Niemelä, Janne Petteri; Marin, Giovanni; Karppinen, Maarit

Titanium dioxide thin films by atomic layer deposition

Published in:
Semiconductor Science and Technology

DOI:
10.1088/1361-6641/aa78ce

Published: 23/08/2017

Document Version
Peer reviewed version

Titanium dioxide thin films by atomic layer deposition: a review

Janne-Petteri Niemelä*, Giovanni Marin and Maarit Karppinen*

Department of Chemistry and Materials Science, Aalto University, FI-00076 Espoo, Finland
**janne.p.niemela@gmail.com; maarit.karppinen@aalto.fi*

Abstract
Within its rich phase diagram titanium dioxide is a truly multifunctional material with a property palette that has been shown to span from dielectric to transparent-conducting characteristics, in addition to the well-known catalytic properties. At the same time down-scaling of microelectronic devices has led to an explosive growth in research on atomic layer deposition (ALD) of a wide variety of frontier thin-film materials, among which TiO_2 is one of the most popular ones. In this topical review we summarize the advances in research of ALD of titanium dioxide starting from the chemistries of the over 50 different deposition routes developed for TiO_2 and the resultant structural characteristics of the films. We then continue with the doped ALD-TiO_2 thin films from the perspective of dielectric, transparent-conductor and photocatalytic applications. Moreover, in order to cover the latest trends in the research field, both the variously constructed TiO_2 nanostructures enabled by ALD and the Ti-based hybrid inorganic-organic films grown by the emerging ALD/MLD (combined atomic/molecular layer deposition) technique are discussed.

CONTENTS

1. Introduction

Titanium dioxide is a wide band gap semiconductor that exhibits various crystal structures, the tetragonal anatase and rutile structures being the most common ones. Although TiO_2 is possibly best known for its photocatalytic properties, it is an interesting material for dielectric and transparent-conductor applications as well. Owing to its higher dielectric constant, rutile is the structure-of-choice for dielectric applications, while the higher electron mobility of anatase makes it more attractive to transparent-conductor applications. Titanium dioxide tends to have *n*-type conducting character due to intrinsic defects that easily form in its crystal lattice. Depending on the targeted application, the intrinsic *n*-type nature can be complemented or compensated for by intentional extrinsic doping.

Atomic layer deposition (ALD) is a chemical thin film fabrication technique that relies on cyclic gas-surface reactions, where the precursor vapors are dosed over the growth surface one at a time. The cyclic nature of the ALD processes ensures excellent control over the film thickness, which is often demanded for today´s microelectronic devices with dimensions down-scaled to a nanometer level. Moreover, the self-limited surface reactions guarantee that the films deposited by ALD grow (sub)atomic layer-by-layer – a fact that enables in addition to the high level of thickness control, conformal deposition of thin films even on high-aspect-ratio nanostructures. These attractive characteristics have led to the apparent increased industrial interest towards ALD in general, and an explosive increase in the number of scientific publications during the last ten years, as is evident from figure 1 in the case of ALD of TiO_2.

The recent outburst of scientific productivity calls for reviewing the activities in the research field, and indeed, numerous general and topical reviews on atomic layer deposition have been published lately. For example, George wrote an overview on ALD in general, covering various more specific topics as well [1]. Miikkulainen *et al.* reviewed ALD processes in general with a special focus on crystallinity of inorganic films [2], while Johnson *et al.* provided a brief review on ALD fundamentals and selected applications [3]. Knez *et al.* introduced the advanced concepts of nanostructuring with ALD [4], and Profijt *et al.* reviewed the merits and challenges of plasma-assisted ALD [5]. Related to recent precursor development, heteroleptic precursors were reviewed with the focus on deposition of group four and five transition metal oxides [6,7]. Fabrication of inorganic-organic thin films by combining atomic and molecular layer deposition (MLD) was reviewed by George *et al.* and by Sundberg *et al.* [8,9]. Motivated by the large number of published works on certain widely studied materials, topical reviews such as the review on ALD of ZnO by Tynell *et al.* have become of increasing interest too [10].

In this work we review the atomic layer deposition of titanium dioxide from various perspectives. We begin by discussing the characteristics of different TiO_2 ALD processes based on halide, alkoxide, alkylamide and heteroleptic precursors. The discussion of the deposition processes is followed by a chapter devoted to film crystallinity. Leaning towards applications we review extrinsic doping of TiO_2 thin films with metal-insulator-metal capacitors, transparent conducting oxides and photocatalysis as case studies. Furthermore, an application-oriented chapter

on TiO_2 nanostructures is included. Finally we summarize the fabrication of titanium-based hybrid thin-film materials obtained *via* the strongly emerging combined ALD/MLD technique.

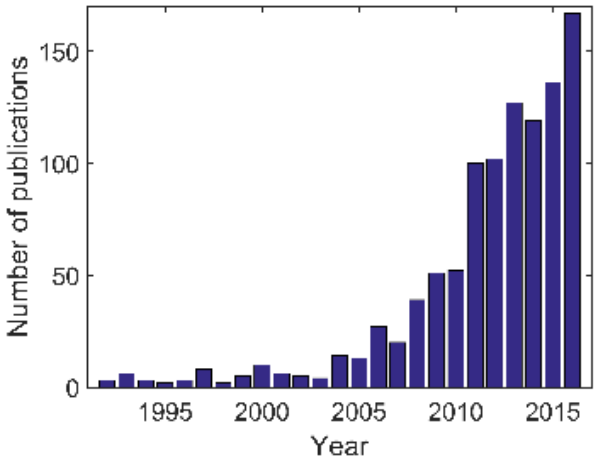

Figure 1. Number of publications on atomic layer deposition of TiO_2 as retrieved with SciFinder.

Table 1. Atomic layer deposition processes for TiO_2.

Reactant: / Precursor:	H_2O	H_2O_2	O_2	O_3	H_2O plasma	O_2 plasma	MeOH	H_3COOH HCOOH	NH_3	N_2O plasma
Halides:										
$TiCl_4$	[11-333];	[334-340];	x	[271,341-343];	x	[344-346];	[347];	x	x	x	x
TiI_4	[348-351];	[352-354];	[355,356];	x	x	x	x	x	x	x	x
TiF_4	[357];	x	x	x	x	x	x	x	x	x	x
Alkoxides:										
$Ti(O^iPr)_4$	[37,87,105,135,146,170,212,267,358-536];	[337,360,398,537-545];	[546]*;	[127,250,486,502,514,547-566];	[384,397];	[362,384,397,507,514,516,556,567-597];	x	[598];	[523,598-603];	[604,605];	[576,606];**
$Ti(OEt)_4$	[37,54,63,91,607-617];	[54,63,91];	x	x	x	x	x	x	x	x	x
$Ti(OMe)_4$	[614,617-633];	x	x	[628-631];	x	x	x	x	x	x	x
$Ti(O^tBu)_4$	x	x	x	[561];	x	x	x	x	x	x	x
Alkylamides:										
$Ti(NMe_2)_4$	[278,384,509,511,634-728];	[688,729-734];	x	[561,683,735-743];	[384,646,744];	[384,646,651,741,745-761];	x	x	x	x	x
$Ti(NEt_2)_4$	[762-766];	x	x	[767];	x	x	x	x	x	x	x
$Ti(NEtMe)_4$	[767];	x	x	[767];	x	x	x	x	x	x	x
***Heteroleptic*:**										
$Ti(O^iPr)_2(dmae)_2$	[768];	x	x	x	x	x	x	x	x	x	x
$Ti(O^iPr)_2(thd)_2$	[636,769-773];	x	x	[774];	x	x	x	x	x	x	x
$Ti(O^iPr)_3(CpMe)$	x	x	x	x	x	[775];	x	x	x	x	x
$Ti(O^iPr)_3(N^iPr\text{-}Me\text{-}amd)$	[776];	x	x	[777];	x	x	x	x	x	x	x
$Ti(OMe)_3(CpMe)$	x	x	x	[767];	x	x	x	x	x	x	x
$Ti(OMe)_3(CpMe_5)$	x	x	x	[767,778-781];	x	[775,782-784];	x	x	x	x	x
$Ti(O^tAm)_2(trhd)_2$	[769];	x	x	x	x	x	x	x	x	x	x
$Ti(NMe_2)_2(O^iPr)_2$	[776];	x	x	[777];	x	x	x	x	x	x	x
$Ti(NMe_2)_3Cp$	x	x	x	[767];	x	x	x	x	x	x	x
$Ti(NMe_2)_3(CpN)$	x	x	x	x	x	[785];	x	x	x	x	x
$Ti(NMe_2)_3(CpMe)$	x	x	x	x	x	[786,787];	x	x	x	x	x
$Ti(NMe_2)_3(CpMe_5)$	x	x	x	[767];	x	x	x	x	x	x	x
$Ti(NMe_2)_3(guan\text{-}NMe_2)$	[788];	x	x	x	x	[789];	x	x	x	x	x
$Ti(NEtMe)_3(guan\text{-}NEtMe)$	[790];	x	x	[790];	x	x	x	x	x	x	x
Ti(CHT)Cp	x	x	x	[791];	x	x	x	x	x	x	x

* Ref. [546] with combined O_2/NH_3 reactant mixture.** Refs. [792-797] without plasma. Note that a process (free from conventional oxygen sources) by combining $TiCl_4$ and $Ti(O^iPr)_4$ has also been demonstrated [798].

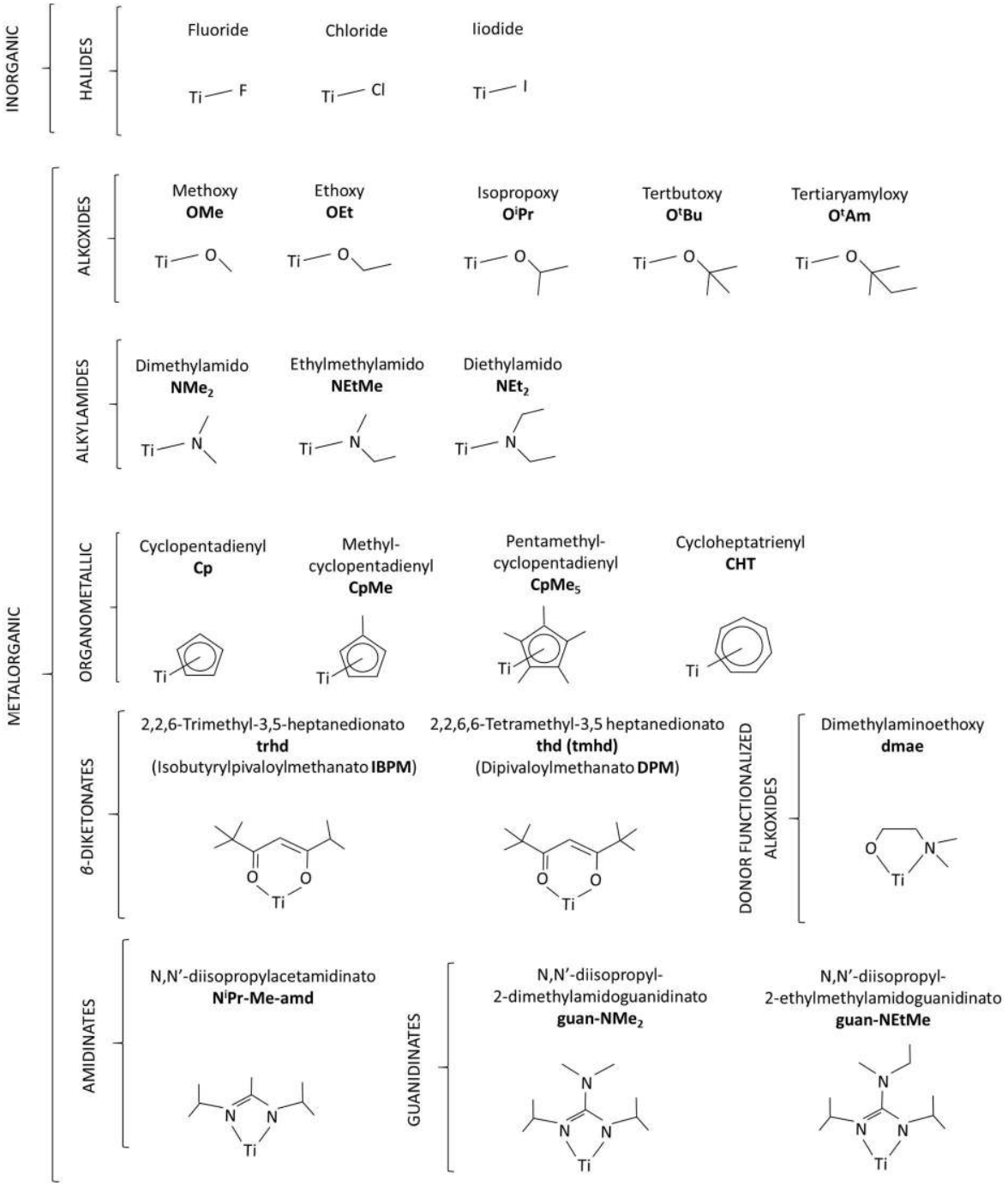

Figure 2. Ligands in the Ti precursors used in the ALD processes for TiO_2 thin films.

2. Precursors and processes

In the last couple of decades numerous ALD routes based on different precursor-reactant couples have been reported for the fabrication of TiO_2 thin films. In table 1 we summarize these processes with an aim to provide an easy access to the corresponding references, while figure 2 provides visualization of the different ligand types in the titanium precursors used. As is seen from table 1, homoleptic halides, alkoxides and alkylamides have been widely employed as Ti precursors. More recently various heteroleptic precursors with *e.g.* cyclopentadienyl ligands have been introduced to improve the poor thermal stability of homoleptic alkoxides and alkylamides. Although water is by far the most common oxygen source, use of alternatives such as ozone or plasmas is sometimes justified to *e.g.*, avoid physisorption of water at low temperatures, or to provide enhanced reactivity in the absence of sufficient thermal energy for water-based routes. In some cases comparison of processes present or missing in table 1 can illustrate interesting trends in the underlying chemistry; for example for the heteroleptic precursors, the lack of reactivity of certain precursors towards water and – on the other hand – the sufficient reactivity towards ozone or O_2 plasma can indeed be revealed from this table.

A common feature of ideal water-based thermal ALD processes is that the film growth proceeds *via* exchange reactions between the hydroxyl groups provided by water and the ligands (L) of the metal precursor. Thus, one water-based thermal ALD cycle for TiO_2 can be described on the basis of equations 1 and 2:

$$n(-OH)(s) + TiL_4(g) \longrightarrow (-O-)_nTiL_{4-n}(s) + nHL(g) \quad (1)$$

$$(-O-)_nTiL_{4-n}(s) + (4-n)H_2O(g) \longrightarrow (-O-)_nTi(OH)_{4-n}(s) + (4-n)HL(g), \quad (2)$$

where n is the average number of ligands released by each TiL_4 molecule during the precursor adsorption, and where *s* and *g* refer to surface and gas-phase species, respectively. However, deviations from this ideal picture are possible. For example, when the surface density of hydroxyl groups decreases due to dehydroxylation at high temperatures, TiL_4 may also react dissociatively or associatively with oxygen bridges on the surface, leading to a decrease in the n value [13,40]. Moreover, the reaction byproducts may play a role in film growth by *e.g.* re-adsorbing onto the surface and blocking the reaction sites. Subsequent completion of surface reactions (1) and (2) forms the so-called ALD cycle, and indeed, the film growth by ALD is realized by repeating this cycle. Stemming from the cyclic nature of the ALD technique, the film deposition rate is often described in terms of the so-called growth-per-cycle (GPC) value. Ideally, for the best repeatability of the ALD process, the GPC value should be constant as a function of the deposition temperature, which however is often not the case. For example with increasing temperature, even under self-saturating growth conditions, the GPC value can decrease for dehydroxylated surfaces, or increase due to increased thermal energy for the surface reactions. For non-self-saturating growth (not ALD)

the GPC value can *e.g.* increase at low temperatures due to physisorption of the precursors or increase at high temperatures due to self-decomposition of the precursors in the gas phase.

In ALD reviews it is typical to tabulate ALD processes together with their respective GPC values. However, provided the large statistical variation observed for the GPC values of the TiO_2 ALD processes, and in order to better illustrate and capture the underlying chemistry, we chose to represent the GPC-*vs.*-temperature trends schematically instead of tabulating them (figures 3-7). When interpreting the figures, it should be kept in mind that the presented GPC values may, to some extent, depend on various factors in addition to temperature and the choice of the ALD process. For example, for very thin films the choice of the substrate can either enhance the GPC values *via* substrate-enhanced growth or reduce the GPC values *via* nucleation delay. For thicker films onset of crystallite formation upon growth propagation may alter the GPC values. Moreover, the type of the ALD reactor used or film-thickness measurement technique applied for determination of the GPC value may also play a small role. Therefore, in order to provide proper statistics and identify general GPC trends large amount of data published by various research groups for films deposited in various types of reactors on various kinds of substrates was gathered. However, owing to the massive amount of the literature, the data from all the references could not be included. Instead, as the halide, alkoxide and alkylamide-based processes have been mostly developed a while ago, the literature published before 2011 was mostly used. As for the heteroleptic precursors the advances in the field are recent, more recent literature was used in this case. From figure 3, that summarizes the GPC-*vs.*-temperature trends for all the titanium-precursor families, the underlying chemistry and research directions are readily visible. For example, while $TiCl_4$ can be used up to high temperatures without decomposition, for alkoxides thermal self-decomposition can become a factor that limits the self-saturating nature of the surface reactions. Moreover, alkylamides show high reactivity at low temperatures, while the research on heteroleptic precursors has boosted up the thermal decomposition temperatures of the alkoxide and alkylamide precursors, often with a compromise in the GPC values. Here in Chapters 2.1-2.4 we present the characteristics of the ALD processes listed in table 1. Although the surface chemistry of ALD is intimately linked to the resultant structural properties of the films, these aspects are not discussed in depth in this chapter; instead, Chapter 3 is devoted to the discussion of the film crystallinity, phase composition and surface topography.

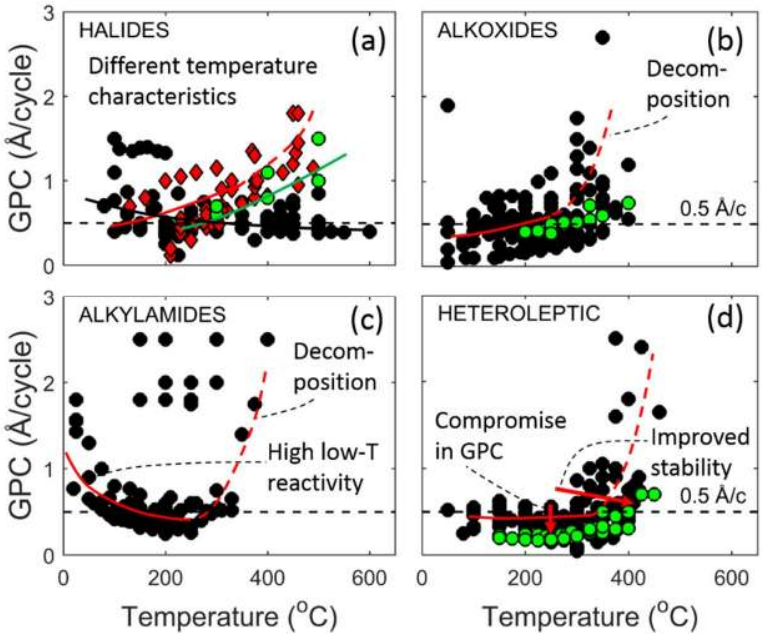

Figure 3. Growth-per-cycle (GPC) trends as a function of deposition temperature as retrieved from literature; the data are from the same references as in figures 4-7. In (a) red diamonds and green spheres indicate the trends for TiI_4- and TiF_4-based processes, respectively, while black spheres indicate $TiCl_4$-based processes. In (b) for alkoxides thermal decomposition and data for $Ti(OMe)_4$ is highlighted, while in (c) high low-temperature reactivity for alkylamides is evident. In (d) for heteroleptic precursors the trend to increase the thermal stability and good-quality data for $CpMe_5$-containing precursors are underlined. The dashed line shows the level of "typical" GPC of 0.5 Å/cycle for TiO_2 ALD as reference.

2.1 Halides

As the atomic layer deposition of TiO_2 was first reported using $TiCl_4$ as the titanium precursor and H_2O as the oxygen source [13,14], a notable part of the early literature discusses the deposition characteristics and the structural properties of the films obtained *via* this ALD route. Note that prior to the works [13,14], molecular layering of TiO_2 seems to have been reported in the USSR literature in Russian [799]. Indeed, detailed reaction mechanism studies have revealed some complexity beyond the simple ligand-exchange picture, such as dissociative or associative adsorption of $TiCl_4$ at high temperatures on dehydroxylated surfaces. However, the $TiCl_4/H_2O$ route has remained as one of the most widely employed ALD process as it can be used in a rather straightforward way in a wide temperature range above 100 °C, even up to 600 °C. For TiI_4, the low dissociation energy of the Ti-I bond enables the easy removal of the iodide ligands, a fact that decreases steric hindrance and increases the GPC value [348]. For the same reason, however, thermal decomposition of the precursor leads to a loss of surface control of the film growth already at temperatures around 275 °C. On the contrary, the fluorine-based precursor TiF_4 is stable at least up to 400 °C [357]. For the halides in general, the drawback is the corrosiveness of the reaction byproducts, which can be

harmful to the deposition instruments and has been one of the drivers in the search for alternative titanium precursors.

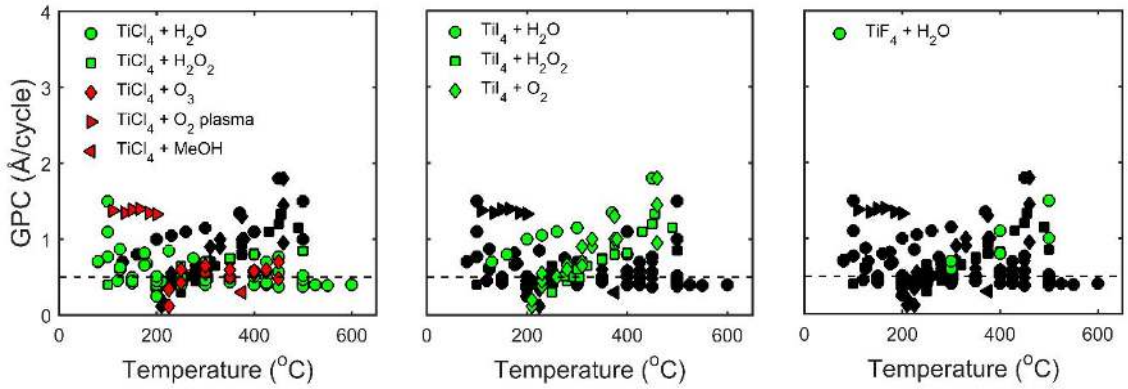

Figure 4. Temperature trends of the growth-per-cycle (GPC) values, as retrieved from literature for the halide-based processes: in each of the three figures data for one of the Ti-halide precursors are highlighted (in green or red) at the time. The data illustrated in color in one of the figures, is shown in black in all the other figures. The data is retrieved from the following references: $TiCl_4/H_2O$ [13,17,19,22,23,28,30,37,38,42,44,45,56,58,83,88,94,123,124], $TiCl_4/H_2O_2$ [334-336], $TiCl_4/O_3$ [271],$TiCl_4/O_2$ plasma [344,345], $TiCl_4$/MeOH [347],TiI_4/H_2O [348], TiI_4/H_2O_2 [352,354], TiI_4/O_2 [356], TiF_4/H_2O [357].

$TiCl_4$ with H_2O, H_2O_2, O_3, O_2 plasma or MeOH. The $TiCl_4/H_2O$ process shows GPC values of around 0.5 Å/cycle, which decrease moderately with increasing deposition temperature (figure 4). The decreasing trend has been linked to a gradual transition in the mechanism of the reactions (1) or (2) as observed via *in-situ* quartz-crystal-microbalance (QCM), quadrupole-mass-spectrometry (QMS) and nuclear-magnetic-resonance (NMR) studies. The *n* value decreases from around 2 at 150 ºC to notably below 1 at 300 ºC [14,40,41], such that the role of dissociative or associative adsorption of $TiCl_4$ without release of any byproducts, and steric hindrance by the –Cl ligands, increase at high temperatures [40,41,46]. At low temperatures the high GPC values may be contributed by condensation of water, and in parallel higher Cl or H impurity levels are seen [13,32,41]. As possible secondary reactions, formation of hydroxychloride species as reaction intermediates have been proposed [16,17,41], but the lack of evidence in QMS experiments has indicated either short life time or very low concentration for these species, which could be explained by their rapid further reactions [40]. Hydroxychlorides could react with the surface hydroxyl groups to form Cl-terminated surface and release water, or decompose to form TiO_2 and water, or decompose releasing oxychloride species and water [16,40,41]. However, neither could have the oxychloride species been detected in QMS measurements [40]. It has been proposed [13] and predicted by computation [26] that the byproduct HCl could react with the surface hydroxyls and/or oxygen bridges such that the number of available reaction sites for the $TiCl_4$ molecules decreases. While the QCM experiments have indicated HCl to create low and unstable surface coverage and hence HCl to not to play a big role in the TiO_2 growth [41], Leem *et al*. saw HCl to

increase or decrease the growth rate in different ways depending on the reaction half-cycle and growth temperature [262].

The GPC values could be enhanced by increasing the reactivity for the second half-reaction (2) by using H_2O_2, O_3, or O_2 plasma as reactants. Indeed, in the case of H_2O_2 GPC values between 0.5 and 0.7 Å/cycle are slightly above the average seen for the $TiCl_4/H_2O$ process, especially at the high end of the temperature range of 100-500 °C [334-339]. Similarly, the O_3-based process yields values around 0.5-0.7 Å/cycle in the temperature range of 250-450 °C [271,341], and slightly lower values at 600 °C [342]. For O_2 plasma, GPC values up to 1.35 Å/cycle at temperatures of 110-200 °C have been reported; for this route molecular chlorine was seen as the only byproduct with QMS and the films were free from Cl impurities, as determined with X-ray photoelectron spectroscopy (XPS) [344,345]. In the absence of –OH groups $TiCl_4$ likely adsorbs dissociatively on oxygen bridges on the film surface [344,345]. Moreover, growth of TiO_2 films *via* the $TiCl_4$/MeOH process has been reported in the context of fabrication of TiO_2–Cr_2O_3 nanolaminates. As a part of these layered structures this process yielded a GPC of 0.3 Å/cycle for the TiO_2 layers [347].

TiI_4 with H_2O, H_2O_2 or O_2. After the first attempts with the TiI_4/H_2O process, resulting in low GPC values [352], higher values from 0.7 Å/cycle at 135 °C to 1.5 Å/cycle at 450 °C were demonstrated [348]. For this process around two iodine ligands are released during the TiI_4 pulse at 135 °C (n = 2), while n decreases to around 1.5 at 200 °C for decreasing hydroxyl coverage of the film surface. Above 275 °C the QCM data indicate thermal decomposition of TiI_4 [348]. For the H_2O_2-based process the GPC-*vs*.-temperature trend is the same as for the H_2O-based process, with the difference that the GPC values are slightly lower with H_2O_2 [352-354]. Contrary to the $TiCl_4$-based routes, for TiI_4 the higher reactivity of H_2O_2 seems thus not to be beneficial. Based on QCM studies the surface reaction for TiI_4 adsorption proceeds by release of one or zero iodine ligands and TiI_4 decomposition yields the rest, summing up to a total of n = 2-3 above 250 °C. The low dissociation energy of the Ti-I bond enables thermal ALD of TiO_2 also by using O_2 as the reactant, so that GPC is around 0.6 Å/cycle at 235 °C – a value that may notably depend on the choice of the substrate though [348,355,356]. In the absence of hydroxyl groups the adsorbing TiI_4 molecules are expected to react with the oxygen bridges on the surface with possible release of iodine ligands in the form of gaseous I_2 byproduct, which in line with the low iodine impurity levels [355]. Low iodine impurity levels seem to be characteristic for the TiI_4-based processes [348,350,354].

TiF_4 with H_2O. This route was studied at 300, 400, and 500 °C and (contrary to what might appear from figure 4) the surface reactions were reported to saturate for both TiF_4 and H_2O exposures at 400 °C. The GPC values were 0.6-0.7 Å/cycle at 300 °C and around 1.0-1.7 Å/cycle at 500 °C such that the growth was faster on soda lime glass in comparison to borosilicate glass [357].

2.2 Alkoxides

The research on the alkoxide precursors has been largely driven by the need for finding alternatives for $TiCl_4$-based processes that suffer from the corrosion issues. Among alkoxides $Ti(O^iPr)_4$ has been the most popular choice, with a benefit of showing reactivity towards H_2O even below 100 °C. Nevertheless, H_2O_2 and O_2 plasma have also been used as oxygen sources with an aim to increase the growth rate. Reaction mechanism studies have shown exchange-reaction governed surface chemistry for the $Ti(O^iPr)_4/H_2O$ process, while more marked role of molecular or dissociative precursor adsorption is seen for the $Ti(OEt)_4/H_2O$ route. The drawback of the alkoxide precursors is that they decompose at relatively low temperatures. For $Ti(O^iPr)_4$ the decomposition starts around 250 °C, while $Ti(OEt)_4$ and in particular $Ti(OMe)_4$ are slightly more stable.

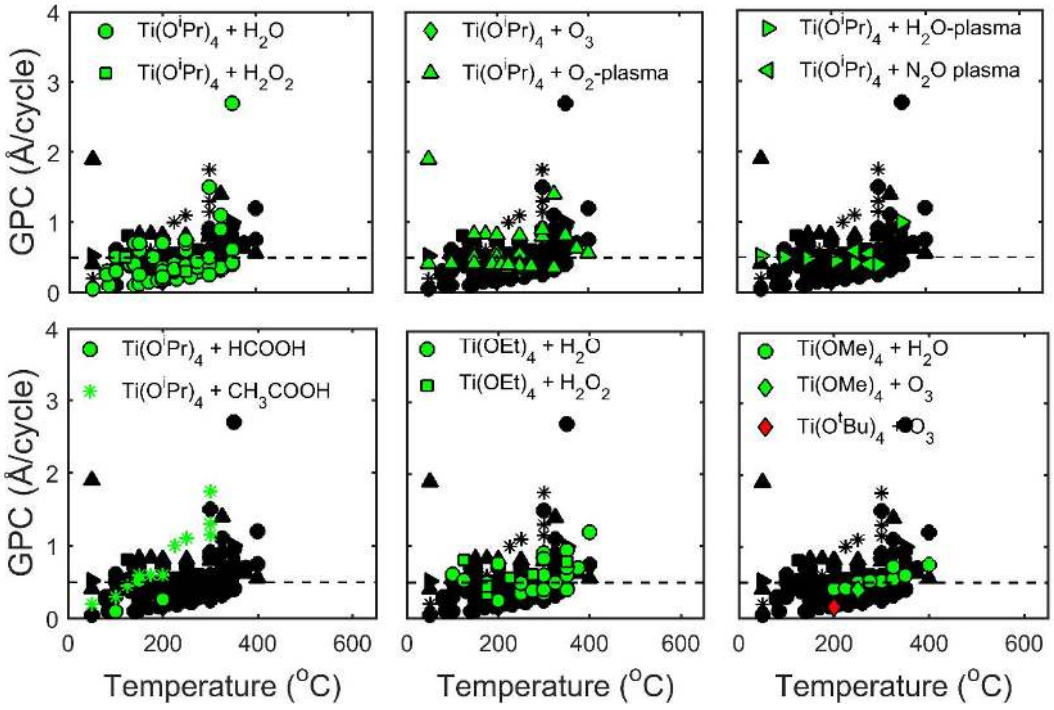

Figure 5. Temperature trends of the growth-per-cycle (GPC) values, as retrieved from literature for the alkoxide-based processes: in each of the six figures data for one to two of the Ti-alkoxide precursors are highlighted (in green or red) at the time. The data illustrated in color in one of the figures, is shown in black in all the other figures. The data was retrieved from the following references: $Ti(O^iPr)_4/H_2O$ [37,359,364,366,368,379,381,382,384,385,387,391-393,396,398,400,402,404], $Ti(O^iPr)_4/H_2O_2$ [540], $Ti(O^iPr)_4/O_3$ [547,551], $Ti(O^iPr)_4/O_2$ plasma [384,397,567,569-571,573,574,578], $Ti(O^iPr)_4/H_2O$ plasma [384,397], $Ti(O^iPr)_4/N_2O$ plasma [576], $Ti(O^iPr)_4$/HCOOH [598], $Ti(O^iPr)_4/CH_3OOH$ [598], $Ti(OEt)_4/H_2O$ [37,63,607,615], $Ti(OEt)_4/H_2O_2$ [54,63,91], $Ti(OMe)_4/H_2O_2$ [614,618,622,627], $Ti(OMe)_4/O_3$ [628], and $Ti(O^tBu)_4/O_3$ [561].

$Ti(O^iPr)_4$ with H_2O, H_2O_2 and H_2O plasma. For the $Ti(O^iPr)_4/H_2O$ process the GPC values around 0.15-0.6 Å/cycle are typical with an increasing trend with increasing deposition temperature (figure 5) [359]. Thermal decomposition of $Ti(O^iPr)_4$ onsets at around 250 °C and becomes marked at 350 °C [359-361,368]. Interestingly, the GPC values can show a notable (almost factor-of-two)

dependence on the water dose (not time), which may to some extent explain the large variation in the reported GPC values [37]. According to QMS and QCM data the number of O^iPr ligands released during the precursor pulse is around two between 150 and 300 °C [360,361]. Owing to the higher reactivity, H_2O_2 as the reactant can improve the GPC values up to 1.2 Å/cycle at 100 °C. At higher temperatures of 200-250 °C the benefit of using H_2O_2 vanishes and essentially similar growth rates of 0.5-0.6 Å/cycle are obtained with both H_2O_2 and H_2O [360]. At 100 °C 2.6-2.9 O^iPr ligands are released during the $Ti(O^iPr)_4$ exposure, while at 200-250 °C *n* values of 1.2-1.7 indicate an increasing effect of steric hindrance to the film growth with increasing temperature [360]. For both H_2O and H_2O_2-based routes, carbon and hydrogen impurities are possible but they tend to decline with increasing temperature (at least in the absence of $Ti(O^iPr)_4$ decomposition of $Ti(O^iPr)_4$) [359,360,368,636]. The $Ti(O^iPr)_4/H_2O$ plasma process yields steady GPC values around 0.5 Å/cycle in the wide temperature range of 50-300 °C, while at 350 °C $Ti(O^iPr)_4$ clearly decomposes [384,397]. The good-quality low-temperature performance should stem from improved reactivity of the H_2O-plasma reactant. In terms of carbon impurities the use of water plasma can be beneficial yielding residue-free films, as verified with XPS [384].

$Ti(O^iPr)_4$ with O_2, O_3 and O_2-plasma. Use of O_2 as the reactant has been mentioned in literature but not studied in detail [29,800]. Instead, for the O_3 reactant GPC values around 0.35-0.5 Å/cycle in the temperature range of 150-250 °C have been reported [547,553]. In the absence of –OH groups, based on *in-situ* Fourier transform infrared (FTIR) spectroscopy, Rai *et al.* proposed the surface reactions to proceed *via* formation of carbonate groups [553]. Probably, combustion of O^iPr ligands with O_3 results in the formation of CO_2 and H_2O; a fraction of the by-product CO_2 would then react with the surface forming carbonates [553]. Upon subsequent exposure to the precursor the carbonates react with the O^iPr ligand again releasing CO_2 [553]. The route based on O_2 plasma shows 0.3-0.8 Å/cycle at temperatures between 150 and 275 °C [362,397,567-569,571,573,576], while at high temperatures above 275 °C the self-limited nature of the surface reactions is lost due to decomposition of $Ti(O^iPr)_4$ [384,567]. Based on *in-situ* FTIR studies, both metal carbonates and hydroxyl groups could serve as reaction sites for the metal precursor [574]. Very high GPC of 1.9 Å/cycle for films grown at 50 °C by using oxygen radicals was reported; these films had density of 3.2 gcm^{-3} with impurity contents of 13 at.% for hydrogen and of 4 at.% for carbon [570]. The impurity contents decline at the higher deposition temperatures as is typical [570,576]. In terms of carbon impurities, O_2 plasma based route might outperform the water-based thermal and plasma processes at 50 °C [384].

$Ti(O^iPr)_4$ with H_3COOH, HCOOH, N_2O-plasma or NH_3. The use of carboxylic acids as the oxygen source has been motivated by the need to minimize the formation of interfacial oxide between Si and a high-k oxide in CMOSFETS, a process that tends to occur when using the ordinary oxygen sources [598-601]. A constant GPC window with 0.6 Å/cycle was reported between 150 and 200 °C for the $Ti(O^iPr)_4/H_3COOH$ process, while the $Ti(O^iPr)_4$/HCOOH process yields the growth of 0.52 Å/cycle at 150 °C; in the latter case the constant-GPC window is narrower and shifted towards the lower temperatures in comparison to the former case [598]. It was proposed that the surface reactions proceed such that an alcohol is released upon the carboxylic acid exposure, while an ester is released upon the $Ti(O^iPr)_4$ exposure. The films have low carbon content

[598]. For N_2O plasma reactant, Choi *et al.* reported a GPC of 0.59 Å/cycle at 250 °C, a notably higher value than obtained for $Ti(O^iPr)_4/O_3$ and $Ti(O^iPr)_4/O_2$-plasma processes in the same study [576]. The improvement was ascribed to the presence of intermediate O-N surface species that increase the ligand removal and decrease the steric hindrance [576]. Nitrogen impurities were not observed in the final full-thickness films [576]. The effect of the substrate was considered in detail in Ref. [606]. Use of the $Ti(O^iPr)_4$ precursor together with NH_3 reactant at 140 °C has also been reported [604,605].

$Ti(OEt)_4$ with H_2O or H_2O_2. The H_2O-based route has shown a range of values between 0.35-0.8 Å/cycle at 100-300 °C [607,609,611], while the precursor decomposition starts at around 250 °C, has slow kinetics below 300 °C, and becomes notable at 350 °C [607,609,610]. Note that, as for the $Ti(O^iPr)_4/H_2O$ process, the GPC values may notably depend on the water doses (not time) [37]. The QMS studies have indicated that only $n < 0.4$ ligands on average were released upon adsorption of the precursor at 250 °C [610], whereas *in-situ* QCM studies by Aarik *et al.* indicated *n* values of 0.6 (225-250 °C), 1.2 (200 °C) and 1.5 (150 °C) [609]. This implies that molecular, dissociative, or side-product-ethanol mediated adsorption of $Ti(OEt)_4$ is more dominant than the surface exchange reaction between the -OH groups [609,610]. The FTIR results have indicated residues of unreacted OEt ligands for the films deposited at 125 °C [91], while at 200 °C the carbon and hydrogen levels were low [63]. Use of H_2O_2 as the oxygen source has not led to marked improvement of the GPC values, the carbon levels were higher though [54,63,90,91].

$Ti(OMe)_4$ with H_2O or O_3, and $Ti(O^tBu)_4$ with O_3. For the deposition from $Ti(OMe)_4$ and H_2O a constant-GPC regime at 0.5 Å/cycle has been seen between 250-300 °C [618]. Below this temperature range the growth rate decreased and above it an increase due to self-decomposition of the precursor was seen [618]. The decomposition was moderate up to 350 °C but notable at 400 °C indicating $Ti(OMe)_4$ to be the most stable alkoxide precursor. The stability order of $Ti(O^tBu)_4 < Ti(O^iPr)_4 < Ti(OEt)_4 < Ti(OMe)_4$ was concluded [618]. Impurity levels were 2 at.% for C and 7 at.% for H for films fabricated at 200 °C, and only fractions of a percent above 200 °C [618]. Film growth *via* the $Ti(OMe)_4/O_3$ process has been demonstrated between 250 and 300 °C [628-631]. Popovici *et al.* grew rutile films on RuO_2 substrates at 250 °C with a GPC of 0.4 Å/cycle [628,629,631], while at 300 °C a similar GPC of 0.4 Å/cycle for films of the anatase structure was reported [630]. The $Ti(O^tBu)_4$ precursor has not received much attention, it has however been used together with O_3 in a batch reactor showing a low GPC value of 0.16 Å/cycle [561].

2.3 Alkylamides

Motivation to use the alkylamide precursors stems from the low binding energy of the Ti-N bond, and hence high reactivity of the amide compounds towards water [634]. This provides a possibility to grow TiO_2 films well below 100 °C. Moreover, the side products of amides are less corrosive than HCl, i.e. the side product from the $TiCl_4/H_2O$ process, which is a benefit when considering the reactor lifetime [634]. The most common alkylamide is $Ti(NMe_2)_4$, but $Ti(NEt_2)_4$ and

$Ti(NEtMe)_4$ based processes are also available. The drawback is that $Ti(NMe_2)_4$ starts to decompose already around 200 °C.

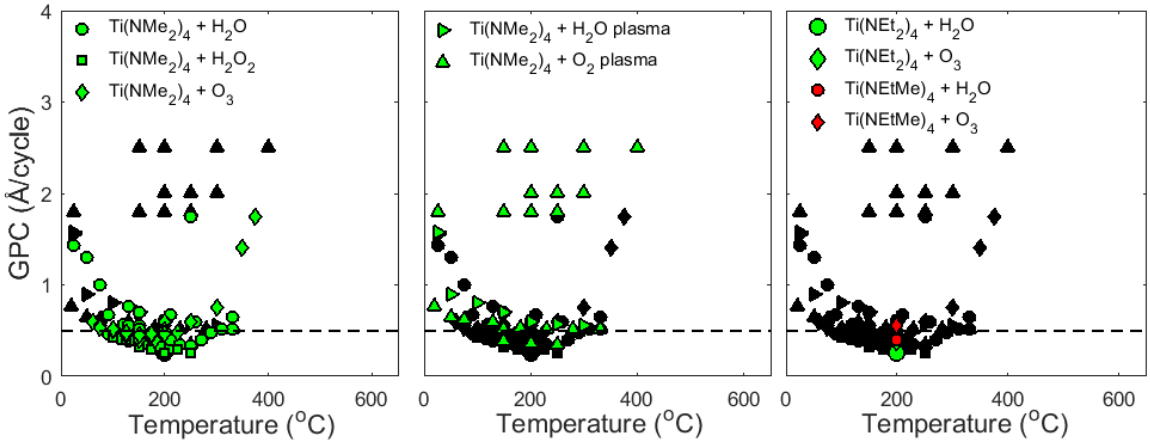

Figure 6. Temperature trends of the growth-per-cycle (GPC) values, as retrieved from literature for alkylamide-based processes: in each of the three figures data for one to two of the Ti-alkylamide precursors are highlighted (in green or red) at the time. The data illustrated in color in one of the figures, is shown in black in all the other figures. The data was retrieved from the following references: $Ti(NMe_2)_4/H_2O$ [384,634,636,637,639,642,643,674,767], $Ti(NMe_2)_4/H_2O_2$ [729], $Ti(NMe_2)_4/O_3$ [735,736,742,767,801], $Ti(NMe_2)_4/H_2O$ plasma [384,744], $Ti(NMe_2)_4/O_2$ plasma [384,651,745-747,749], $Ti(NEt_2)_4/H_2O$ [767], $Ti(NEt_2)_4/O_3$ [767], $Ti(NEtMe)_4/H_2O$ [767], $Ti(NEtMe)_4/O_3$ [767].

$Ti(NMe_2)_4$ with H_2O, H_2O_2 or O_3. Typically, as is seen from figure 6, the $Ti(NMe_2)_4/H_2O$ process exhibits a decreasing trend of the GPC with increasing deposition temperature. At low temperatures around 100 °C and below, the GPC values increase rapidly which might relate to physisorption of water and/or the $Ti(NMe_2)_4$ precursor. In this respect, in-situ IR studies have shown that physisorbed water has long lifetime on the film surface, up to 30 seconds even at 110 °C, and that it can contribute to the film growth [696]. On the other hand, saturating behaviour of the precursor and the reactant pulses at 50 °C have been used as an argument against the physisorption [636,646]. At high temperatures around 200-260 °C, the low binding energy of the Ti-N bond leads to early self-decomposition of the $Ti(NMe_2)_4$ precursor [635,636]. Absence of nitrogen impurities has indicated that the NMe_2 ligands are removed as a whole [636]. Interestingly, by using H_2O_2 as the oxygen source, crystalline films with anatase structure have been obtained already at 150 °C [729]. This is a lower temperature than is typically needed for crystallization via the water-based route (see chapter 3.1). No impurities were detected in the H_2O_2-based films in the temperature range 100-250 °C [729]. The $Ti(NMe_2)_4/O_3$ process shows similar temperature characteristics to those of the water-based process, with slightly lower GPC values at low temperatures [735,736,742,767,801].

$Ti(NMe_2)_4$ with O_2 plasma or H_2O plasma. Also for the O_2 plasma-based route the GPC-*vs.*-temperature data shows an increasing trend with decreasing temperature, and as for O_3, the GPC values for O_2 plasma process at low temperatures are slightly lower than for the water-based thermal route [384]. AES depth profiles showed presence of carbon impurities only at the sample surface for the film deposited at 200 °C [745]. The films deposited at 50 and 150 °C showed 3.5

and 2% of carbon impurities [384]. Lee *et al.* reported very high GPC values around 2 Å/cycle even around 100-200 °C, however neither the carbon content, nor pulse saturation was commented [747,749]. For the $Ti(NMe_2)_4/H_2O$ plasma process the GPC-*vs*.-temperature trend was very similar to that of the thermal process [384]. The films deposited at 50 and 150 °C showed no carbon impurities [384].

$Ti(NEt_2)_4$ and $Ti(NEtMe)_4$ with H_2O or O_3. Katamreddy *et al.* have demonstrated TiO_2 film growth also *via* different combinations of the $Ti(NEt_2)_4$, $Ti(NEtMe)_4$ precursors and the H_2O and O_3 reactants [767]. The processes yielded the following GPCs: $Ti(NEt_2)_4/H_2O$ 0.25 Å/cycle (125-250 °C), $Ti(NEt_2)_4/O_3$ 0.4 Å/cycle (125-225 °C), $Ti(NEtMe)_4/H_2O$ 0.4 Å/cycle (125-225 °C), $Ti(NEtMe)_4/O_3$ 0.55 Å/cycle (125-225 °C) [767].

2.4 Heteroleptic precursors

Heteroleptic precursors are molecules in which the ligands bonding to the central titanium atom are of more than one type. The synergetic effects in these precursors are expected to arise from the fact that one type of ligand can compensate for the drawbacks of the other type of ligand. Although $TiCl_4$ is thermally stable up to high temperatures, the corrosive byproduct HCl of the $TiCl_4$-based processes may be harmful for the deposition instruments. The processes based on the homoleptic alkoxides and alkylamides do not suffer from corrosion issues, however, thermal self-decomposition limits their use in general below 300 °C. Therefore, various routes for boosting up the thermal-decomposition temperature of the non-halide precursors have been investigated by replacing one or more of the original ligands of the alkoxide or alkylamide precursors. In this respect, thd and Cp ligands have been found to have a particularly stabilizing effect; for Cp this seems to be enhanced for Me-substituted Cp rings, especially for $CpMe_5$. It is worth noting that typically insufficient reactivity of water towards the Cp-based precursors requires the use of more reactive co-reactants such as ozone or O_2 plasma. The bulkiness of the Cp ligand may lead to a decrease in the GPC values due to steric hindrance, which could however be overcome by using O_2 plasma instead of ozone. The main driver for this development is the deposition of rutile-structured TiO_2 and $SrTiO_2$ thin films, which are interesting high-*k* materials for dynamic random access memories (DRAM).

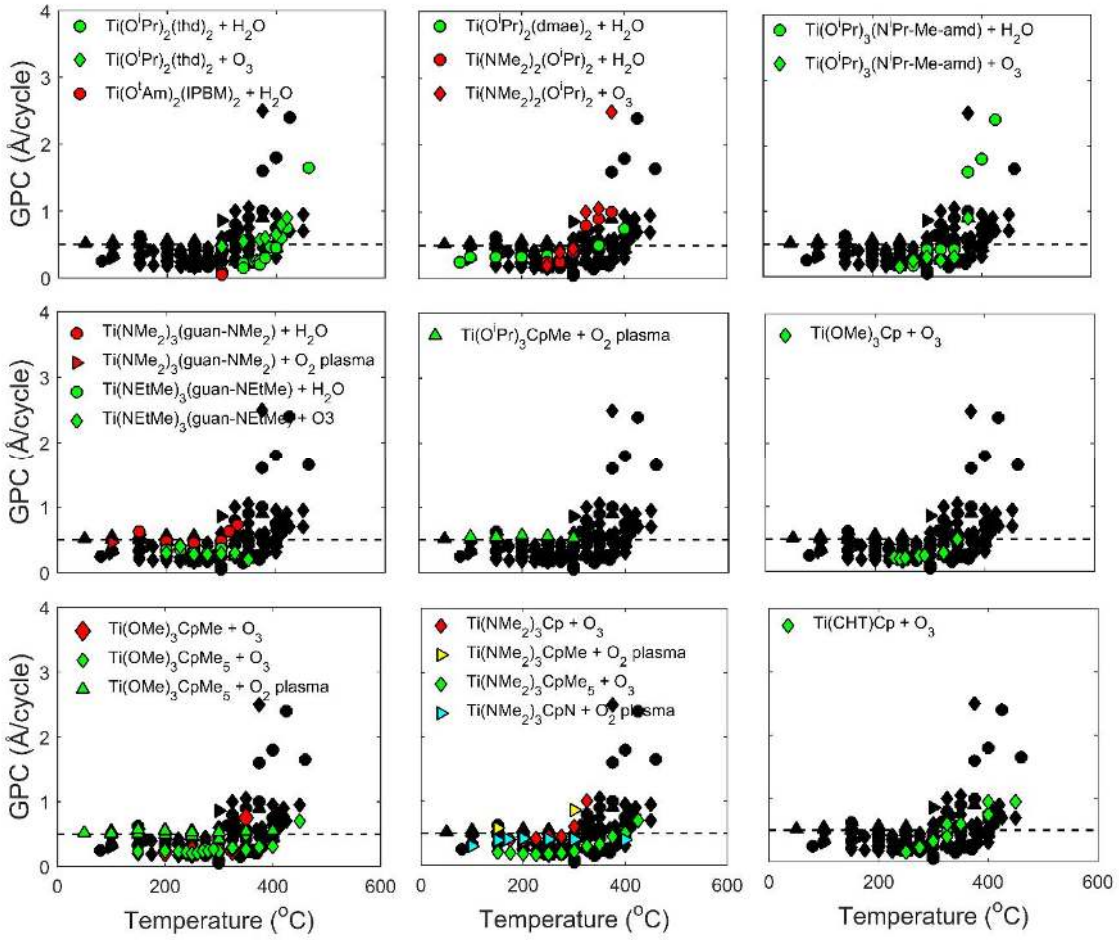

Figure 7. Temperature trends of the growth-per-cycle (GPC) values, as retrieved from literature for processes based on heteroleptic precursors: in each of the nine figures data for one to four of the heteroleptic precursors are highlighted (in green, red, yellow or blue) at the time. The data illustrated in color in one of the figures, is shown in black in all the other figures. The data was retrieved from the following references: $Ti(O^iPr)_2(thd)_2/H_2O$ [769,771-773], $Ti(O^iPr)_2(thd)_2/O_3$ [774], $Ti(O^tAm)_2(IPBM)_2/O_3$ [769], $Ti(O^iPr)_2(dmae)_2/H_2O$ [768], $Ti(NMe_2)_2(O^iPr)_2/H_2O$ [776], $Ti(NMe_2)_2(O^iPr)_2/O_3$ [777], $Ti(O^iPr)_3(N^iPr\text{-}Me\text{-}amd)/H_2O$ [776], $Ti(O^iPr)_3(N^iPr\text{-}Me\text{-}amd)/O_3$ [777], $Ti(NMe_2)_3(guan\text{-}NMe_2)/H_2O$ [788], $Ti(NMe_2)_3(guan\text{-}NMe_2)/O_2$ plasma [789], $Ti(NEtMe)_3(guan\text{-}NMe_2)/H_2O$ [790], $Ti(NEtMe)_3(guan\text{-}NMe_2)/O_3$ [790], $Ti(O^iPr)_3(CpMe)/O_2$ plasma [775], $Ti(OMe)_3(CpMe)/O_3$ [767], $Ti(OMe)_3(CpMe_5)/O_3$ [767,778], $Ti(OMe)_3(CpMe_5)/O_2$ plasma [775,784], $Ti(NMe_2)_3Cp/O_3$ [767], $Ti(NMe_2)_3(CpMe_5)/O_3$ [767], $Ti(NMe_2)_3(CpMe)/O_2$ plasma [787,802], $Ti(NMe_2)_3(CpN)/O_2$ plasma [785], $Ti(CHT)Cp/O_3$ [791].

$Ti(O^iPr)_2(dmae)_2$ with H_2O. In the study of this ALD route, the self-decomposition temperature was reported to shift by around 50 °C towards the higher temperatures in comparison to the $Ti(O^iPr)_4/H_2O$ process [768]. The improved stability was thought to stem from the fact that the precursor exists as a monomeric complex with a pseudo-octahedral coordination and hence increased coordinative saturation for the central Ti atom. The GPC values around 0.3 Å/cycle between 80 and 300 °C were obtained, while above 300 °C the precursor started to self-decompose. However, the high level of impurities for the films' surfaces (15 at.% for carbon and up to 5 at.%

of nitrogen below 300 °C) indicated incomplete hydrolysis of the metal precursor below 300 °C, which was also reflected to the crystallization behavior of the films such that anatase-structured films were obtained only at 400 °C [768].

Ti(O^{i}Pr)$_2$(thd)$_2$ with H$_2$O or O$_3$, and Ti(O^{t}Am)$_2$(trhd)$_2$ with H$_2$O. The Ti(O^{t}Am)$_2$(trhd)$_2$/H$_2$O process proceeds as a saturated growth at 300 °C, however it suffers from very low growth rate of around 0.05 Å/cycle [769]. The Ti(O^{i}Pr)$_2$(thd)$_2$/H$_2$O process shows better performance: it exhibits self-saturating growth with GPC values up to 0.46 Å/cycle at 390 °C [769], with notable decomposition of the β-diketonate ligands and increasing carbon-impurity levels seen above 470 °C [772]. Moreover, Lee *et al.* observed self-saturating growth for the Ti(O^{i}Pr)$_2$(thd)$_2$/H$_2$O process at 370 °C with a GPC value of 0.25 Å/cycle [773], whereas the use of ozone as the reactant enabled notably higher GPC of 0.43 Å/cycle on a Ru substrate. The GPC value increases with increasing temperature for both the reactants, even for self-saturating surface reactions. The differences in the GPC values stem from interfacial reactions between the substrate and the oxygen source: strong oxidation power of ozone leads to *in-situ* oxidation of the Ru substrate to the rutile-structured RuO_2, on top of which the growth of rutile-structured TiO_2 with a high GPC is promoted. Note that, the alkoxide ligands add reactivity towards water as compared to homoleptic *β*-diketonates [773].

Ti(O^{i}Pr)$_3$(CpMe) and Ti(OMe)$_3$(CpMe$_5$) with O$_2$ plasma. Potts *et al.* reported film growth for the Ti(O^{i}Pr)$_3$(CpMe) precursor in the temperature range of 100-300 °C with a rather constant GPC values around 0.55 Å/cycle, while the use of the Ti(O^{i}Pr)$_3$(CpMe$_5$) precursor yielded a GPC of around 0.5 Å/cycle. Film densities were high, comparable to the ideal anatase density of 3.9 g/cm^3 even at the deposition temperatures as low as 100 °C; for the Ti(O^{i}Pr)$_3$(CpMe$_5$)/O$_2$ plasma process even at 50 °C the density was around 3.6 g/cm^3. No carbon was detected in the films as measured with RBS for neither of the processes, while elastic recoil detection (ERD) showed 2-3 % of hydrogen to be present in the films. The Cp-containing precursors are not decently reactive towards water, so use of ozone or plasma is necessary. Note that here the O_2-plasma based route seems to give higher GPC values [775] in comparison to the O_3-based route discussed below.

Ti(OMe)$_3$(CpMe) and Ti(OMe)$_3$(CpMe$_5$) with O$_3$. The Ti(OMe)$_3$(CpMe)/O$_3$ process shows a GPC of around 0.25 Å/cycle between 200 and 325 °C, with a marked precursor decomposition seen at 350 °C. The Ti(OMe)$_3$(CpMe$_5$)/O$_3$ process enabled film growth with a GPC slightly below 0.3 Å/cycle between 200 and 400 °C with a significant decomposition seen only above 450 °C [767]. On the other hand Rose *et al.* saw precursor decomposition already at 350 °C [778]. The GPC values were around 0.25 Å/cycle. QMS studies indicated that one OMe ligand is released during the chemisorption of the metal precursor, while the Cp ligand and the rest of the OMe ligands are removed during the O_3 pulse. XPS showed only surface carbon and TOF-SIMS only moderate carbon levels, decreasing with increasing deposition temperature. The films deposited at 280 °C on TiN had anatase structure and the films deposited on Ru had a mixed amorphous and rutile structure. The drawback in using non-symmetric molecules is that they may have lower sticking coefficients [779]. Computational aspects of the Ti(OMe)$_3$(CpMe$_5$)/O$_3$ are discussed in [781,803].

Ti(NMe$_2$)$_3$Cp and Ti(NMe$_2$)$_3$(CpMe$_5$) with O$_3$. The Ti(NMe$_2$)$_3$Cp/O$_3$ process shows GPC of around 0.4 Å/cycle between 175 and 275 °C, and at 350 °C the precursor decomposition becomes marked. For the Ti(NMe$_2$)$_3$(CpMe$_5$)/O$_3$ process GPC is slightly below 0.23 Å/cycle between 150

and 350 °C, so that at 350 °C the precursor decomposition becomes marked [767]. These data by Katamreddy *et al.* indicate the substitution of the Cp ring to have a stabilizing role on the Cp-based precursors [767]. This could be due to the methyl groups serving as electron donors to the Cp ring hence strengthening the Cp-Ti bond [7].

Ti(NMe$_2$)$_3$(CpMe) and Ti(NMe$_2$)$_3$(CpN) with O$_2$ plasma. Profijt *et al.* studied the role of substrate biasing in Ti(NMe$_2$)$_3$(CpMe)-based route between 100 and 300 °C. GPC values around 0.9 Å/cycle were obtained, with a slight increase with increased biasing. Notably, without epitaxial stabilization, formation of the rutile structure was observed at temperatures as low as 200 °C for films deposited on Si substrates, by applying substrate biasing. Together with the formation of the rutile structure, more impurities such as –OH groups were incorporated in the films, so that the films became slightly over-stoichiometric with increased biasing [786]. This process was also used to fabricate compact layers for flexible perovskite solar cells [787]. For the Ti(NMe$_2$)$_3$(CpN)-based route nearly constant GPC of 0.4 Å/cycle was reported between 200 and 400 °C. Between 100 and 200 °C the GPC values drop with decreasing temperature [785]. The films deposited (on oxygen plasma treated Ru substrates) at 200 °C were amorphous, while the films deposited at 400 °C possessed the rutile structure. [785]

Ti(CHT)Cp with O$_3$. Ti(CHT)Cp is different from the common Ti precursors in that instead of having four ligands it has only two, such that the metal center is surrounded by one η^5-coordinated cyclopentadienyl ligand and one η^7-coordinated cycloheptatrienyl ligand; the oxidation state of Ti has been debated but IV+ is considered the most likely one [791]. The ALD process with ozone shows GPC values around 0.35 Å/cycle at 300 °C with an increasing trend with increasing temperature in the range of 250-450 °C; precursor decomposition manifests itself at 400 °C, but it likely starts at around 350 °C. For films grown at 300 °C the carbon content is below 1 at%. The films deposited at 300 °C and below are predominately of the anatase structure, while at 325 and above the rutile structure starts to dominate. The Cp precursor does not react with water and requires ozone as the reactant [791].

Ti(O^{i}Pr)$_3$(N^{i}Pr-Me-amd) with H$_2$O or O$_3$. The Ti(O^{i}Pr)$_3$(N^{i}Pr-Me-amd)-based process using water as the reactant shows constant GPC around 0.5 Å/cycle between 300 and 350 °C with self-limiting growth demonstrated at 325 °C [776]. Carbon and nitrogen levels are below 1 at% within the temperature range of 275-375 °C. In the thermal decomposition regime above 375 °C the carbon levels jump up to 10-20 at%. The films had anatase structure within the entire temperature range studied. When ozone was used as the reactant the GPC was around 0.3 Å/cycle between 275-325 °C, being slightly lower than for the water-based process. However, similarly to the water process decomposition of the precursor was seen above 350 °C [777]. The films had anatase structure at 275 °C and above, and the carbon impurities were reported to be below the detection limit. Film purity was good and the films were stoichiometric regardless of the decomposition at 375 °C [777]. Ti(O^{i}Pr)$_3$(N^{i}Pr-Me-amd) has the benefit of being liquid, hence avoiding particle incorporation into the films [776].

Ti(NMe$_2$)$_2$(O^{i}Pr)$_2$ with H$_2$O or O$_3$. The homoleptic alkoxide and alkylamide counterparts of Ti(NMe$_2$)$_2$(O^{i}Pr)$_2$ start to decompose around 250 °C, however the heteroleptic Ti(NMe$_2$)$_2$(O^{i}Pr)$_2$ shows an improvement in stability up to 325 °C [776,777]. The films deposited with water as the

reactant exhibited an increasing trend for the GPC value with increasing deposition temperature in the temperature range of 250-375 °C with a high value around 0.8 Å/cycle at 325 °C. Carbon and nitrogen levels were below 1 at.%. In the thermal decomposition regime above 375 °C the carbon levels were high 10-20 at.%. The films had anatase structure within the temperature range studied [776]. The films deposited with ozone as the reactant showed very similar characteristics to the films deposited *via* the water-based process, including self-saturate surface reactions and high GPC of 0.9 Å/cycle at 325 °C; moreover, the *in-situ* studies indicated that combustion reactions are taking place during both metal precursor and ozone pulses [777].

Ti(NMe$_2$)$_3$(guan-NMe$_2$) with H$_2$O or O$_2$ plasma. For this process film growth shows a region of rather constant GPC around 0.45 Å/cycle between 200 and 300 °C and strong increase below and above this temperature range up to values around 0.7 Å/cycle [788]. Regardless of this increase the GPC does not show a marked dependence on the precursor pulse length at 330 °C. Impurities were below 1 at.% for N and below 3 at.% for C below 300 °C, while above 300 °C a slight increase was observed. The anatase structure dominated in the films for deposited temperatures at around 250 °C, while small inclusions of the brookite phase were seen at 300 °C. Above 300 °C notable rutile inclusions appeared. Moreover, the authors noted that that shorter process time favors the growth of smaller crystallites and smoother films. The phase composition seemed to depend on the process time such that shorter times favored the growth of rutile phase [788]. O_2 plasma-based films demonstrated by Dang *et al.* were amorphous in the temperature range 100-225 °C and contained 10 at.% of carbon [789].

Ti(NEtMe)$_3$(guan-NEtMe) with H$_2$O and O$_3$. This ALD route exhibits rather constant GPC around 0.3-0.4 Å/cycle between 200 and 325 °C, independent on the oxygen source used [790]. For the water (for ozone not reported) process the GPC at 350 °C drops slightly, which hints absence of decomposition at such a high temperature. The stability is notably enhanced in comparison to the Ti(NEtMe)$_4$ precursor [767], perhaps due to chelate effect of the guanidinate ligand [790]. The ozone-based process yields very pure films with 1.3 at.% for carbon, 0.3 at.% for nitrogen and 0.5 at.% for hydrogen, whereas the water-based process incorporates more impurities into the films, such that the levels are 4.7 at.% for carbon, 1.6 at.% for nitrogen and 0.5 at.% for hydrogen. The impurity levels are reflected to the crystallization temperature of the films such that for the ozone-based process anatase-structured films are obtained at 275 °C (amorphous below), while for the water-based process the films grow with the anatase structure at 300 °C (amorphous below) [790].

3. Structural characteristics

Crystal structure and morphology are crucial properties for various potential applications of ALD-fabricated TiO_2 thin films. Both the dielectric and the electrical transport properties depend on the crystal structure of the material: rutile exhibits a high dielectric constant, while anatase possesses a high electron mobility for applications where high conductivity is needed. Texture of the films is of importance, as the tetragonal crystal structure may yield anisotropic physical properties. Moreover, grain boundaries may provide current leakage pathways in dielectric applications and reduce the carrier mobility in conducting applications; control of film morphology is vital for surface-area-sensitive applications such as catalysis.

3.1 Crystal structure

Atomic layer deposited TiO_2 thin films can be grown either as amorphous or in several different crystalline forms; crystal structures reported for the films are anatase, rutile, brookite, TiO_2-II phase and suboxide phases. With properly chosen deposition conditions some of these polymorphs can be obtained as a phase-pure material but often two or more crystal structures coexist and form a mixed-phase material. The key factors that determine the crystal structure of the as-deposited thin film are the deposition temperature, the choice of the ALD process and the substrate material, and the film thickness. Post-deposition annealing treatments can be employed to obtain the targeted crystal structure. In general, amorphous films are obtained at low deposition temperatures, films with anatase structure at intermediate temperatures and mixed-phase anatase-rutile or pure rutile TiO_2 films at high temperatures.

For the $TiCl_4/H_2O$ process anatase crystals start forming (often within an amorphous TiO_2 matrix) already at 125-165 °C or above [19,42,88,91,100,117]. The rutile structure begins to form at around 350 °C [19], or above [74]. For the films deposited *via* the $TiCl_4/H_2O_2$ route no formation of rutile was seen up to 440 °C [335]. Lower crystallization temperatures are apparently realized when using O_2 plasma as the oxygen source, as anatase was observed by XRD at 135 °C and already at 110 °C by FTIR [344,345]. Onset temperatures comparable to those of the $TiCl_4/H_2O$ process for anatase and rutile formation have also been reported for the TiI_4/O_2 [356] and the TiI_4/H_2O [348] processes, while for the TiI_4/H_2O_2 process rutile started to form already at around 300 °C [352-354]. Note that for the TiI_4-based processes the self-limited nature of the film growth may be compromised at the temperatures were rutile forms. For the TiF_4/H_2O process the rutile structure was observed starting from 400 °C on soda-lime glass, whereas on borosilicate glass the anatase structure still predominated at 500 °C [357]. Interestingly, after very careful process optimization the $TiCl_4/H_2O$ route can enable fabrication of the TiO_2-II phase (α-PbO_2-type high-density TiO_2 polymorph) on Si(111) substrates in the temperature range of 375-450 °C [21,22,25]. Growth of Ti_9O_{17} suboxide films was achieved *via* the TiI_4/H_2O_2 route on glass substrates in a narrow temperature range of 300-325 °C; this structure was unstable upon storage though. Furthermore, some Ti_3O_5 inclusions were observed in the films fabricated *via* the TiI_4/H_2O route [352].

For the alkoxide-based processes the onset temperatures for the anatase formation appear to be slightly higher than for the halide-based processes. For the $Ti(O^iPr)_4/H_2O$ process the first signs of

the anatase formation are seen at 180 °C [360]; or above, and in the temperature range 200-325 °C films have the anatase or amorphous-anatase structure [359,368,373,391,547]. Similar to the water-based process the $Ti(O^iPr)_4/O_3$ route yields anatase-structured films at 250 °C on a silicon substrate [547]. On an Ru substrate O_3 oxidizes the substrate surface to rutile-structured RuO_2 which seeds the growth of rutile TiO_2 [547,548]. If the Ru seed layer is grown on TiN, anatase content is minimized [555]. Note that the use of RuO_2 substrates directly yields similar results [391,555]. Similar to ozone, both O_2 plasma or N_2O plasma serve as powerful oxidizers on Ru surfaces in a way that the N_2O plasma yields slightly purer rutile films with higher GPC values [576]. On silicon, also the O_2 plasma yields anatase films at 250 °C [568]. If an Ru surface is pretreated with O_3, films in which the rutile structure dominates can be also grown *via* the $Ti(O^iPr)_4/H_2O$ process [371]. Similarly, rutile films can be obtained on oxidized Ir surfaces *via* the O_2 plasma-based process at 250 °C [397]. It is worth noting that Rai *et al.* reported mixed anatase-rutile films at temperatures as low as 150 °C *via* the $Ti(O^iPr)_4/O_2$ plasma process on HF-cleaned silicon [574]. For the $Ti(OEt)_4/H_2O$ process anatase formation begins at around 180 °C or above [54,63,91,609,611]. Use of H_2O_2 as the oxygen source instead of H_2O has been reported to suppress crystallization slightly, presumably due to increased level of impurities [63]. For the $Ti(OMe)_4/H_2O$ process, anatase formation has been reported to begin at 225 °C, as evidenced with XRD [618,625]. In general, for the alkoxide-based processes the film crystallinity might be suppressed at temperatures where the self-decomposition of the precursor starts to take place, as more and more impurities are incorporated in the films [607,618]. Moreover, for alkoxide-based processes it may also be difficult to obtain the rutile structure in the decomposition-free temperature regime without epitaxial seeding of the film growth.

For alkylamide-based processes the poor thermal stability of the precursors limits the decomposition-free film growth to temperatures below 200-260 °C [635,636]. Hence, in most of the cases obtaining crystalline as-deposited films becomes difficult, or the processes may not be decomposition free in the temperature region where crystalline films are obtained. For the $Ti(NMe_2)_4/H_2O$, $Ti(NMe_2)_4/H_2O$ plasma and $Ti(NMe_2)_4/O_2$ plasma processes growth of amorphous films has been reported to take place below 250 °C [384,634,636,746,747,749]. The anatase phase has been seen to appear at 250 °C, while at 300 °C rutile inclusions have been potentially observed [635,746,749]. The poor crystallization tendency is not necessarily related to incomplete surface reactions and consequent high carbon and/or nitrogen content, as the films are reported to be of high purity [384,634,636]. Regarding the O_2 plasma-based process, formation of the rutile structure was seen for films deposited on stainless steel substrates at 400 °C, while on silicon substrates mixed-phase anatase-rutile structure formed at 300 °C and above [746,747,749]. Xie *et al.* compared H_2O, H_2O plasma and O_2 plasma as the oxygen source for $Ti(NMe_2)_4$; the highest level of carbon impurities was found for the $Ti(NMe_2)_4/O_2$ plasma process, which correlated with the poor crystallization tendency upon annealing [384]. The report regarding film crystallization when using H_2O_2 as the oxygen source makes a noteworthy exception, as the formation of anatase structure was reported to onset already at 150 °C [729].

For the processes based on heteroleptic precursors crystalline anatase films can typically be deposited in the decomposition-free regime, as the self-decomposition temperatures are shifted

towards the higher temperatures in comparison to the homoleptic alkoxides and alkylamides. For the $Ti(NMe_2)_2(O^iPr)_2$ precursor TiO_2 films crystallize with the anatase structure starting from 250 °C be the oxygen source H_2O or O_3 [776,777]. For $Ti(O^iPr)_2(thd)_2$ as the Ti precursor, the anatase structure was found to form in the temperature range of 340-470 °C when H_2O was used as the oxygen source [769,772,773], while using ozone as the oxygen source rutile structure forms on Ru substrate at 370 °C [773], in a similar way that has been reported for the $Ti(O^iPr)_4/O_3$ process and discussed above [547]. Regarding the cyclopentadienyl-based processes anatase formation has been reported at 280 °C for the $Ti(OMe)_3(CpMe_5)/O_3$ [778] and at 250 °C for the $Ti(Cp)(CHT)/O_3$ process [791]; for $Ti(OMe)_3(CpMe_5)$ amorphous-rutile films grow on Ru at 280 °C [778]. Notably, for the $Ti(NMe_2)_3(CpMe)/O_2$ plasma process formation of the rutile structure was observed at temperatures as low as 200 °C for films deposited on Si substrates, by applying substrate biasing [786]. For the $Ti(Cp)(CHT)/O_3$ process, the rutile content progressively increases starting from 300 °C being higher than the anatase content above 325 °C [791]. For amidinate-based processes the crystallization onset is similar such that the films fabricated using $Ti(O^iPr)_3(N^iPr\text{-}Me\text{-}amd)$ and H_2O reactants crystallize in the anatase phase at 250-375 °C [776], while use of O_3 as the oxygen source increases the onset of the crystallization slightly to 275 °C [777]. For guanidinate precursors the film crystallization takes place at slightly higher temperatures, at 275 °C for the O_3-based process and at 300 °C for the H_2O-based process, when $Ti(NEtMe)_3$(guan-NEtMe) is used as the Ti precursor [790]. However, for the $Ti(NMe_2)_3$(guan-NEtMe) precursor the anatase formation was seen already at 250 °C, brookite inclusions seen in the temperature range of 300-315 °C and disappearing at 330 °C; rutile formation was seen to onset at 315 °C for films grown on Si [788]. The $Ti(O^iPr)_3(N^iPr\text{-}Me\text{-}amd)$ precursor yields anatase structure at 275 °C and above with H_2O or O_3 as co-reactants. For the $Ti(O^iPr)_2(dmae)_2/H_2O$ process the high level of impurities indicated incomplete hydrolysis of the metal precursor below 300 °C, so that anatase-structured films were obtained only at 400 °C [768]. For the $Ti(O^iPr)_2(thd)_2/H_2O$ and $Ti(O^tAm)_2(trhd)_2/H_2O$ processes all the films exhibited anatase structure above 300 °C [772].

Role of film thickness. In the vicinity of the film surface and the film-substrate interface the crystal structure of the film may differ from that in the bulk of the film. For example, Aarik *et al.* observed that phase-pure TiO_2-II films can only be obtained below a critical thickness above which an increasing amount of the rutile phase forms [25]. Depending on the surface conditions of the substrate the ALD growth of TiO_2 may begin as amorphous or crystalline, even at temperatures where crystalline films eventually form. Removal of the native oxide layer from the surface of a silicon substrate can promote immediate crystallization *via* island-type growth mode, whereas on native-oxide-covered silicon surfaces the film growth begins with an amorphous layer and the crystallization only starts within the amorphous matrix after the film thickness exceeds the critical thickness [44]. Aarik *et al.* reported such critical thicknesses to be 10 nm at 210 °C and 2 nm at 300 °C for films grown on soda lime, fused silica or Si(111) substrates [19]. The thickness of the initial amorphous layer thus decreases with increasing deposition temperature.

Post-deposition treatments. In many cases a post-deposition annealing can be used to obtain the desired crystal structure, if it has not be reached during the film deposition. The phase-transition temperatures upon the post-deposition annealing treatments tend to be higher than those revealed

for as-deposited thin films from experiments with different deposition temperatures. Moreover, the structure of the as-deposited films may affect the transition temperature during the annealing. For example, for films obtained *via* the $TiCl_4/H_2O$ process, annealing of an amorphous as-deposited (chlorine-rich) film in air/O_2 results in the anatase structure at 400 °C, and the structure remains as anatase at least up to 900 °C. On the other hand, if the as-deposited matrix is anatase, the rutile structure is obtained already at 750 °C [74,91]. An interesting exception is the amorphous-anatase transition seen upon a ten-hour hydrothermal treatment at 120 °C; this treatment however results in coarse-grained films rich in voids at crystal perimeters and at the film-substrate interface [83].

Epitaxial films. Epitaxial seeding of the film growth can provide further control over the desired crystal structure of TiO_2 films. Rutile structure is favored over the anatase structure and amorphous films for high-*k* applications; however, for lattice-mismatched substrates thermal energy needed for the formation of the rutile structure is high. In this respect, epitaxial seeding can provide means for lowering the processing temperature and control over the film orientation (table 2). Epitaxial rutile $TiO_2(101)$ films have been deposited on α-$Al_2O_3(1\bar{1}02)$ [43], *α*-$Al_2O_3(012)$ [348,354,356] and $RuO_2(101)$ [94] surfaces. The rutile $TiO_2(100)$ growth can be seeded by *α*-$Al_2O_3(001)$ [123,354] and Ru surfaces; in the latter case high-reactivity oxygen source such as ozone is required to in-situ oxidize the Ru surface to RuO_2, which stabilizes the growth of rutile TiO_2 [547]. Note that according to Lee *et al.* anatase-structured TiO_2 is formed on an RuO_2 substrate from the $Ti(O^iPr)_2(thd)_2$ precursor when H_2O is used as the reactant [773]. Most likely the RuO_2 substrate surface is reduced to Ru by the first precursor pulse; ozone could reverse this such that RuO_2 is reformed, while the oxidation power of water is not enough for the oxidation [773]. Moreover, $SnO_2(110)$ and $SnO_2(001)$ surfaces can be used as substrates for film growth along 110 and 001 directions of TiO_2 rutile structure, respectively [543]. It is worth noting that, in Refs. [547] and [543] the rutile structure was obtained at temperatures as low as 250 °C, which is a marked improvement in comparison to the case of lattice-mismatched substrates. At high temperatures the TiO_2 II structure (mixed with the anatase/rutile structures) can form on sapphire surfaces with certain orientations [206,343]. Considering TCO applications for the anatase phase, it stems from the anisotropy of the crystal structure that the electron mobility in the (*a*,*b*) plane is notably higher than along the *c*-axis direction; hence growth of *c*-axis oriented films is favorable if electrons are to be transported in the in-plane direction. In this respect, Luka *et al.* recently demonstrated the growth of both anatase $TiO_2(001)$ and anatase Nb:$TiO_2(001)$ films on $LaAlO_3(100)$ substrates at 220 °C [323]. Similar to $LaAlO_3(100)$ surfaces, also $SrTiO_3(100)$ surfaces can seed the growth of *c*-axis oriented anatase-structured TiO_2 [308,441,448]. Furthermore, MgO(001) surfaces have been reported to seed the growth of *a*-axis oriented anatase films [58,335,356].

Table 2. Epitaxially seeded ALD growth of TiO_2 thin films.

Substrate	TiO_2 structure (orientation)	Growth temperature	ALD process	Reference
α-$Al_2O_3(1\bar{1}02)$	Rutile(101)	425-500 °C	$TiCl_4/H_2O$	[43]
α-$Al_2O_3(012)$	Rutile(101)	445 °C	TiI_4/H_2O	[348]
α-$Al_2O_3(012)$	Rutile(101)	275-455 °C	TiI_4/H_2O_2	[354]
α-$Al_2O_3(012)$	Rutile(101)	330-455 °C	TiI_4/O_2	[356]
α-$Al_2O_3(001)$	Rutile(100)	450 °C	$TiCl_4/H_2O$	[123]
α-$Al_2O_3(001)$	Rutile(100)	455 °C	TiI_4/H_2O_2	[354]
α-$Al_2O_3(001)$	TiO_2 II(100)*	425-475 °C	$TiCl_4/H_2O$	[206]
α-$Al_2O_3(001)$	TiO_2 II(100)*	425-500 °C	$TiCl_4/O_3$	[343]
α-$Al_2O_3(100)$	TiO_2 II(001)*	425-475 °C	$TiCl_4/H_2O$	[206]
$RuO_2(101)$	Rutile(101)	425 °C	$TiCl_4/H_2O$	[94]
Ru	Rutile(100)	250 °C	$Ti(O^iPr)_4/O_3$**	[547]
Ir	Rutile	250 °C	$Ti(O^iPr)_4/O_3$**	[558]
$SnO_2(110)$	Rutile(110)	250 °C	$Ti(O^iPr)_4/H_2O_2$	[543]
$SnO_2(001)$	Rutile(001)	250 °C	$Ti(O^iPr)_4/H_2O_2$	[543]
MgO(001)	Anatase(100)	390 °C	$TiCl_4/H_2O_2$	[335]
MgO(001)	Anatase(100)	300 °C	$TiCl_4/H_2O$	[58]
MgO(001)	Anatase(100)	230-375 °C	TiI_4/O_2	[356]
$SrTiO_3(100)$	Anatase(001)	250 °C	$TiCl_4/H_2O$	[308]
$SrTiO_3(100)$***	Anatase(001)	225-250 °C	$Ti(O^iPr)_4/H_2O$	[441,448]
$LaAlO_3(100)$	Anatase(001)	220 °C	$TiCl_4/H_2O$	[323]

*Mixed with anatase and rutile phases.
**Ozone oxidizes Ru to RuO_2 or Ir to IrO_2 during the first TiO_2 ALD cycles.
***Subtrate is Si(001) with few unit cell thick $SrTiO_3(100)$ buffer layer.

3.2 From nucleation to film morphology

Deposition temperature and the conditions on the substrate surface largely determine how the thin-film growth begins and how the initial conditions are reflected to the evolution of the film morphology and grain size with increasing film thickness.

First deposition cycles. The nature and surface density of functional groups on the substrate surface are among the key factors that determine the first steps of the film growth. This was systematically studied for the $TiCl_4/H_2O$ process by comparing the film-growth characteristics on hydroxyl-rich (Radio Corporation of America (RCA)-cleaned) and hydride-ending (HF-cleaned) Si(100) surfaces at 300 °C [45]. On a hydroxyl-rich surface the growth initiates with a homogeneous amorphous layer, while on a predominately hydride-ending surface the growth starts

from the very few spots rich in hydroxyl groups [45]. A plausible explanation is that the abundant hydroxyl groups are hydrogen bonded and form low-mobility bidentate species upon chlorination; then the surface does not arrange itself towards the anatase structure with ease, and the film growth onsets as amorphous. Provided that the temperature is high enough, crystalline anatase grains can then form within/on the amorphous layer regardless of the substrate [30,117]. On the other hand, for a low degree of hydroxyl coverage monodentate high-mobility species form upon chlorination and the deposition onsets *via* formation of small island-type crystalline grains [45]. Island-type growth has also been reported for TiO_2 films grown on phlogopite mica at 500 °C, and also for amorphous films grown on soda-lime glass at 300 °C [17]. Mechanisms proposed for the island formation include migration of surface species [17] and cleaving the surface Si-O-Ti linkages by the first H_2O pulses; in the latter case hydroxychloride species would be produced leading to local restoration of Si-OH-termination of the surface [59]. Note that for the growth proceeding *via* island formation, reaching the full coverage of the substrate may take up to some 100-200 ALD cycles [17,28]. The growth on hydride ending surfaces may also be considered as substrate inhibited [208,263,652]; this could even be used as a means for area-selective deposition such that growth rate is notably higher on –OH terminated areas, while growth is inhibited on –H terminated areas [208,263].

It is good to note that the potential nucleation delay or substrate-enhanced growth might influence the GPC values for very thin films. For example for the $TiCl_4/H_2O$ process the GPC value may be enhanced during approximately first 5 ALD cycle on both hydroxyl-rich native oxide surface and hydrogen-terminated silicon surface, such that higher GPC is seen on hydroxyl-rich surface (at 100 °C) [118]. After the 5 cycles the effect of the substrate-enhanced growth levels off and the GPC becomes constant with increasing number of ALD cycles [118]. For higher number of ALD cycles film growth is typically linear with increasing number of cycles, regardless of the surface treatment of the Si substrate [44,124]. Other examples are substrate-enhanced growth observed for $Ti(O^iPr)_4/N_2O$ plasma and $Ti(O^iPr)_4/O_2$ plasma processes on Ru surfaces [606], and for the $Ti(O^iPr)_4/O_2$ plasma process on TiN [573].

Bulk of the film. When the film growth begins with the formation of amorphous TiO_2, crystalline grains start forming within/on top of the amorphous layer after the film has reached the critical thickness, which can be as much as 1400 cycles [41,117,198,611,614,615]. At low temperatures the nucleation of the crystallites begins from fewer sparsely-spaced sites than at the higher temperatures [117]. Hence, as more and more cycles are applied and the grains expand laterally, the crystalline nuclei are free to grow larger at the low temperatures compared to the situation at the higher temperatures (>300 °C) where the growing grains sooner collide with the neighboring ones [117]. Provided that there is sufficient thermal energy available, at high temperatures thermally activated coalescence of the neighboring grains (Ostwald ripening) may increase the mean grain size (figure 8). Hence, the temperature dependence of the grain growth is governed by the density of the nucleation sites such that the grain size decreases with increasing temperature, and that an upturn at around 250-300 °C can be possibly seen due to Ostwald ripening [117]. This grain size *vs.* temperature trend is in reasonable accordance with the data from several authors for TiO_2 films deposited on various substrates [38,44,75,88,100]. Roughly speaking the

minimum grain size in reasonably-thick (>50 nm) films is somewhere below 100 nm, while at low-enough and at high-enough temperatures grain size is above 100 nm, likely larger at low temperatures. The micron-size grains observed for TiO_2 films grown on Al_2O_3 surface can be mentioned a rare exception [144]. The substrate pre-treatments can also lead to a difference in grain size as reported by Mitchell *et al.*: grain sizes larger than 100 nm were seen for TiO_2 films grown on RCA-treated silicon substrates and smaller than 100 nm for films deposited on HF-treated silicon [44]. It is worth noting that, even though the film growth would begin by formation of an amorphous layer, the subsequent grain growth can progressively consume the initial amorphous regions eventually resulting in throughout-crystalline films [75]. Note also that the transition from amorphous to crystalline film growth after reaching the critical film thickness may influence the GPC values if the growth rates for the amorphous and crystalline phases differ from each others [611].

Film surface. The roughness of the film surface is largely determined by the deposition temperature and the film thickness, *via* the aforementioned mechanisms [17,19,625]. At low temperatures where TiO_2 grows amorphous, films with smooth surfaces are obtained. As the deposition temperature is increased (> 150 ºC) and anatase crystallites start to form within the amorphous TiO_2 matrix, the surface roughness increases in parallel with the grain size [19]. Surface roughness increases also with increasing film thickness, such that *e.g.* at 150 ºC TiO_2 films become notably rougher when the film thickness increases from 2 to 30 nm (1000 to 3000 ALD cycles); however after 3000 cycles the increase in roughness seems to somewhat level off [30]. Moreover, as ascribed to improved grain alignment, epitaxial films can be less rough on the surfaces than the corresponding films on lattice-mismatched substrates [58].

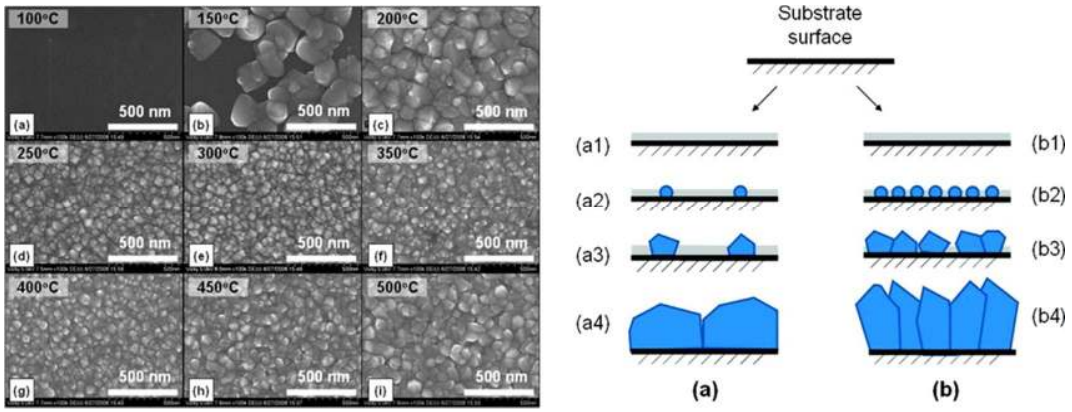

Figure 8. (left) SEM micrographs of TiO_2 films deposited with 1000 ALD cycles at various temperatures. (right) Schematic grain-growth models of ALD TiO_2 films: (a) at low deposition temperatures (150−250 °C) and (b) high deposition temperatures (above 300 °C). Reprinted with permission from Lee W and Hon M 2010 *J Phys Chem C* **114** 6917. Copyright 2010 American Chemical Society [117]

4. Towards applications - doped films

For many applications undoped stoichiometric semiconductor materials fail to provide the required functionalities. Frequently though, the lattice of an intrinsic material is not fully stoichiometric but comes with a notable concentration of cationic or anionic vacancies or self-interstitial ions that largely define the physical properties of the material. To complement or to compensate for the intrinsic properties, and to fully unlock the needed functional properties, doping *via* incorporation of extrinsic cations or anions is often needed. In atomic layer deposition of oxide materials elemental substitutions are realized by replacing single ALD cycles of the parent oxide with single cycles of the oxide of the dopant metal, which in principle leads to layer-wise localization of the dopant atoms. However, the dopant atoms may diffuse during the deposition or post-deposition treatments to substitutional sites in the host lattice, to a larger or to a lesser extent.

For ALD-fabricated TiO_2 thin films typical extrinsic cation dopants are Al and Nb, while anion-site doping is mainly attempted with N (table 3). The literature discussing Al doping is in particular motivated by the implementation of the rutile-structured TiO_2 films for high-*k* applications, while Nb doping of anatase-structured films is mainly investigated transparent-conducting-oxide (TCO) applications in mind. The anion-site doping with N decreases the band-gap of TiO_2, hence sensitizing the material to visible light; this is highly relevant for photocatalytic applications. Moreover, Ta [406,626], Co [630] and Zn [292] cation substitutions have been reported, the first case showing TCO properties close to those of Nb-doped films, and the second case being related to interesting magnetic properties. Furthermore, H_2S-modified TiO_2 films have shown promising photocatalytic performance [81]. In this chapter we cover the literature regarding doping of ALD-fabricated TiO_2 thin films discussing the deposition chemistry in relation to the targeted functional properties.

Table 3. Doping of TiO_2 thin films in ALD.

ALD process	Subst.	Temp. (°C)	Crystal structure	Doping ratio[1]			Ref.
Al doping					**EOT (nm)**	**Leakage current at 0.8 V (A/cm²)**	
$Ti(O^iPr)_4/AlMe_3/O_3$	Ru	250 (400)	rutile[2]	1/60 – 1/120	0.48 (1/60)	0.8×10^{-7} (1/60)	[551, 552, 554]
$Ti(O^iPr)_4/AlMe_3/O_2$ plasma	Ru	250 (400)	rutile/anatase	1/30 – 1/90	0.5 (1/60)	0.5×10^{-7} (1/60)	[576]
$Ti(O^iPr)_4/AlMe_3/N_2O$ plasma	Ru	250 (400)	rutile	1/30 – 1/90	0.6 (1/90)	0.2×10^{-7} (1/90)	[576]
$Ti(O^iPr)_4/AlMe_3/H_2O$	RuO_2	225	rutile[2]	1/60 – 1/120	2.9 (1/60)	0.3×10^{-7} (1/60)	[402]
$TiCl_4/AlCl_3/H_2O$	RuO_2	400 (300)	rutile	1/10 – 1/100	0.9	1×10^{-5}	[130]
$Ti(O^iPr)_4/AlMe_3/O_3$	Ir	250 (400)	rutile	1/60	0.50, 0.53	1×10^{-7}, 0.5×10^{-8}	[558]
$Ti(O^iPr)_4/AlMe_3/H_2O$	Ge	250 (500)	amorphous	1/5 – 1/20	1.6 (1/10)	1×10^{-5} (1/10)	[418]

$Ti(NMe_2)_4/AlMe_3/H_2O$	Si	150 (600)	amorphous	1/20 – 1/50	7.7 (1/20)	1×10^{-7} (1/20)	[650]
$Ti(O^iPr)_4/AlMe_3/O_3$	RuO_2	250 (400)	rutile[2]	1/60	0.44, 0.50	3×10^{-7}, 0.7×10^{-8}	[127]
$Ti(O^iPr)_4/AlMe_3/O_2$ plasma	RuO_2	250 (400)	rutile[2]	-	0.46	1×10^{-8}	[556]
$TiCl_4/AlMe_3/H_2O$	RuO_2[3]	400 (300)	rutile	1/60	0.39, 0.46	3×10^{-7}, 2×10^{-8}	[186]
$Ti(O^iPr)_4$, $Ti(O^tBu)_4$, $Ti(NMe_2)_4$, $Ti(OEt)_4/AlMe_3/H_2O$	TiN, TaN, W	150-240 (up to 600)	amorphous/ anatase	1/15 – 1/40	12 (on TaN)	5×10^{-7} (at 2 V)	[561]
$TiCl_4/AlMe_3/H_2O,O_3$	RuO_2[4]	400 (300)	rutile	1/60	0.5	0.46×10^{-7}	[189]
$TiCl_4/AlCl_3/O_3$ $TiCl_4/AlMe_3/H_2O$	RuO_2[4], Si	350 (300)	rutile, anatase	1/2 – 1/126	0.57 (on RuO_2) 0.51 (on RuO_2)	0.7×10^{-7} 0.5×10^{-7}	[265]
$Ti(O^iPr)_4/AlMe_3/O_3$	RuO_2	250 (400)	rutile	1/100, 3/100	0.37 (1/100)	0.5×10^{-7} (1/100)	[564]
$Ti(NMe_2)_4/AlMe_3/O_2$ plasma	RuO_2, Pt	250 (400)	rutile, anatase	1/30 – 1/120	0.8 (1/60)	2×10^{-7} (1/60)	[757]
$Ti(O^iPr)_4/AlMe_3/O_3$	RuO_2	250 (400)	rutile[2]	1/250			[565]
Nb doping					ρ (mΩcm)		
$Ti(OMe)_4/Nb(OEt)_5/H_2O$	SiO_2	215 (600)	anatase[5]	1/20-1/2	1.9		[626]
$Ti(Cl)_4/Nb(OEt)_5/H_2O$	glass	210 (500-600)	anatase[5]	1/20-1/2	1.4		[240, 311]
$Ti(Cl)_4/Nb(OEt)_5/H_2O$	glass	100-280 (600)	anatase[5]	1/20	1.5		[315]
$Ti(Cl)_4$/TBTDEN/H_2O	LAO[6] (100)	220	anatase	1/25	3.1		[323]
$Ti(Cl)_4$/TBTDEN/H_2O	Al_2O_3 (0001)	220	rutile	1/25	39		[323]
N doping					***Photoactivity measurement***		
$TiCl_4/H_2O/NH_3$	glass	500	anatase, rutile	1/6-3/4	Stearic acid degradation, contact angle		[65]
$TiCl_4/(NH_3$-H_2O mixture)	Si	400	anatase, rutile	-	Photocurrent		[128]
$Ti(NMe_2)_4/H_2O/N_2$ plasma	Si	150 (>500)	amorphous(anatase,rutile)	1/3-1/10	Stearic acid degradation		[689]
$TiCl_4/H_2O/N_2$ plasma	Si	300	-	-	Methylene blue degradation, contact angle		[242]
$TiCl_4/H_2O/(N_2$-H_2 plasma)	Si,Ti, nanotubes	250,350	-	-	Photocurrent		[804]
Other dopants					***Research/application interest***		
$Ti(NEt_2)_4/Hf(NEt_2)_4/H_2O$	Si	175-250	amorphous	1/6-1/2	-		[762]
$Ti(OMe)_4/Ta(OEt)_5/H_2O$	SiO_2	215 (600)	(anatase)	1/20-1/2	Transparent conductor		[626]
$Ti(O^iPr)_4$/TATTDMTa[7]/H_2O	[8]	220	anatase	1/16-1/7	Dye-sensitized solar-cell electrode		[406]
$Ti(OMe)_4/Co(acac)_3/H_2O$ $Ti(OMe)_4/Co(acac)_3/O_3$	Si, glass	300 (650)	(anatase-rutile)[9]	1/101-1/2	Magnetic properties		[630]

$Ti(O^iPr)_4/Mn(DPM)_3/H_2O$	Si	200-400 (550)	amorphous/ anatase	-	Magnetic properties	[410, 494]
$TiCl_4/ZnEt_2/H_2O$	Si,PC[10]	100 (300-600)	(anatase)	1/200-1/25	Nanotubes	[292]

Temperatures listed represent the deposition temperature (and the annealing temperature in the brackets). Annealing atmospheres are N_2/O_2 (95%/5%) [551,552,554,556,558,565], O_2 [127,130,186,189,265], N_2 [418], O_2 plasma [757].
[1] Doping ratio is defined as (Al cycles)/(Al cycles + Ti cycles).
[2] Rutile structure deduced from the high *k*-value, too high for anatase.
[3,4]Ar/O_2 plasma pretreatment. [3]Epitaxial *c*-axis oriented rutile films $TiO_2(001) \mid RuO_2(001)$.
[5]After annealing at 500-600 °C in hydrogen containing atmosphere.
[6]LAO stands for $LaAlO_3$.
[7] TATDMTa stands for tertiaryamylimidotris(dimethylamido)tantalum.
[8] Fluorine-doped tin oxide glass and/or 3D colloidal crystals of monodisperse silica spheres.
[9] With $CoTiO_3$ or $CoTi_2O_5$ impurity phases.
[10] PC stands for Polycarbonate.

4.1. Al doping

The massive part of the work done on the Al substitutions has found the motivation from application of Al-doped ALD-TiO_2 thin films as the dielectric layers in metal-insulator-metal (MIMs) capacitors for dynamic-random-access memories (DRAMs). As the dielectric constant of rutile-structured TiO_2 is around 170 along the *c* axis and around 90 along the *a* axis (notably larger than the values around 40 for anatase), it is the rutile structure that is of the interest for the dielectric applications [556]. However, leakage current through the TiO_2 layers tends to be unacceptably high, which is the main bottleneck for the use of undoped TiO_2 as a dielectric material [551]. Remarkably, Kim *et al.* showed a decrease in leakage current values of multiple orders of magnitude by doping Al in the rutile TiO_2 matrix [551]; this was the discovery that largely inspired the later research on the topic.

Deposition characteristics. As $AlMe_3$ is by far the most common metal precursor for the ALD growth of Al_2O_3, it is not surprising that $AlMe_3$ has typically been used to realize the Al doping of ALD-TiO_2 films (see table 3). Besides $AlMe_3$, $AlCl_3$ has been studied as a hydrogen-free alternative [130,265]. The choice of the oxygen source is important particularly when TiO_2 is grown directly on a metal surface. For example in the case of Ru substrates, use of water leads to the formation of anatase/amorphous TiO_2, while the higher oxidation powers of O_3, O_2 plasma and N_2O plasma enable the *in-situ* formation of interfacial RuO_2 that promotes the growth of rutile-structured TiO_2 at notably low temperatures around 250 °C, owing to the lattice-matching structures of the two compounds [551,552,554,576]. However, when RuO_2 is used as the growth surface, also the H_2O-based process can provide rutile-structured TiO_2 films *via* local epitaxy [130,186,189,402]. Furthermore, comparing the different oxygen sources in terms of the growth characteristics, Choi *et al.* noticed that N_2O plasma provided notably higher GPC values than O_3 and O_2 plasma, without significantly compromising the electrical properties [576].

It is often seen that the film-growth characteristics for the doped ALD films deviate to some extent from those for the constituent binary oxides, which is typically reflected to the GPC values. For example, Kim *et al.* found that for the $Ti(O^iPr)_4/AlMe_3/O_3$ process the GPC values for Al-doped TiO_2 films are lower compared to the value for undoped TiO_2: for the doping ratios 1/120, 1/90, and 1/60 the values were 0.28, 0.27, and 0.26 Å/cycle, respectively, while for the undoped film GPC was 0.33 Å/cycle [552]. This was ascribed to retarded adsorption of the $Ti(O^iPr)_4$ precursor molecules on the film surface right after the dopant $AlMe_3/O_3$ cycle, as in contrast, the adsorption of $AlMe_3$ is reported to be higher on the Ti-O surface than on the Al-O surface [552]. The measured atomic content Al/(Al+Ti) can be notably higher (6, 8, and 12 at.%) than expected from the ALD-cycle ratio $((AlMe_3/O_3)/(Ti(O^iPr)_4/O_3 + AlMe_3/O_3)$ = 1/120, 1/90, and 1/60) [551], which is in line with the enhanced adsorption of $AlMe_3$ on the TiO_2 surface. Note that, the Al content can be fine-tuned by omitting the O_3 pulse preceding the $AlMe_3$ exposure which leads to a slightly lower Al/(Al+Ti) ratio [554]. Note also that for the $TiCl_4/AlMe_3/H_2O$ process the Al precursor adsorption has been reported to be hindered such that the ALD doping cycle ratio of 1/60 leads to Al content of Al/(Al+Ti) = 0.5 at.% only [186]. For the $Ti(O^iPr)_4/AlMe_3/O_3$ process, film growth proposedly shows the lowest rate right after the $AlMe_3/O_3$ cycle and then recovers to a constant value before the next $AlMe_3/O_3$ cycle. However this constant GPC value is still lower than for the undoped TiO_2, as some Al diffuses to the film surface when the deposition proceeds, thus hindering the chemisorption of the precursor for the $Ti(O^iPr)_4/O_3$ cycles [552].

Contrary to *e.g.* Al doping of ALD-ZnO thin films where the absence of significant Al diffusion can result in layer-wise localization of the Al-dopant atoms [805], Al doping of TiO_2 is reported to lead to more homogenous cross-plane distribution of the dopant atoms [551]. It has been proposed that the diffusion pathway for the Al ions is likely provided by Ti vacancies present in over-stoichiometric films (with O:Ti = 2.2 in this case) [552]. Moreover, first-principle calculations have indicated that Al atoms find energetically favourable positions on the surface of rutile TiO_2, such that there is a driving force for Al atoms towards the film surface during the growth [552]. These conclusions by Kim *et al.* [551,552,554] are supported for example by the results of Hudec *et al.* who detected Al on the film surface for a 20-nm thick film doped only in its bottom 2.5-nm part; the through-thickness Al concentration was far from constant though [130]. Apart from the higher-than-average Al content on the top surface, the depth profile of the Al concentration may also exhibit a peak at the film-substrate interface [130]. Furthermore, from XPS investigation it has been shown that Al ions form in rutile-structured films a chemically uniform Al–Ti–O film without any phase separation [551]; also, for anatase films peak shifts in Raman data have indicated that Al^{3+} substitutes for Ti^{4+} in the anatase lattice [650].

Dielectric properties. The capability of a dielectric material to store charge can be described by the so-called equivalent-oxide-thickness value: EOT = $d\times(3.9/k)$, where d is the physical film thickness and k the dielectric constant. To achieve the goal of the international technology road map for semiconductors, the effort has been to reach EOT values below 0.5 nm together with leakage current values below 10^{-7} A/cm^2 at 0.8 V for capacitor dielectrics in DRAMS (memory elements consisting of a capacitor and a transistor). Attempts to achieve the 0.5-nm limit by decreasing the thickness of ordinary-k materials (k around 20-30) lead to excessively high leakage

current values, and hence high-*k* materials are demanded for [186,551]. Rutile-structured TiO_2 with its notably high *k* value in the range of 90-170 is thus among the considerable candidates [130,186,551]. However, due to the relatively small band gap of rutile around 3 eV, and in-gap donor states due to intrinsic oxygen vacancies and titanium interstitials, the energy offset between the Fermi level of the metal electrode and the conduction band bottom of TiO_2 is low [551]. This leads to too high leakage currents through the TiO_2 layers, which is the main bottleneck for the use of undoped TiO_2 in dielectrics applications [551]. When doped in the TiO_2 matrix, Al in the oxidation state 3+ is expected to create acceptor states that should compensate for the intrinsic donor states, and hence lead to the lower leakage currents and better overall dielectric performance [551].

Indeed, trivalent Al has been evidenced to create acceptor states in the TiO_2 band gap such that Fermi level is seen to shift towards the valence band, by 0.2-0.5 eV as revealed from XPS and capacitance-voltage measurements, and by 0.25-0.65 eV *via* first-principle calculations [551]. This shift of Fermi level increases the Schottky barrier between Al:TiO_2 and the capacitor electrode and is thus the likely explanation for the reduction of the leakage current [551]. Considering the Al:TiO_2-RuO_2 interface properties, thicker RuO_2 layers enable higher Schottky barriers than thin RuO_2 layers obtained on Ru *via in-situ* oxidation, as in the latter case the work function of RuO_2 is reduced due to the close presence of the thick Ru bottom layer [556]. Moreover, regarding the Al:TiO_2-RuO_2 interface properties oxygen-plasma pretreatment of the RuO_2 surface has been reported to enhance the barrier height between the metal and the dielectric layer [186,189]. Locating the dopant layers closer to the Al:TiO_2-RuO_2 interface may further enhance the barrier height simultaneously allowing for higher *k* in the bulk of the TiO_2 layer with lower Al concentration [565]. Use of hydrogen-free processes may furthermore lead to lower leakage current values [265].

After Kim *et al.* had demonstrated that Al doping provides a viable means for decreasing the leakage current value for rutile TiO_2 films [551], similar results by various authors followed, as summarized in table 3. It is evident from the table that anatase-structured or amorphous films do not provide the required dielectric performance, achieved only for the rutile-structured films. When rutile-structured films are obtained *via* epitaxial growth, leakage current values below 10^{-7} A/cm^2 with EOT below 0.5 (or very close to it) are generally observed. The dielectric performance observed appears to be rather independent of the ALD process used, such that aside of the original $Ti(O^iPr)_4/AlMe_3/O_3$ route [551,552,554], *e.g.* the $Ti(O^iPr)_4/AlMe_3/H_2O$ [130] and $TiCl_4/AlMe_3/H_2O$ [186,265] routes give similar results once RuO_2 is used as the substrate instead of Ru. It is worth noting that post-metallization annealing treatments for metal-insulator-metal stacks are frequently used to optimize the electrical performance. Typically the annealing atmosphere contains a small amount of oxygen together with nitrogen or oxygen only.

4.2. Nb doping

Niobium in the oxidation state 5+ is highly soluble in the TiO_2 matrix, which allows for turning the rather robust dielectric material into a highly conducting material. Indeed, the resultant high electrical conductivity together with the wide band gap of around 3.2 eV make Nb-doped TiO_2 an interesting candidate for applications where transparent conducting oxides are needed. In comparison to the rutile structure, the lower electron effective mass and thereby the higher mobility make the anatase-TiO_2 structure of interest for TCO applications.

Deposition characteristics. Fabrication of Nb:TiO_2 films has been demonstrated using either $Ti(OMe)_4$ [626] or $TiCl_4$ [240,311,315,323] as the titanium precursor, $Nb(OEt)_5$ [240,311,315,626] or tert-butylimido-tris-diethylamido-niobium (TBTDEN) [323] as the niobium precursor and H_2O as the oxygen source (table 3). The fact that niobium chloride is known to have an etching effect on niobium oxide surfaces [806], might complicate its use as the dopant precursor. The reasonable deposition temperature window for these processes spans roughly from 100 to 300 °C, being limited at the lower end by the reactivity of $TiCl_4$ and at the higher end by the thermal stability of the alkoxide precursors. Regarding the growth characteristics, the GPC of the doped films decreases progressively with increasing doping level, implying that TiO_2 exhibits delayed growth after the dopant $Nb(OEt)_5/H_2O$ cycle, at least for the $TiCl_4$-based process [240]. Even though at temperatures above 150-200 °C undoped TiO_2 tends to start to crystallize in the anatase structure even on lattice-mismatched surfaces, the picture for the doped films is slightly different. Namely, Nb doping suppresses the crystallization of the films (at growth temperatures around 210 °C) in a way that the as-deposited films are amorphous with the exception of the lightly doped (Nb/(Nb+Ti) < 0.10) films for the $TiCl_4$-based process [240,626]. Once the films are crystallized through a post-deposition annealing treatment at around 500-600 °C under reducing conditions, Nb is found to substitute Ti in the anatase lattice, seen as an increased lattice-plane spacing determined by XRD [240,311,626].

It stems from the anisotropy in the transport properties of the anatase structure that the highest in-plane conductivity is obtained for *c*-axis oriented films [807]. Growth of *c*-axis oriented films is possible on single-crystal substrates that provide epitaxial seeding for the film growth. However, often for applications epitaxial growth may not be possible and control over the film orientation without epitaxial seeding is needed. Interestingly, ALD-fabricated Nb:TiO_2 films crystallized *via* annealing of amorphous as-deposited films, may exhibit remarkable degree of *c*-axis orientation and exceptionally large lateral grain size up to around 10-100 µm for films with a thickness below 100 nm [311,315,626]. This has been explained in terms of explosive crystallization [626], in other words, crystallization onsets from few sparsely spaced points in an amorphous film, after which the grain growth propagates rapidly until the growth fronts collide with the neighbouring ones. As the grain growth is extremely fast, there is no time for the crystallization to start from the higher-activation-energy onset points upon temperature increase during annealing. The process results in highly *c*-axis oriented grains spanned by cross-shaped domains of single-crystalline *c*-axis oriented anatase [311,626]. This crystallization behaviour is prominent for heavily Nb-doped TiO_2 (Nb/(Nb+Ti) > 0.15) films. For the low-doping regime (Nb/(Nb+Ti) < 0.10), at least in case of the $TiCl_4$-based process, films with large grain size can be obtained by annealing amorphous as-deposited films grown at lower temperatures around 170 °C; in this case however the grains do not

feature cross-shapes and the preferred *c*-axis orientation is lost [315]. For low level of doping, growth of *c*-axis oriented films is though possible on *e.g.* single crystal $LaAlO_3$(100) substrates [323].

TCO properties. Transparent conducting oxides are materials frequently used in optoelectronic devices as electrodes. A good TCO has as-high-as-possible electronic conductivity and is as transparent as possible. For maximum conductivity ($\sigma = \mu en$) the material should have high free-carrier density (n) and high mobility (μ) (e stands for electron charge). Typically, transparency of TCOs around the visible range is limited by band-gap absorption at the high-energy side of the transparency window and by the free-electron gas absorption at the low-energy side. Both of these absorption processes depend on n such that increasing n shifts the absorption edges towards higher energies. Hence, too high n can severely limit transparency in the Vis-NIR range *via* free-carrier absorption and in terms of carrier density, the high transmittance and the high conductivity are thus contradicting properties – a fact that underlines the importance of high carrier mobility for the best TCO performance. A general criterion for transparent conductors is that they should show a room-temperature resistivity of the order of 10^{-3} Ωcm, or below, and transparency above 80% in the visible range [808].

When Nb:TiO_2 films are grown from $Ti(OEt)_4$ or $TiCl_4$, $Nb(OEt)_5$ and H_2O precursors at around 210 ºC on borosilicate glass or thermal SiO_2, followed by a reductive post-deposition annealing at 500-600 ºC (in hydrogen-containing atmospheres), very low resistivity values of ~1 mΩcm can obtained for highly-doped films (Nb/(Nb+Ti) ≥ 0.2) [240,311,626]. However, for the films with lower substitution ratios the resistivity values are more than an order of magnitude higher [240,311,626]. Hall-effect measurements (2-300 K) have indicated a signature of phonon-scattering dominated mobility for the highly-doped films, while for the low-doping regime comparison of the Hall mobility values against the optical mobility values have revealed grain-boundary scattering limited mobility [311]. The transport data are in good agreement with the microscopy and XRD results that have shown larger grain size and high degree of *c*-axis orientation of the grains for the high-doping regime [240,311,626]. However, for TCO applications, the excessive electron doping of the high-doping regime is not beneficial, as the free carrier absorption progressively suppresses the transparency window in the vis-NIR side of the electromagnetic spectrum. Formation of too small grains in lightly-doped films can be avoided by decreasing the deposition temperature to around 170 ºC (at least for the $TiCl_4$/$Nb(OEt)_5$/H_2O process); then the charge transport becomes virtually free from grain-boundary scattering and the conduction electrons are predominately scattered by phonons inherent to the anatase TiO_2 lattice and by impurities [315]. Most importantly, achieving the low resistivity with the low doping level enables the improved vis-NIR transmittance *via* decreased free-carrier absorption, thus improving the overall TCO performance of the material [315]. Moreover, high-quality as-deposited crystalline films grown on epitaxial $LaAlO_3$ substrates grown at 220 ºC *via* the $TiCl_4$/TBTDEN/H_2O process have shown resistivity values around 3 mΩcm for 4% Nb doping [323].

Niobium works as an efficient electron donor in the anatase lattice such that high carrier-density values with close to one-to-one ratio with the Nb atomic density values are obtained [311]. As a result the Nb:TiO_2 films can be regarded as degenerate semiconductors – a fact indicated by the

lack of temperature activation in the carrier density values and the Burstein-Moss shift seen for the fundamental absorption edge [311,315]. Stemming from the anisotropy in the effective mass of anatase the future challenge is to increase the control over film orientation such that electron conduction along the low-effective-mass (*a*,*b*) plane is maximized for lightly-doped films grown on non-lattice-matched substrates. Furthermore, lowering the temperature required for the annealing step would broaden the spectrum of possible applications. Note that also tantalum serves as a dopant that notably lowers the resistivity of TiO_2 films, however, the lowest resistivity values reported for Ta-doped TiO_2 are around 10×10^{-3} Ωcm [626].

4.3 N doping

Titanium dioxide is well known for its photocatalytic properties, however, the wide band gap of the material limits the light-activation regime above 3.2 eV. In order to reduce the band gap and sensitize TiO_2 to visible light, doping with nitrogen is a prominent approach.

Deposition characteristics. Fabrication of N-doped TiO_2 films has been demonstrated *via* various ALD routes. A thermal ALD process that employs $TiCl_4/H_2O$ cycles for TiO_2 and $TiCl_4/NH_3$ cycles for incorporation of nitrogen was reported by Pore *et al.* [65], while Cheng *et al.* employed a similar approach using $TiCl_4$ together with H_2O-NH_3 vapour mixture [128]. Plasma-assisted ALD processes employing N_2 plasma as the nitrogen source and $Ti(NMe_2)_4/H_2O$ [689] or $TiCl_4/H_2O$ [242] cycles for TiO_2 have also been developed. Moreover, Zhang *et al.* demonstrated a deposition route based on H_2-N_2 plasma and $Ti(NMe_2)_3(CpMe)$ [804]. The GPC values fall in the range typically reported for undoped TiO_2 films, with a trend of decreasing GPC with increasing N content [65,128].

As TiN has a strong tendency towards oxidation, the incorporation of N into the anion site of the TiO_2 lattice may not be as straightforward as the cation-site doping with metal atoms. This was seen in the report by Pore *et al.* where replacing single $TiCl_4/H_2O$ cycles in the TiO_2 process by $TiCl_4/NH_3$ cycles at the $(TiCl_4/NH_3)/(TiCl_4/H_2O + TiCl_4/NH_3)$ ratios as high as 1/2 led to low level (< 1 at.%) of nitrogen content in the form of molecularly absorbed N_2 [65]. Only when the approach was changed (perhaps counter intuitively) such that three or more consecutive $TiCl_4/NH_3$ cycles were followed by single $TiCl_4/H_2O$ cycles (or simple H_2O-oxidation cycles), respectable N doping (>3.8 at.%) was achieved and Ti-N bond formation was seen [65]. The approach of using H_2O-NH_3 vapour mixture for doping shows a good control over the N content in a way that N levels of 0.2, 0.7, 1.2, 1.5, and 4.3 at.% are achieved by increasing the relative amount of NH_3 in the vapour mixture [128]. Incorporation of N atoms *via* the conventional single-cycle doping approach using plasma-based processes may be more feasible than *via* thermal process: Deng *et al.* reported substitution ratios of 1/10, 1/6, and 1/3 to lead to N levels of 3.3, 4.7 and 9.4 at.%, respectively; Ti-N bonding was moreover seen by XPS [689].

Regarding crystallization, according to the results by Pore *et al.* the higher N content together with the Ti-N bond formation seem to favour the growth of anatase-structured films with preferred *c*-axis orientation, while mixed-phase anatase-rutile films are obtained for low N levels (at 500 °C) [65]. With the exception of the preferred orientation this observation is supported by the results of

Cheng *et al.*, who furthermore saw a shift in the anatase (101) peak position (in an XRD pattern) with increasing doping level as an indication of substitutional incorporation of N into the O site in the TiO_2 lattice (at 400 °C) [128]. When the deposition was realized through the $Ti(NMe_2)_4/H_2O/N_2$ plasma process at a relatively low temperature of 150 °C, amorphous films were obtained [689]. These amorphous films were then crystallized upon annealing at a temperature of ~500 °C; note that the required crystallization temperature increases slightly for increasing N levels [689]. Lack of oxygen in the annealing atmosphere favours the rutile structure, whereas air anneal leads to the formation of anatase-structured films with preferred *c*-axis orientation that becomes more pronounced at higher N levels [689].

Photocatalytic properties. When a material is irradiated with light with energy larger than its band gap electrons from the valence band are excited to the conduction band, leaving holes behind in the valence band. These photo-generated holes and electrons can drive oxidation and reduction reactions on the material surface. Due to its large band gap of around 3.2 eV, TiO_2 can only exploit UV-range photons and activation of the material to the visible light has been an active research topic. Often the anatase structure or an anatase-rutile mixture is considered better than the rutile structure regarding the photocatalytic performance, though the topic yet has remained a subject of discussion [809,810].

Indeed, lowering the TiO_2 band gap by N doping has been proven successful through different ALD routes [65,242,313,689]. For thermal ALD Pore *et al.* reported a modest shift in the band-gap value down to 2.9 eV (anatase TiO_2) for nitrogen content of 8.1 at.%, while a plasma-based process yielding a similar nitrogen level of 9.4 at.% enabled a more pronounced decrease of the band gap down to 1.9 eV (amorphous TiO_2) [65]. However, attempts to anneal the amorphous films to obtain the anatase structure drove out the N dopants and the band gap was found to increase to a value close to that seen for undoped TiO_2 [689].

Looking into the photocatalytic properties of ALD fabricated N-doped TiO_2, simple reduction in the band gap may not directly imply improved photocatalytic performance. Pore *et al.* reported heavy recombination of the photogenerated electron-hole pairs for their N-doped film obtained *via* thermal ALD, such that the films showed poor performance both in the UV and visible range in terms of stearic acid decomposition [65]. Photocurrent experiments by Cheng *et al.* also pointed towards prominent recombination for the higher N content, however films within the low-doping regime below 1.2 at.% exhibited enhanced photocurrent production in the visible range while largely maintaining the UV activity [128]. Furthermore in this respect, it has been proposed that substitutional N is linked to the presence of Ti^{3+} that functions as a recombination centre [804]. However, Rao *et al*. showed improved performance for films from the N_2 plasma-based process in comparison to the undoped TiO_2 in the visible range in terms of methylene blue degradation, again for a rather low N level of around 1%. Deng *et al.* showed enhanced stearic acid decomposition for annealed N-doped films where most of the nitrogen was driven out by the annealing step; in this case the enhanced performance was ascribed to the increased surface area of the films [689]. Indeed, enhanced surface area is beneficial for surface-driven processes such as catalysis, a fact that has inspired research on N-doped TiO_2 nanotubes: Liu *et al*. showed enhanced water-splitting power for post-deposition doped samples [313], while Chen *et al*. fabricated N-doped nanotubes

by annealing molecular-layer-deposited films and showed degradation of methylene blue under visible light [811].

5. Towards applications – nanostructures

The unique capability enabled by the ALD technique is the conformal deposition of ultrathin films on high-aspect-ratio nanostructures. Recalling the well-known catalytic activity of TiO_2 in particular, ALD provides us with an attractive means for fabrication of high-surface-area nanostructured surfaces for catalysis [320,566,739]. As TiO_2 is furthermore photoactive, the research examples related to the employment of ALD for nanostructuring of TiO_2 can be mostly found in the fields of chemical catalysis [114,515,812], photovoltaics [155,325,813,814], photoelectrolysis [812,814], and photochemical hydrogen generation [188]. Apart from catalysis, another field where high surface area is beneficial is sensors; indeed TiO_2 has also been investigated as a gas barrier layer [815], a gas sensor [816] and a biological sensor [175]. Titanium dioxide is also biocompatible and ALD-fabricated TiO_2 thin films could potentially offer superior performances in some frontier medical applications [817]. Moreover, the interesting properties of nanostructured TiO_2 include UV-light-switchability combined with hydrophilicity/phobicity and photoactivity [303,818]. The variety of different ALD-TiO_2 nanostructures and their potential applications are highlighted in figure 9.

In this chapter we discuss the different nanostructuring approaches demonstrated in literature. A distinction is made between the approaches where TiO_2 serves as a mere coating layer and approaches where the substrate is used as a sacrificial template for fabrication of (self-supporting) TiO_2 nanostructures. Deposition on planar carbon-based substrates is also discussed here, as the goals are often very similar to those with the nanostructures.

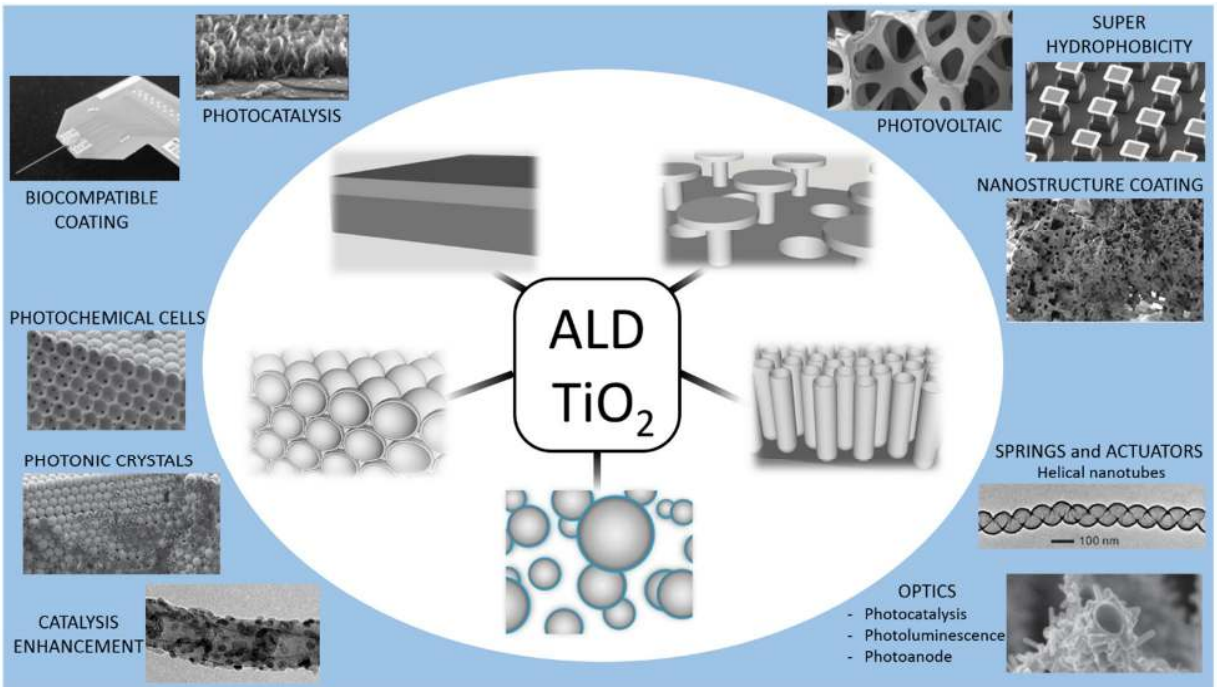

Figure 9. Pictorial overview of ALD-TiO_2 nanostructures and their applications. Reprinted with permission from: Hoshian S *et al.* 2015 ACS Appl Mater Interfaces 7 15593. 2015 Americal Chemical Society; Schröder S *et al.* 2015 2015 6th International Workshop on Advances in Sensors and Interfaces (IWASI) 21. 2015 IEEE; Kurttepeli M *et al.* 2014 J Phys Chem C 118 21031. 2014 American Chemical Society; Kubrin R *et al.* 2012 J Am Ceram Soc 95 2226. 2012 American Chemical Society; Qin Y *et al.* 2010 Small 6 910. 2010 John Wiley and Sons; Acauan L *et al.* 2016 ACS Appl Mater Interfaces 8 16444. 2016 American Chemical Society; Tian L *et al.* 2015 J Vac Sci Technol A 33 01A141. 2015 AIP Publishing LLC; Li Z *et al.* 2014 Nanotechnology 25 504005. 2014 IOP; Sasha Hoshian, author permission.

5.1 Coatings/overlayers on nanostructures

Nanoparticles. Zinc oxide nanoparticles show good photocatalytic activity, but they suffer from lower chemical stability [566]. This drawback of ZnO nanoparticles was overcome by coating them with an ALD-TiO_2 overlayer without compromising the excellent photochemical activity of the original ZnO particles [566]. Another example related to nanoparticle catalysts is the core-shell Au-Al_2O_3 and Au-SiO_2 nanoparticles coated with a 1.5-nm-thick ALD-TiO_2 layer used for CO reduction [819]. For such a thin layer, the film growth was observed to proceed by formation of islands, such that TiO_2 grew preferentially on the under-coordinated Au sites [819]. The island-type growth mode can even be exploited to fabricate structures, where TiO_2 nanoparticles form on supporting nanoparticles, *e.g.* silica or titania nanoparticles [812,813]. The high surface area makes these nanostructures attractive for water splitting, decomposition of organic contaminants [812] and improvement of dye-sensitized solar-cell performance [813]. When an ALD-TiO_2 layer is deposited on nanoparticles, the coating can furthermore provide improved inter-particle and

particle-substrate adhesion [813]. Moreover, Kim *et al.* obtained improved chemical water-splitting performance for Co/C nanoparticles by coating them with an ALD-TiO_2 layer [320].

Carbon nanotubes. Acauan *et al.* deposited TiO_2 on carbon nanotube (CNT) surfaces that had undergone different surface treatments prior to the deposition [820]. On the pristine CNT surface TiO_2 grew as small particles with broad size distribution and poor and non-uniform coverage. The treatment of CNTs with nitrogen improved the coverage such that crystalline uniformly distributed particles of TiO_2 formed, with a narrow size distribution of 7-8 nm. When the CNTs were treated with oxygen, continuous films instead of nanoparticles were formed. The work suggests that the nucleation of TiO_2 preferentially onsets on C-X sites (with X being N or O atoms) rather than on C-C defects. Also Marichy *et al.* studied the deposition of TiO_2 on carbon nanotubes [821]. The morphology of the TiO_2 film depended strongly on the functionality of the CNTs, a property that was controlled with heat treatments of the CNTs *prior* to the deposition of the TiO_2 layer. Consequently, the morphology of the TiO_2 overlayer varied from homogeneous and conformal amorphous (pre-deposition heat treatment at 700 °C) to a more granular and particulate amorphous (pre-treatment at 1500-3000 °C). The homogeneous layer showed a significant change in resistivity in the presence of NO_2 and O_2 gases indicating continuous layers to perform better for gas sensing purposes. The TiO_2 layer was observed to have *p*-type response towards oxygen and nitrogen dioxide [821]. Apart from the catalytic applications, amorphous TiO_2 films deposited on CNTs have been tested as anodes for lithium ion batteries [822]. The ALD-TiO_2 films displayed high specific capacity resulting from the high surface area of the underlying CNTs. The high capacity achieved was higher than the theoretical bulk value. The TiO_2/CNT system was also fabricated as a free-standing structure reinforcing the idea that the combination could provide the high-power and high-capacity anodes for Li-ion battery applications.

Graphitic and polymeric carbon. Carbon nanosheets (CNS) have been studied as high-surface area substrates for photocatalytic TiO_2 films deposited by ALD [739]. After the deposition the samples were annealed at 600°C to form a porous, nanocrystalline and photocatalytically active CNS-TiO_2 composite film. The annealing treatment transformed the as-deposited amorphous titanium oxide to anatase with the morphology remaining unchanged (figure 10). Ismagilov *et al.* used nanographite films (few-layer graphene nanowalls with cross-plane oriented nanoscrolls) as a substrate for the TiO_2 deposition [289]. The ALD-TiO_2 film grown on them with a thickness ranging from 50 to 250 nm covered the nanowalls homogeneously while only partially coating the needle-like nanoscrolls where rather individual spherical particles were formed. Even when the thickness of the TiO_2 coating was as much as 200 nm, the field emission characteristics of the graphene were not significantly affected. The application proposed for the structure is as cold anode in vacuum electronic devices since TiO_2 was also found to form a protective passivation layer on top of the graphite.

Titanium dioxide deposited by ALD on graphene nanosheets (GNSs) could find application in Li-ion batteries as well. Li *et al.* deposited amorphous TiO_2 on GNSs for an anode material [823]. The amorphous nature of TiO_2 provided the structure with short Li^+-ion diffusion pathways while the CNSs offered excellent electrical conductivity and large electrode/TiO_2 contact area. These characteristics contributed to the remarkable electrochemical performance of the structure. In

another work, the authors utilized ALD to coat mesoporous activated carbon (AC) electrodes with TiO_2 [824]. The mesoporous AC substrate was chosen in order to enhance the low electrical conductivity, poor cyclic performance and low Li^+-ion diffusivity of TiO_2. The thus fabricated TiO_2-coated AC electrode showed improved performance with a high specific capacitance, high rate cabability and enhanced cycle life compared to pristine AC electrodes.

Lange *et al.* used TiO_2 grown on top of low-density polyethylene as a gas-barrier enhancer of the plastic film [815]. The growth of the TiO_2 layer starts inside the polyethylene film with the first 10-15 cycles penetrating the surface, after which the deposition continues normally on top of the surface. To avoid cracks, the deposition temperature was kept at a maximum of 50 °C, when the TiO_2 layer was confirmed to be an effective oxygen barrier.

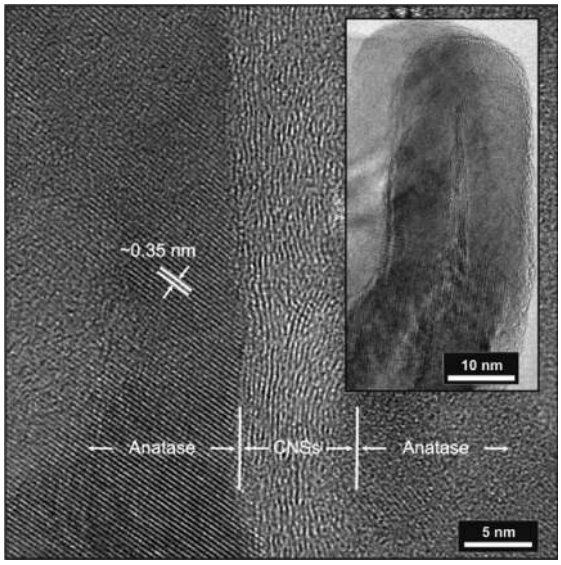

Figure 10. HRTEM image showing the anatase crystallites grown on a graphite wall of a carbon nanosheet. Reprinted with permission from Verbruggen S W *et al.* 2014 Appl Catal , B **160-161** 204. Copyright 2014 American Chemical Society [739].

Other substrates. Hoshian *et al.* utilized the photoactivity of TiO_2 to fabricate photoswitchable hydrophilic/hydrophobic surfaces [303,818]. Titanium oxide has phototunable hydrophilic properties that arise from its surface chemistry and, when deposited on top of microscale overhanging pillars the surface can be made hydrophobic, as illustrated in figure 11. Thus, the switching of the state of the surface can be controlled by UV exposure. The combination of photoswitching, micropillar design and surface nanostructuring made the switching/recovery possible. Moreover, Tian *et al.* have demonstrated the coating of nickel foam with ALD-TiO_2 for antireflection layer of solar cells (figure 12) [325].

Microfabricated silicon nanowires (NWs) can be used as anode material in Li-ion batteries but their performance is not ideal. Lotfabad *et al.* coated the structure with ALD-TiO_2 [825]. The amorphous coating was conformal and not only enhanced the electrochemical properties but also prevented the agglomeration of Si NWs that would lead to delamination from the conductive substrate in the battery. Also, TiO_2 has been found advantageous as a coating for $LiMO_2$ cathodes

where M = (Ni,Mn,Co) or (Ni,Co,Al) [826,827]. Here the thin TiO_2 layer acts mostly as a protective layer for the active $LiMO_2$ cathode material preventing its dissolution and promoting the Li^+-ion diffusion.

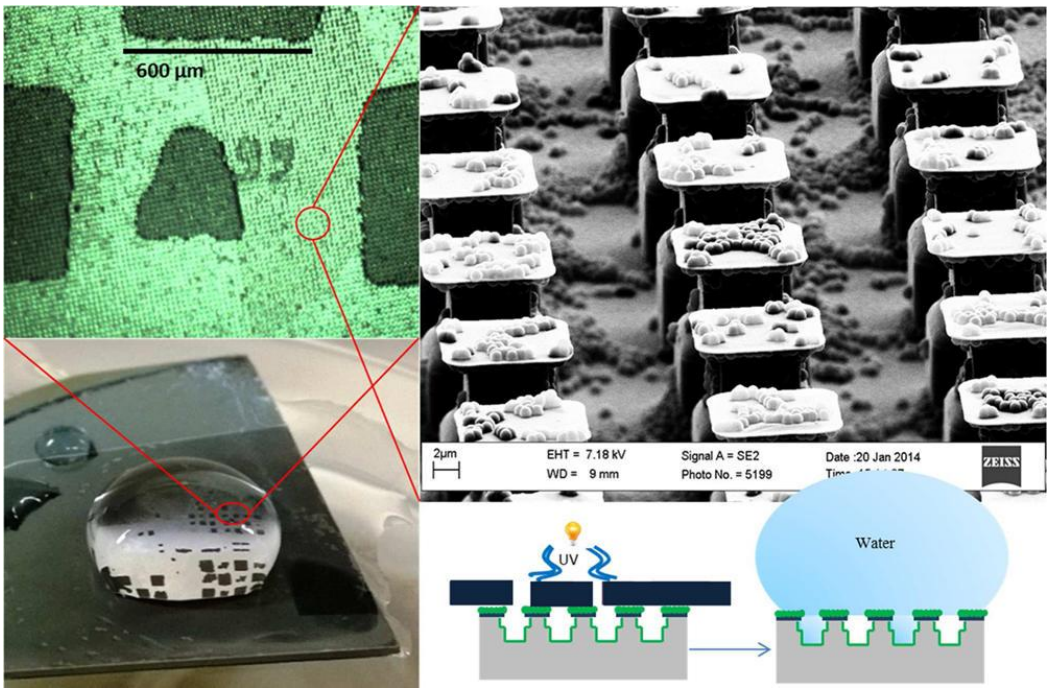

Figure 11. (bottom, left) Image of the hydrophobic structure in macro scale. (top, right) Microscale scanning-electron-microscope image of the same. (bottom, right) The working principle of the structure is schematically explained. Reprinted with permission from Hoshian S *et al*. 2015 ACS Appl Mater Interfaces **7** 15593. Copyright 2015 American Chemical Society [303]

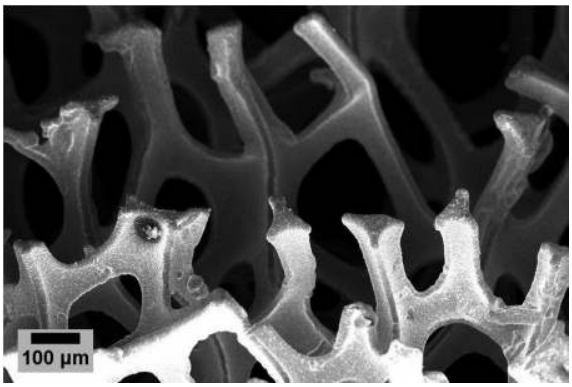

Figure 12. Scanning electron micrograph of nickel foam coated with TiO_2 Reprinted with permission from Tian L *et al. 2015 J Vac Sci Technol* A **33** 01A141. Copyright 2015 AIP Publishing LLC [325].

5.2 Template-assisted nanostructures

Nanotubes. In template-assisted nanostructuring an ALD-TiO_2 layer of a desired thickness is first conformally deposited on a sacrificial template. Then the template is selectively removed by etching or by a heat treatment, which yields the TiO_2 nanostructure shaped by the template. In general ALD-based nanotubes are probably most commonly fabricated using porous anodic alumina (PAA) as a sacrificial template; in case of TiO_2, nanotubes have also been fabricated using other type of templates such as carbon nanocoils [399], carbon nanotubes [828], nanocellulose aerogel [138], polyvynilpyrollidone-modified polysulfone [247] or polycarbonate membrane [292]. Note that, as the TiO_2 deposition on nanotube templates are often performed at low temperatures, subsequent annealing in the temperature range of 300-500°C can convert the as-deposited amorphous nanotubes into the anatase crystal structure [85,114,159]. Owing to the high surface area and functionalization possibilities, the TiO_2 nanotube structures are highly interesting for photocatalysis and photovoltaics [148,246,272,320,829,830].

Nanotube arrays can be fabricated using PAA as a template, such that the outer diameter of the nanotubes is controlled by the PAA pore width, while the thickness of the ALD layer deposited on the pore walls determines the inner radius of the nanotubes, as illustrated in figure 13. Besides the width of the pores, the depth and spacing of the hexagonally arranged pores can be tuned by the fabrication parameters of the through-porous PAA template [85,172,381]. The well-defined structure of the template enables fabrication of consistent and homogeneous arrays of nanotubes with good contact between the closed bottom of the nanotubes and the substrate [85,114,476].

In an early work by Shin *et al.* on ALD-grown TiO_2 nanotubes, the structures were fabricated utilizing a polycarbonate filter as a template, and excellent control over the wall thickness of the nanotubes was achieved [829]. However, the control of the other dimensions of the nanotubes was not so good compared with the level of control typically seen for PAA-templated nanotubes. Su *et al.* reported the use of a polycarbonate membrane as a template [292]. Moreover, helical TiO_2 nanotubes have been fabricated using carbon nanocoils as a sacrificial template and studied for their mechanical properties [399]. These nanotubes showed improved elastic modulus values compared to the ordinary non-helical ones, therefore having potential applications as nanosensors, mechanical springs, actuators and elastic electrical conductors [399]. Deng *et al.* used CNTs as a template and showed that the as-deposited TiO_2 layer could continuously coat the CNT surfaces [828]. However, after calcination above 475 °C the TiO_2 layer transformed to a stack of interconnected nanoparticles in place of the removed CNTs. Upon increasing the temperature, TiO_2 was transformed from the as-deposited amorphous phase to crystalline anatase phase while the carbon was gradually removed.

Possible nanotube structures are not limited to arrays, as use of network-structured templates enables fabrication of nanotube networks. Korhonen *et al.* coated nanocellulose fibers, organized in a random mesh, with ALD-TiO_2 [138]. After removal of the template, a hollow nanotube network of anatase TiO_2 was obtained. When these TiO_2 nanotubes were tested as a humidity sensor, they showed a relatively fast response time in the 40-80% humidity region. Other proposed

applications include non-wetting surfaces, carriers, encapsulation, drug-release, catalysis, microfluidics and filtration. Similar nanotube networks have also been fabricated by using cellulose nanofibers as a template [272]. Both pure TiO_2 and ZnO-TiO_2 bilayer nanotubes were fabricated with the wall thicknesses of 100 and 150 nm, respectively, and tested as photoelectrochemical (PEC) photoanodes. Moreover, use of polyvynilpyrollidone-modified polysulfone [246] and tris-8-hydroxyquinoline gallium [148] can be used as a template to obtain hollow TiO_2-network structures.

Currently TiO_2 nanotubes realized through template-assisted ALD are also investigated as Li-ion battery anode materials. Both sacrificial templates and intermediate layers to obtain hollow tubular structures have been utilized. A common material here used in combination with TiO_2 is SnO_2 [831-833]. In the case of Carvajal *et al.* the template made of vertically aligned SnO_2 nanorods was not sacrificial [831]; on top of these nanorods two layers were deposited by ALD, first a sacrificial ZnO layer and then TiO_2. Removal of the ZnO layer then created a 30 nm gap between the active materials, SnO_2 and TiO_2. In another work, a hollow SnO_2/TiO_2 structure was employed to obtain good initial discharge capacity and cycling performance [832]. In this case too, ZnO was used as a sacrificial template grown as nanotubes on the surface of flexible carbon cloth. On these ZnO nanotubes, SnO_2 (utilizing $SnCl_4$ and H_2O as precursors) was grown by ALD followed by ZnO etching and ALD of TiO_2 (with $TiCl_4$ and H_2O). This structure was able to accommodate the large internal stress from the volume expansion of SnO_2 while the TiO_2 layer protects it from pulverization and exfoliation. Similar SnO_2/TiO_2 nanotube structures have been fabricated also using the traditional PAA template method. First ALD of TiO_2 is performed inside the template holes, followed by the ALD of SnO_2 [834]. The thinner walls of the nanotubes resulted in enhanced capacity retention.

Recently Zhong *et al.* fabricated a nanotube array made of TiO_2/Fe_2O_3 utilizing $Co_2(OH)_2CO_3$ as a sacrificial template [835]. According to the article the performance of the structure was superior compared to most reported TiO_2/metal oxide composites. This was attributed to the combination of the high specific capacity of Fe_2O_3 and the usual structural stability of the TiO_2 backbone.

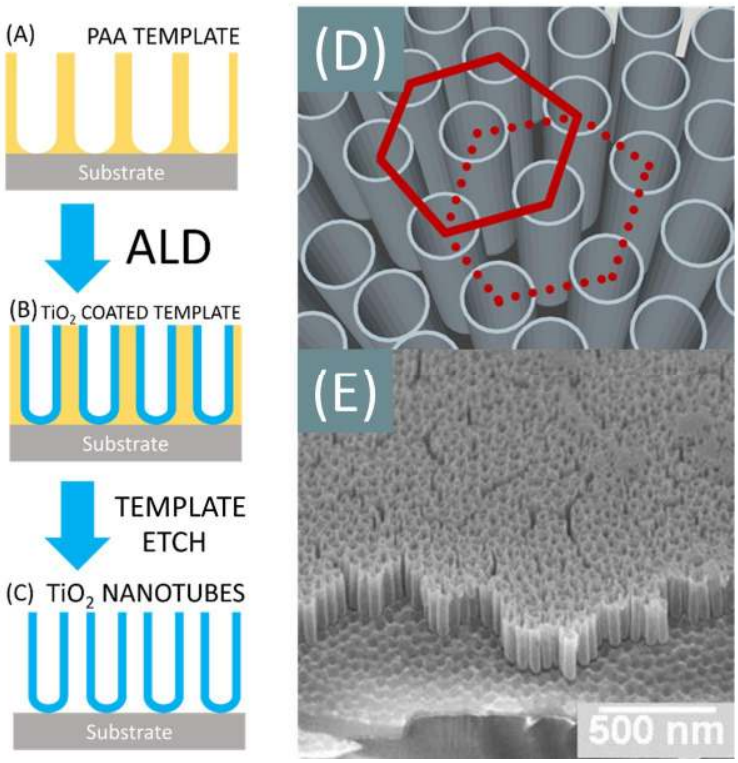

Figure 13. Fabrication route for TiO_2 nanotubes using a porous anodic alumina (PAA) template. (A) The PAA template prepared from an aluminum film. (B) TiO_2 is conformally deposited by ALD inside the pores of the PAA template. (C) Template is removed by etching, which leaves an array of TiO_2 nanotubes on the substrate. (D) Illustration of the hexagonal arrangement of the PAA-based nanotubes. (E) Scanning electron micrograph of a nanotube array with hexagonal packing Reprinted with permission from Deng S *et al.* 2014 RSC Adv 4 11648. Copyright 2014 American Chemical Society [836].

Inverse opals. Inverse opals are structures formed from an opal template (amorphous SiO_2 or polystyrene spheres organized in regular, closely packed planes) infiltrated with a material (*e.g.* TiO_2). The template is then removed leaving a TiO_2 structure that is the inverted of the initial opal. One of the main characteristics of these TiO_2 nanostructures is the high surface area together with a high void volume (74 % in [188]). These nanostructures could be interesting material candidates for applications such as photochemical hydrogen generators [188], photochemical cells [530], dye-sensitized solar cells [837] or photonic crystal displays [140].

Conventionally inverse opals are formed by means of infiltrating liquid into the opal template. However, by using ALD a better control on the wall thickness is achieved, together with an improved infiltration that yields filling fractions close to the theoretical maximum [72]. The ALD processes used to fabricate the inverse opals are all operating with long pulse or long hold times depending on the reactor type. Long processing times are needed because the infiltration of the precursors needs to be complete and uniform. The infiltration, being a diffusion process, cannot be sped up and the thickness of the template will define the deposition time. During the post-deposition template-removing calcination (for polystyrene templates) or HF etching (for silica

templates) the inverse opal structure is formed, while the TiO_2 is transformed to the anatase crystalline phase. Figure 14 presents a schematic and a SEM cross-section image of an inverse-opal structure fabricated with a template formed by stacked particles, while figure 15 shows how the dimensions of an inverse-opal structure can be further controlled with ALD after the template removal.

The inverse opals are porous structures that can then again be used as a substrate for further processing, such as fabrication of multi-layered inverse opals. For example, Graugnard *et al.* fabricated non-close-packed inverse-opal photonic crystals on opal templates [72]. The opal template was first coated with a sacrificial Al_2O_3 layer and then with a TiO_2 dielectric layer. When both the template and the sacrificial layer were removed by etching, the remaining structure was composed of TiO_2 structured as spherical voids connected by air channels. The dielectric structure can then be further coated to adjust the size of the air channels and the thickness of the walls. Other examples on further tailoring of TiO_2 inverse opals include sensitization with CdS quantum dots for photoelectrochemical hydrogen generation [188], and sensitization with indoline for dye-sensitized solar cells [837].

Other structures. Titanium oxide coating has also been used to enhance the hydrophobicity of nanostructured surfaces replicated on polydimethylsiloxane (PDMS) from an aluminum template [818]. Aluminum was etched to create the nanostructures and then coated with 25-nm thick ALD-TiO_2 layer. Then, PDMS was casted and cured on top of the structure. After the removal of aluminum by etching, the nanostructures remained replicated on the PDMS surface with the TiO_2 coating transferred on them. The final surface showed enhanced hydrophobicity compared to the nanostructured PDMS alone thus confirming the benefits provided by the added TiO_2 layer.

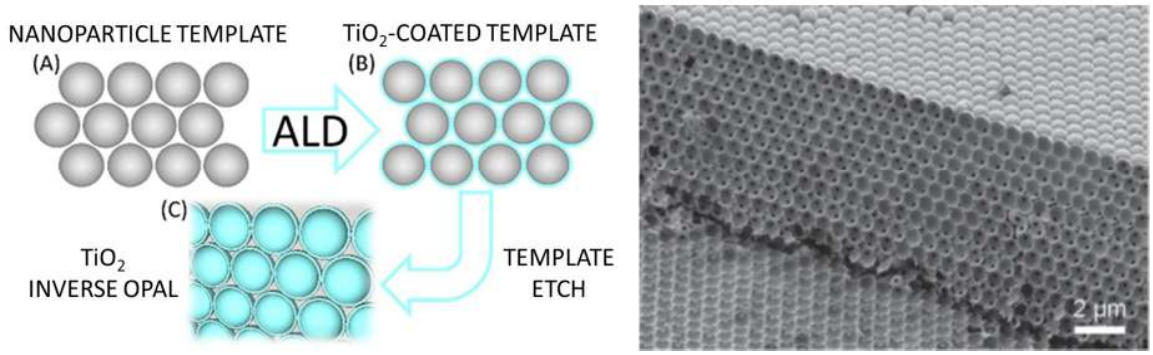

Figure 14. (left) Schematic of the fabrication of TiO_2 inverse opal structure. Starting from an ordered nanoparticle template (A) the ALD coating is applied (B). When the template is removed the TiO_2 coating remains forming the inverse-opal structure (C). (right) Scanning electron micrograph of a TiO_2 inverse-opal structure fabricated with a template with particle size of 756 nm. Reprinted with permission from Kubrin R *et* al. 2012 J Am Ceram Soc 95 2226. Copyright 2012 John Wiley and Sons. [431]

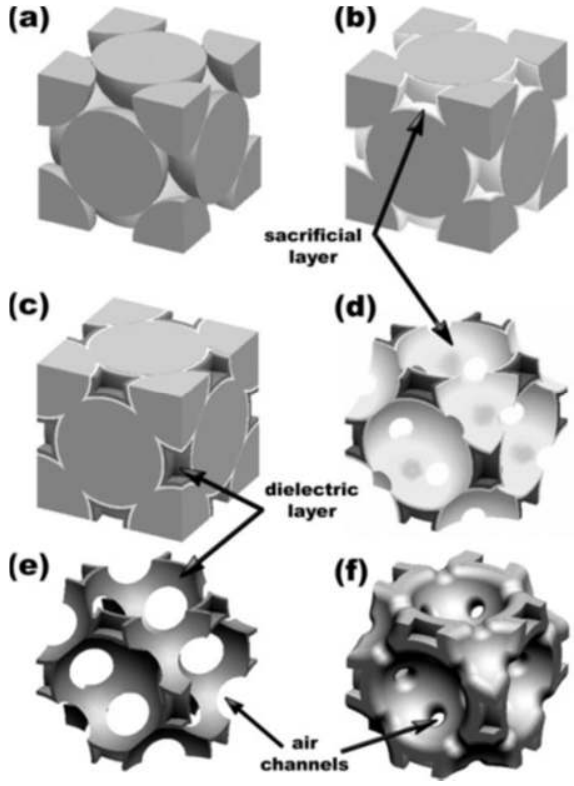

Figure 15. Fabrication route for a coated inverse opal structure. Starting from packed nanoparticles (NP) in (a), a sacrificial coating is applied in (b) and then the dielectric TiO_2 is deposited by ALD in (c). The NPs and the sacrificial layer are etched away in (d) and (e) with another TiO_2 deposition is performed in (f) to control the size of the air channels. Reprinted with permission from Graugnard E *et al*. 2006 Adv Funct Mater 16 1187. Copyright 2006 John Wiley and Sons. [838]

6. Hybrid TiO_2-organic structures

Molecular layer deposition (MLD) is a technique analogous to ALD with the difference that in MLD the film growth proceeds *via* deposition of molecular monolayers instead of atomic monolayers. When two (or more) different organic MLD precursors are reacted on a substrate surface in a cyclic self-limited manner, purely organic thin films such as polyimide [839] and polyamide [840] can be grown; this is an approach that dates back to 1990s. More recently, an interesting way to combine organic MLD precursors and metal-containing ALD precursors to produce inorganic-organic thin films has been demonstrated [841-843]. In addition to enabling the fabrication of completely new types of inorganic-organic hybrid materials, this novel combinatorial approach (ALD/MLD) adds an additional degree of freedom for tailoring inorganic materials such as TiO_2, as the ratio of the inorganic and organic constituents in these layered hybrid materials can be freely tuned with an accuracy of atomic or molecular monolayer [307,841,844-846]. In this chapter we briefly introduce the literature on Ti-based hybrid thin films by ALD/MLD.

In the first published work on Ti-based hybrid films by ALD/MLD the film growth was achieved from $Ti(O^iPr)_4$ and $CH_2=CH(CH_2)_6SiCl_3$ precursors [841]. After this, attention regarding the organic precursors has shifted more and more on aliphatic and aromatic organic alcohols, amines and carboxylic acids [9]. In most of the works $TiCl_4$ has been used as the Ti precursor; it has been combined with ethylene glycol [847,848], glycerol [847,849], 8-hydroxyquinoline [842,850], ethanolamine [811], malonyl chloride [811] and 4,4'-oxydianiline [851,852]. Ideally, the growth of a hybrid thin film takes place *via* self-saturating ligand-exchange reactions between *e.g.* the –OH groups of an organic alcohol and –Cl groups of $TiCl_4$, that is, in a way familiar from ALD. Note that the reaction sequences are not limited to two-precursor processes but multi-precursor processes are also possible, as illustrated by the work by Chen *et al.* who demonstrated the growth of hybrid films using $TiCl_4$, ethanolamine and malonyl chloride [811]. The possible complications with the ALD/MLD film growth relate to unwanted double surface reactions, such that both functional groups of an organic precursor react during one half-cycle reaction with the surface. This is a problem that may lead to slowing down of the film growth as the functional group density on the surface of the growing film decreases with increasing film thickness. This can be though largely avoided by using aromatic molecules with rigid backbones [9].

Thermal post-deposition treatments provide a powerful tool for tuning the structure and properties of these hybrid films, such that annealing in oxygen-containing environments may provide a pathway to porous inorganic structures, while annealing in reductive conditions leads to formation of TiO_2:C composite-type materials where the carbon is present in graphitic form [845,849]. Inorganic-organic thin films where the thickness of the organic layers is kept at a mono-molecular level while expanding the thickness of the inorganic layers, the organic layers can be used to fine-tune the properties of the inorganic matrix. In this regards, examples are TiO_2:polydiacetylene hybrid superlattices obtained combining the $TiCl_4/H_2O$ process with single intermediate $TiCl_4$/HDD/UV-exposure cycles for the polydiacetylene layers (HDD stands for 2,4-

hexadiyne-1,6-diol) [844], TiO_2:hydroquinone superlattices for tuning the optical properties and TiO_2:C superlattices for thermal conductivity suppression of TiO_2 [307,845,846]. The ability to combine the properties of inorganics and organics in one material holds a great promise, yet the research on these hybrid materials is still in its infancy and a lot remains to be understood regarding *e.g.* the local structure of the films and finding the key inorganic-organic material pairs and properties for break-through applications.

7. Summary and outlook

During the past decades over fifty different ALD processes have been developed for TiO_2 by combining homoleptic halide, alkoxide, alkylamide, and also heteroleptic precursors with *e.g.*, water, ozone, and oxygen plasma. The most common halide-based process is $TiCl_4/H_2O$, which can be used in a wide temperature range above 100 °C. Other halides, namely TiI_4 and TiF_4, have also been studied but are not as common as $TiCl_4$. For the halides in general, the drawback is the corrosiveness of the reaction byproducts, which can be harmful to the deposition instruments and has been one of the drivers in the search for alternative titanium precursors among alkoxides, alkylamides and heteroleptic precursors. While $Ti(O^iPr)_4$ has been the most popular alkoxide precursor, showing reactivity towards H_2O even below 100 °C, $Ti(OEt)_4$ and $Ti(OMe)_4$ have also received some attention. The drawback of the alkoxide precursors is that they decompose at relatively low temperatures, such that for $Ti(O^iPr)_4$ the decomposition starts around 250 °C, while $Ti(OEt)_4$ and in particular $Ti(OMe)_4$ are slightly more stable. Alkylamides are highly reactive towards water, so that TiO_2 films can be grown well below 100 °C. The most common alkylamide is $Ti(NMe_2)_4$, but $Ti(NEt_2)_4$ and $Ti(NEtMe)_4$ based processes are also sometimes employed. The drawback is that $Ti(NMe_2)_4$ starts to decompose already around 200 °C. In order to boost up the thermal-decomposition temperature of the non-halide precursors, various heteroleptic precursors have been developed. In this respect, Cp ligands have shown a particularly positive stabilizing effect when combined in a single precursor molecule with alkoxide or alkylamide ligands. The stabilizing effect seems to be enhanced for Me-substituted Cp rings, especially for $CpMe_5$. It is worth noting that typically insufficient reactivity of water towards these Cp-based precursors requires the use of more reactive co-reactants such as ozone or O_2 plasma.

Depending on the deposition conditions, as-grown TiO_2 thin films can be amorphous, one of the crystalline forms, *i.e.*, anatase, rutile, brookite, TiO_2-II phase, suboxide phases, or – as also often being the case – a mixture of some of these. Amorphous films are obtained at low temperatures, films of the anatase structure at intermediate temperatures and films of the rutile structure at high temperatures. For the halide-based processes anatase crystals start forming within the amorphous matrix at around 130 °C or above, while formation of the rutile structure is observed around 300 °C or above. For the alkoxide-based processes the onset temperature for the anatase structure appears to be slightly higher than for the halide-based processes, *i.e.*, 180 °C or higher. The low decomposition temperature of the precursor makes it difficult to obtain rutile films within the decomposition-free deposition temperature regime. This holds also for alkylamides, for which even the anatase-formation temperatures may overlap with the precursor decomposition regime. Heteroleptic precursors typically enable anatase films to be obtained in the decomposition-free regime, starting from 250 °C, while the onset temperatures for rutile formation are typically above 300 °C. Evidently, the choice of the growth surface plays a role in the formation of the crystal structure. The growth of TiO_2 films is often initiated by a formation of a homogeneous amorphous layer, being presumably linked to a high density of hydroxyl groups on the surface. In the opposite

low-hydroxyl-group-density case, the deposition may initiate *via* formation of small island-type crystal grains. When the film growth begins with the formation of an amorphous layer, crystalline anatase grains can subsequently form within/on the amorphous layer, provided that the deposition temperature is high enough. Moreover, lattice match between TiO_2 and the substrate plays a role, such that for example epitaxial growth of rutile films at the notably low temperatures around 250 ^oC is possible on rutile-structured RuO_2, SnO_2 and IrO_2 surfaces.

For ALD-fabricated TiO_2 the common dopant cations are Al and Nb, while anion-site doping with N is also possible. $AlMe_3$ has typically been used as the Al-dopant precursor, while $AlCl_3$ has been studied as a hydrogen-free alternative. The choice of the oxygen source can be important when TiO_2 is grown on a metal surface; *e.g.* on Ru the high oxidation power of O_3, O_2 plasma or N_2O plasma is needed for *in-situ* formation of interfacial RuO_2 that promotes the growth of rutile-structured TiO_2 at notably low temperatures around 250 ^oC. Interesting for high-*k* applications, Al-doping has been shown to decrease the leakage current values for rutile TiO_2 films by multiple orders of magnitude in comparison to undoped TiO_2. This has been ascribed to increased Schottky barrier at the metal-insulator interface, as Al^{3+} acceptors lower the Fermi level in TiO_2. Contrary to Al^{3+}, Nb^{5+} in the anatase structure makes TiO_2 a degenerate semiconductor and hence an interesting transparent conductor. Fabrication of Nb:TiO_2 films has been demonstrated using either $Ti(OMe)_4$ or $TiCl_4$ as the Ti precursor, $Nb(OEt)_5$ or TBTDEN as the Nb precursor and H_2O as the oxygen source. Via reductive heat treatment of amorphous as-deposited films, the films on glass substrates exhibit large crystal grains and hence high mobility with resistivity values as low as 1 mΩcm. Especially for high Nb contents the crystal grains are extraordinarily large and highly *c*-axis oriented. Doping TiO_2 with nitrogen is a prominent approach to reduce the band gap and sensitize the material to visible light, and has been attempted *via* various thermal and plasma ALD routes. Indeed, lowering the TiO_2 band gap by N doping together with improved photocatalytic properties has been reported. However, the decreased band gap may not directly imply improved photocatalytic performance, as due to doping, simultaneously enhanced recombination has been reported.

The unique feature of the ALD technique is the ability to conformally deposit ultrathin films on high-aspect-ratio nanostructures. A distinction can made between the nanostructuring approaches where TiO_2 serves as a mere coating layer and approaches where a substrate is used as a sacrificial template for fabrication of TiO_2 nanostructures. Having the eye on the utilization of the well-known catalytic activity of TiO_2, ALD therefore is a promising technique for tailoring/fabricating high-surface-area nanostructured surfaces for catalysis by coating *e.g.*, different nanoparticles and carbon nanotubes. The template-assisted approach enables fabrication of TiO_2 nanotube arrays, again interesting for catalysis, and for example inverse-opal structures interesting for solar-cell electrodes or photonic crystals.

During the past decade, an increasing number of ways to combine organic MLD precursors and metal-containing ALD precursors for the fabrication of inorganic-organic thin films has been demonstrated. In addition to enabling fabrication of completely new hybrid materials, the ALD/MLD approach brings in additional freedom for tuning inorganic materials, TiO_2 among the others, as the ratio of the inorganic and organic constituents in these layered hybrid materials can

be freely tuned with an accuracy of atomic or molecular monolayer. For these hybrid materials, post-deposition treatments provide a powerful tool for tuning their structure and properties. For example annealing in oxygen may provide a route to porous inorganic structures, while use of reductive conditions can lead to the formation of nanocomposite-type materials with carbon in graphitic form.

In the future, the continuing downscaling of microelectronic devices implies ever increasing demand for atomic-level thickness control for deposition of ultrathin films on three-dimensional nanostructures – extremely stringent conditions that can be met by atomic layer deposition but not necessarily by other thin-film techniques. The literature overviewed in this work shows that a wide range of ALD processes with specific characteristics is available for tailoring TiO_2 films for different applications. Besides nanostructuring, enhanced control over the material properties achieved by doping, and by combining TiO_2 with organics by means of atomic/molecular layer deposition, are foreseen as future research directions on the way to further enhanced technological applicability of TiO_2 thin films.

Acknowledgement

This work has been supported by the European Research Council under the European Union's Seventh Framework Programme (FP/2007-2013)/ERC Advanced Grant Agreement (No. 339478) and also by the Strategic Research Council at the Academy of Finland (No. 303452) and the Mineral Resources and Material Substitution Programme of the Academy of Finland (No. 292431).

References

[1] George S M 2010 *Chem Rev* **110** 111
[2] Miikkulainen V, Leskelä M, Ritala M and Puurunen R L 2013 *J Appl Phys* **113** 021301
[3] Johnson R W, Hultqvist A and Bent S F 2014 *Materials Today* **17** 236
[4] Knez M, Nielsch K and Niinistö L 2007 *Adv Mater* **19** 3425
[5] Profijt H B, Potts S E, Van de Sanden, M. C. M. and Kessels W M M 2011 *J Vac Sci Technol A* **29** 050801
[6] Niinistö J, Blanquart T, Seppälä S, Ritala M and Leskelä M 2014 *ECS Trans* **64** 221
[7] Blanquart T, Niinistö J, Ritala M and Leskelä M 2014 *Chem Vap Dep* **20** 189
[8] George S M, Lee B H, Yoon B, Abdulagatov A I and Hall R A 2011 *J Nanosci Nanotechnol* **11** 7948
[9] Sundberg P and Karppinen M 2014 *Beilstein J Nanotechnol* **5** 1104
[10] Tynell T and Karppinen M 2014 *Semicond Sci Technol* **29** 043001
[11] Lakomaa E, Haukka S and Suntola T 1992 *Appl Surf Sci* **60** 742
[12] Desu S B 1992 *Mater Sci Eng B* **13** 299
[13] Ritala M and Leskelä M 1993 *Thin Solid Films* **225** 228
[14] Haukka S, Lakomaa E and Roots A 1993 *J Phys Chem* **97** 5085
[15] Haukka S, Lakomaa E and Suntola T 1993 *Thin Solid Films* **225** 280
[16] Haukka S, Lakomaa E, Jylha O, Vilhunen J and Hornytzkyj S 1993 *Langmuir* **9** 3497
[17] Ritala M, Leskelä M, Johansson L and Niinistö L 1993 *Thin Solid Films* **228** 32
[18] Haukka S, Lakomaa E and Suntola T 1994 *Appl Surf Sci* **82/83** 548
[19] Aarik J, Aidla A, Uustare T and Sammelselg V 1995 *J Cryst Growth* **148** 268
[20] Rosental A, Adamson P, Gerst A and Niilisk A 1996 *Appl Surf Sci* **107** 178
[21] Aarik J, Aidla A, Sammelselg V, Siimon H and Uustare T 1996 *J Cryst Growth* **169** 496
[22] Aarik J, Aidla A and Uustare T 1996 *Philos Mag Lett* **73** 115
[23] Aarik J, Aidla A, Kiisler A, Uustare T and Sammelselg V 1997 *Thin Solid Films* **305** 270
[24] Drozd V E, Kopilov N N and Aleskovski V B 1997 *Appl Surf Sci* **112** 258
[25] Aarik J, Aidla A, Sammelselg V and Uustare T 1997 *J Cryst Growth* **181** 259
[26] Siimon H and Aarik J 1997 *J Phys D* **30** 1725
[27] Rosental A, Adamson P, Gerst A, Koppel H and Tarre A 1997 *Appl Surf Sci* **112** 82
[28] Dolgushev N V, Malkov A A, Malygin A A, Suvorov S A, Shchukarev A V, Beljaev A V and Bykov V A 1997 *Thin Solid Films* **293** 91
[29] Lindblad M, Haukka S, Kytökivi A, Lakomaa E, Rautiainen A and Suntola T 1997 *Appl Surf Sci* **121-122** 286
[30] Sammelselg V, Rosental A, Tarre A, Niinistö L, Heiskanen K, Ilmonen K, Johansson L and Uustare T 1998 *Appl Surf Sci* **134** 78
[31] Suisalu A, Aarik J, Mändar H and Sildos I 1998 *Thin Solid Films* **336** 295
[32] Sammelselg V, Aarik J, Aidla A, Kasikov A, Heikinheimo E, Peussa M and Niinistö L 1999 *J Anal At Spectrom* **14** 523
[33] Schrijnemakers K, Impens N R E N and Vansant E F 1999 *Langmuir* **15** 5807
[34] Rosental A, Tarre A, Adamson P, Gerst A, Kasikov A and Niilisk A 1999 *Appl Surf Sci* **142** 204
[35] Matero R, Ritala M, Leskelä M, Salo T, Aromaa J and Forsén O 1999 *J Phys IV France* **09** Pr8-493
[36] Turkovic A 2000 *Mater Sci Eng B* **75** 85
[37] Matero R, Rahtu A, Ritala M, Leskelä M and Sajavaara T 2000 *Thin Solid Films* **368** 1
[38] Aarik J, Aidla A, Mändar H and Sammelselg V 2000 *J Cryst Growth* **220** 531
[39] Cameron M A, Gartland I P, Smith J A, Diaz S F and George S M 2000 *Langmuir* **16** 7435
[40] Matero R, Rahtu A and Ritala M 2001 *Chem Mater* **13** 4506
[41] Aarik J, Aidla A, Mändar H and Uustare T 2001 *Appl Surf Sci* **172** 148
[42] Tarre A, Rosental A, Sammelselg V and Uustare T 2001 *Appl Surf Sci* **175-176** 111
[43] Aarik J, Aidla A, Mändar H, Uustare T, Schuisky M and Hårsta A 2002 *J Cryst Growth* **242** 189
[44] Mitchell D R G, Attard D J and Triani G 2003 *Thin Solid Films* **441** 85
[45] Finnie K S, Triani G, Short K T, Mitchell D R G, Attard D J, Bartlett J R and Barbé C J 2003 *Thin Solid Films* **440** 109
[46] Puurunen R L 2003 *Chemical Vapor Deposition* **9** 327

[47] Ninness B J, Bousfield D W and Tripp C P 2003 *Colloids Surf Physicochem Eng Aspects* **214** 195
[48] Sander M S, Côté M J, Gu W, Kile B M and Tripp C P 2004 *Adv Mater* **16** 2052
[49] Wang X D, Graugnard E, King J S, Wang Z L and Summers C J 2004 *Nano Lett* **4** 2223
[50] Ferguson J D, Yoder A R, Weimer A W and George S M 2004 *Appl Surf Sci* **226** 393
[51] Xiong G, Elam J W, Feng H, Han C Y, Wang H, Iton L E, Curtiss L A, Pellin M J, Kung M, Kung H and Stair P C 2005 *J Phys Chem B* **109** 14059
[52] Wang X D, Neff C, Graugnard E, Ding Y, King J S, Pranger L A, Tannenbaum R, Wang Z L and Summers C J 2005 *Adv Mater* **17** 2103
[53] King J S, Graugnard E and Summers C J 2005 *Adv Mater* **17** 1010
[54] Dueñas S, Castán H, García H, San Andrés E, Toledano-Luque M, Mártil I, González-Díaz G, Kukli K, Uustare T and Aarik J 2005 *Semicond Sci Technol* **20** 1044
[55] King J S, Heineman D, Graugnard E and Summers C J 2005 *Appl Surf Sci* **244** 511
[56] Mitchell D R G, Attard D J, Finnie K S, Triani G, Barbé C J, Depagne C and Bartlett J R 2005 *Appl Surf Sci* **243** 265
[57] Elam J W and Pellin M J 2005 *Anal Chem* **77** 3531
[58] Mitchell D R G, Attard D J and Triani G 2005 *J Cryst Growth* **285** 208
[59] Gu W and Tripp C P 2005 *Langmuir* **21** 211
[60] Lulla M, Asari J, Aarik J, Kukli K, Rammula R, Tapper U, Kauppinen E and Sammelselg V 2006 *Microchim Acta* **155** 195
[61] Losic D, Triani G, Evans P J, Atanacio A, Mitchell J G and Voelcker N H 2006 *J Mater Chem* **16** 4029
[62] Sinha A, Hess D W and Henderson C L 2006 *J Vac Sci Technol B* **24** 2523
[63] Jõgi I, Aarik J, Laan M, Lu J, Kukli K, Käämbre H, Sajavaara T and Uustare T 2006 *Thin Solid Films* **510** 39
[64] Sinha A, Hess D W and Henderson C L 2006 *J Electrochem Soc* **153** G465
[65] Pore V, Heikkilä M, Ritala M, Leskelä M and Areva S 2006 *J Photochem Photobiol A* **177** 68
[66] Mahurin S, Bao L, Yan W, Liang C and Dai S 2006 *J Non Cryst Solids* **352** 3280
[67] King J S, Graugnard E, Roche O M, Sharp D N, Scrimgeour J, Denning R G, Turberfield A J and Summers C J 2006 *Adv Mater* **18** 1561
[68] Ritala M, Kemell M, Lautala M, Niskanen A, Leskelä M and Lindfors S 2006 *Chem Vap Dep* **12** 655
[69] Law M, Greene L E, Radenovic A, Kuykendall T, Liphardt J and Yang P 2006 *J Phys Chem B* **110** 22652
[70] Graugnard E, King J S, Gaillot D P and Summers C J 2006 *Advanced Functional Materials* **16** 1187
[71] Triani G, Evans P J, Attard D J, Prince K E, Bartlett J, Tan S and Burford R P 2006 *J Mater Chem* **16** 1355
[72] Graugnard E, Gaillot D P, Dunham S N, Neff C W, Yamashita T and Summers C J 2006 *Appl Phys Lett* **89** 181108
[73] Kasikov A, Aarik J, Mändar H, Moppel M, Pärs M and Uustare T 2006 *J Phys D* **39** 54
[74] Niilisk A, Moppel M, Pärs M, Sildos I, Jantson T, Avarmaa T, Jaaniso R and Aarik J 2006 *Cent Eur J Phys* **4** 105
[75] Mitchell D R G, Triani G, Attard D J, Finnie K S, Evans P J, Barbé C J and Bartlett J R 2006 *Smart Mater Struct* **15** S57
[76] Triyoso D H, Hegde R I, Wang X -, Stoker M W, Rai R, Ramon M E, White B E and Tobin P J 2006 *J Electrochem Soc* **153** G834
[77] Latella B A, Triani G, Zhang Z, Short K T, Bartlett J R and Ignat M 2007 *Thin Solid Films* **515** 3138
[78] Puurunen R L, Saarilahti J and Kattelus H 2007 *ECS Trans* **11** 3
[79] Greene L E, Law M, Yuhas B D and Yang P 2007 *J Phys Chem C* **111** 18451
[80] Jõgi I, Kukli K, Kemell M, Ritala M and Leskelä M 2007 *J Appl Phys* **102** 114114
[81] Pore V, Ritala M, Leskelä M, Areva S, Järn M and Järnström J 2007 *J Mater Chem* **17** 1361
[82] Fröhlich K, Tapajna M, Rosová A, Dobrocka E, Hušeková K, Aarik J and Aidla A 2008 *Electrochem Solid-State Lett* **11** G19
[83] Mitchell D R G, Triani G and Zhang Z 2008 *Thin Solid Films* **516** 8414
[84] Ng C J W, Gao H and Tan T T Y 2008 *Nanotechnology* **19** 445604
[85] Tan L K, Gao H, Zong Y and Knoll W 2008 *J Phys Chem C* **112** 17576
[86] Tan L K, Chong M A S and Gao H 2008 *J Phys Chem C* **112** 69
[87] Zhang Z, Triani G and Fan L 2008 *J Mater Res* **23** 2472
[88] Cheng H and Chen C 2008 *J Electrochem Soc* **155** D604

[89] Martinson A B F, Elam J W, Liu J, Pellin M J, Marks T J and Hupp J T 2008 *Nano Lett* **8** 2862
[90] Dueñas S, Castán H, García H, Bailón L, Kukli K, Lu J, Ritala M and Leskelä M 2008 *J Non Cryst Solids* **354** 404
[91] Jõgi I, Pärs M, Aarik J, Aidla A, Laan M, Sundqvist J, Oberbeck L, Heitmann J and Kukli K 2008 *Thin Solid Films* **516** 4855
[92] Kawakami H, Ilola R, Straka L, Papula S, Romu J, Hänninen H, Mahlberg R and Heikkilä M 2008 *J Electrochem Soc* **155** C62
[93] Kemell M, Färm E, Ritala M and Leskelä M 2008 *Eur Polym* **44** 3564
[94] Fröhlich K, Aarik J, Ťapajna M, Rosová A, Aidla A, Dobročka E and Hušková K 2009 *J Vac Sci Technol B* **27** 266
[95] Ghosal S, Baumann T F, King J S, Kucheyev S O, Wang Y, Worsley M A, Biener J, Bent S F and Hamza A V 2009 *Chem Mater* **21** 1989
[96] Narayan R J, Monteiro-Riviere N, Brigmon R L, Pellin M J and Elam J W 2009 *JOM* **61** 12
[97] Nevalainen K, Suihkonen R, Eteläaho P, Vuorinen J, Järvelä P, Isomäki N, Hintze C and Leskelä M 2009 *J Vac Sci Technol A* **27** 929
[98] Vilhunen S, Bosund M, Kääriäinen M, Cameron D and Sillanpää M 2009 *Sep Purif Technol* **66** 130
[99] Kumar M K, Tan L K, Gosvami N N and Gao H 2009 *J Phys Chem C* **113** 6381
[100] Cheng H, Hsu C and Chen Y 2009 *J Electrochem Soc* **156** D275
[101] Belyaev A P, Malygin A A, Antipov V V and Rubets V P 2009 *Phys Solid State* **51** 495
[102] Santala E, Kemell M, Leskelä M and Ritala M 2009 *Nanotechnology* **20** 035602
[103] Antipov V V, Belyaev A P, Malygin A A, Rubets V P and Sosnov E A 2009 *Russ J Appl Chem* **81** 2051
[104] Kääriäinen M, Kääriäinen T O and Cameron D C 2009 *Thin Solid Films* **517** 6666
[105] Lu J, Kosuda K M, Van Duyne R P and Stair P C 2009 *J Phys Chem C* **113** 12412
[106] Hwang D, Noh H, Cao H and Chang R P H 2009 *Appl Phys Lett* **95** 091101
[107] Malkov A A, Sosnov E A and Malygin A A 2010 *Russ J Appl Chem* **83** 1511
[108] Guo H, Kemell M, Heikkilä M and Leskelä M 2010 *Appl Catal B* **95** 358
[109] Minton T K, Wu B, Zhang J, Lindholm N F, Abdulagatov A I, O'Patchen J, George S M and Groner M D 2010 *ACS Appl Mater Interfaces* **2** 2515
[110] Peng Q, Tseng Y, Darling S B and Elam J W 2010 *Adv Mater* **22** 5129
[111] Kemell M, Härkönen E, Pore V, Ritala M and Leskelä M 2010 *Nanotechnology* **21** 035301
[112] Cheng H, Hsiao S H and Lu D 2010 *Electrochem Solid-State Lett* **13** D19
[113] Chang Y, Liu C, Tseng Y, Chen C, Chen C and Cheng H 2010 *Nanotechnology* **21** 225602
[114] Tan L K, Kumar M K, An W W and Gao H 2010 *ACS Appl Mater Interfaces* **2** 498
[115] Guo D J, Abdulagatov A I, Rourke D M, Bertness K A, George S M, Lee Y C and Tan W 2010 *Langmuir* **26** 18382
[116] Li W, Auciello O, Premnath R N and Kabius B 2010 *Appl Phys Lett* **96** 162907
[117] Lee W and Hon M 2010 *J Phys Chem C* **114** 6917
[118] Methaapanon R and Bent S F 2010 *J Phys Chem C* **114** 10498
[119] Karuturi S K, Liu L, Su L T, Zhao Y, Fan H J, Ge X, He S and Yoong A T I 2010 *J Phys Chem C* **114** 14843
[120] Aaltonen T, Alnes M, Nilsen O, Costelle L and Fjellvåg H 2010 *J Mater Chem* **20** 2877
[121] Testa G, Huang Y, Zeni L, Sarro P M and Bernini R 2010 *IEEE Photon Technol Lett* **22** 616
[122] Lu S, Tang C, Lin Y, Kuo H, Lai Y, Tsai M, Ouyang H and Hsu W 2010 *Appl Phys Lett* **96** 231915
[123] Kumagai H, Tanaka Y, Murata M, Masuda Y and Shinagawa T 2010 *J Phys : Condens Matter* **22** 474008
[124] Triani G, Campbell J A, Evans P J, Davis J, Latella B A and Burford R P 2010 *Thin Solid Films* **518** 3182
[125] Liu C, Chen C and Cheng H 2011 *Electrochem Solid-State Lett* **14** K33
[126] Biluš Abaffy N, McCulloch D G, Partridge J G, Evans P J and Triani G 2011 *J Appl Phys* **110** 123514
[127] Hudec B, Hušeková K, Tarre A, Han J H, Han S, Rosová A, Lee W, Kasikov A, Song S J, Aarik J, Hwang C S and Fröhlich K 2011 *Microelectron Eng* **88** 1514
[128] Cheng H, Chen Y, Wu W and Hsu C 2011 *Mater Sci Eng B* **176** 596
[129] Wang C, Kei C and Perng T 2011 *Nanotechnology* **22** 365702
[130] Hudec B, Hušeková K, Dobročka E, Aarik J, Rammula R, Kasikov A, Tarre A, Vincze A and Fröhlich K 2011 *J Vac Sci Technol B* **29** 01AC09
[131] Deng Y, Tüysüz H, Henzie J and Yang P 2011 *Small* **7** 2037

[132] Abdulagatov A I, Yan Y, Cooper J R, Zhang Y, Gibbs Z M, Cavanagh A S, Yang R G, Lee Y C and George S M 2011 *ACS Appl Mater Interfaces* **3** 4593
[133] Biener M M, Biener J, Wichmann A, Wittstock A, Baumann T F, Baumer M and Hamza A V 2011 *Nano Lett* **11** 3085
[134] Lee J, Kim D H, Hong S and Jho J Y 2011 *Sensors Actuators B: Chem* **160** 1494
[135] Yanguas-Gil A, Peterson K E and Elam J W 2011 *Chem Mater* **23** 4295
[136] Yang Z, Gao S, Li W, Vlasko-Vlasov V, Welp U, Kwok W and Xu T 2011 *ACS Appl Mater Interfaces* **3** 1101
[137] Wu J, Wu J, Lee K, Hsu W and Lin S 2011 *J Mater Chem* **21** 11730
[138] Korhonen J T, Hiekkataipale P, Malm J, Karppinen M, Ikkala O and Ras R H 2011 *ACS Nano* **5** 1967
[139] Wei Y, Liu H, Sheng O, Liu Z, Chen S and Yang L 2011 *Appl Opt* **50** 4720
[140] Liu L, Karuturi S K, Su L T, Wang Q and Tok A I Y 2011 *Electrochem Commun* **13** 1163
[141] Lee J and Jho J Y 2011 *Sol Energy Mater Sol Cells* **95** 3152
[142] Marin E, Lanzutti A, Guzman L and Fedrizzi L 2011 *J Coat Technol* **8** 655
[143] Kumagai H, Masuda Y and Shinagawa T 2011 *J Cryst Growth* **314** 146
[144] Puurunen R L, Sajavaara T, Santala E, Miikkulainen V, Saukkonen T, Laitinen M and Leskelä M 2011 *J Nanosci Nanotechnol* **11** 8101
[145] Kumar M K, Krishnamoorthy S, Tan L K, Chiam S Y, Tripathy S and Gao H 2011 *ACS Catal* **1** 300
[146] Kalanyan B and Parsons G 2011 *ECS Trans* **41** 285
[147] Jalkanen P, Kulju S, Arutyunov K, Antila L, Myllyperkioe P, Ihalainen T, Kääriäinen T, Kääriäinen M and Korppi-Tommola J 2011 *Thin Solid Films* **519** 3835
[148] Wang C, Kei C and Perng T 2011 *Nanotechnology* **22** 365702/1
[149] Lee H and Bent S F 2011 *Chem Mater* **24** 279
[150] Vapaavuori J, Valtavirta V, Alasaarela T, Mamiya J, Priimagi A, Shishido A and Kaivola M 2011 *J Mater Chem* **21** 15437
[151] Lee W, Hon M, Chung Y and Lee J 2011 *Jpn J Appl Phys* **50** 06GH06
[152] Tan L K, Liu X and Gao H 2011 *J Mater Chem* **21** 11084
[153] Lee J, Hon M, Chung Y and Leu I 2011 *Applied Physics A* **102** 545
[154] Lee W and Hon M 2011 *Appl Phys Lett* **99** 251102
[155] Liu L, Karuturi S K, Su L T and Tok A I Y 2011 *Energy Environ Sci* **4** 209
[156] Liu C, Chen C and Cheng H 2011 *J Electrochem Soc* **158** K58
[157] Saleem M R, Stenberg P, Alasaarela T, Silfsten P, Khan M B, Honkanen S and Turunen J 2011 *Opt Express* **19** 24241
[158] Sanjo Y, Murata M, Tanaka Y, Kumagai H and Chigane M 2011 *Proc SPIE* **7922** 79220L/1
[159] Liang Y C, Wang C C, Kei C C, Hsueh Y C, Cho W H and Perng T P 2011 *J Phys Chem C* **115** 9498
[160] Liu Z, Wei Y, Chen S, Luo J and Ma P 2011 *Proc SPIE* **8190** 81900C/1
[161] Wang W, Tian M, Abdulagatov A, George S M, Lee Y and Yang R 2012 *Nano Lett* **12** 655
[162] Lee H and Bent S F 2012 *Chem Mater* **24** 279
[163] Sundberg P, Sood A, Liu X, Johansson L and Karppinen M 2012 *Dalton Trans* **41** 10731
[164] Sun X, Xie M, Wang G, Sun H, Cavanagh A S, Travis J J, George S M and Lian J 2012 *J Electrochem Soc* **159** A364
[165] Jensen L O, Maedebach H, Maula J, Guertler K and Ristau D 2012 *Proc SPIE* **8530** 853010
[166] Li X, Hu H, Li D, Shen Z, Xiong Q, Li S and Fan H J 2012 *ACS Appl Mater Interfaces* **4** 2180
[167] Campbell J A, de Borniol M, Mozer A J, Evans P J, Burford R P and Triani G 2012 *J Vac Sci Technol , A* **30** 01A157/1
[168] Kääriäinen M and Cameron D C 2012 *Surf Sci* **606** L22
[169] Ao X, Tong X, Kim D S, Zhang L, Knez M, Mueller F, He S and Schmidt V 2012 *Appl Phys Lett* **101** 111901/1
[170] Kukli K, Aarik J, Aidla A, Jogi I, Arroval T, Lu J, Sajavaara T, Laitinen M, Kiisler A, Ritala M, Leskelä M, Peck J, Natwora J, Geary J, Spohn R, Meiere S and Thompson D M 2012 *Thin Solid Films* **520** 2756
[171] Baca A I, Brown J J, Bertness K A and Bright V M 2012 *Nanotechnology* **23** 245301/1
[172] Chang Y, Liu C, Chen C, Cheng H and Lu T 2012 *J Electrochem Soc* **159** K136
[173] Jiang C Y, Koh W L, Leung M Y, Chiam S Y, Wu J S and Zhang J 2012 *Appl Phys Lett* **100** 113901
[174] Sanjo Y, Murata M, Tanaka Y, Kumagai H and Chigane M 2012 *J Laser Micro/Nanoeng* **7** 375

[175] Purniawan A, Pandraud G, Moh T S Y, Marthen A, Vakalopoulos K A, French P J and Sarro P M 2012 *Sens Actuators A* **188** 127
[176] Miranda E, Sune J, Das T, Mahata C and Maiti C K 2012 *J Appl Phys* **112** 064113/1
[177] Mahata C, Mallik S, Das T, Maiti C K, Dalapati G K, Tan C C, Chia C K, Gao H, Kumar M K, Chiam S Y, Tan H R, Seng H L, Chi D Z and Miranda E 2012 *Appl Phys Lett* **100** 062905
[178] Liu Z, Chen S, Ma P, Wei Y, Zheng Y, Pan F, Liu H and Tang G 2012 *Opt Express* **20** 854
[179] Chang Y, Liu C, Chen C and Cheng H 2012 *J Electrochem Soc* **159** D401
[180] Chang Y, Liu C, Chen C and Cheng H 2012 *Nanoscale Res Lett* **7** 231
[181] Saleem M R, Zheng D, Bai B, Stenberg P, Kuittinen M, Honkanen S and Turunen J 2012 *Opt Express* **20** 16974
[182] Saleem M R, Silfsten P, Honkanen S and Turunen J 2012 *Thin Solid Films* **520** 5442
[183] Hwang Y J, Hahn C, Liu B and Yang P 2012 *ACS Nano* **6** 5060
[184] Huang Y, Pandraud G and Sarro P M 2012 *Nanotechnology* **23** 485306
[185] Luo J, Karuturi S K, Liu L, Su L T, Tok A I Y and Fan H J 2012 *Sci Rep* **2** 451
[186] Aarik J, Hudec B, Husekova K, Rammula R, Kasikov A, Arroval T, Uustare T and Frohlich K 2012 *Semicond Sci Technol* **27** 074007/1
[187] Roy A K, Schulze S, Hietschold M and Goedel W A 2012 *Carbon* **50** 761
[188] Cheng C, Karuturi S K, Liu L, Liu J, Li H, Su L T, Tok A I Y and Fan H J 2012 *Small* **8** 37
[189] Frohlich K, Hudec B, Tapajna M, Husekova K, Rosova A, Elias P, Aarik J, Rammula R, Kasikov A, Arroval T, Aarik L, Murakami K, Rommel M and Bauer A J 2012 *ECS Trans* **50** 79
[190] Marin E, Lanzutti A, Guzman L and Fedrizzi L 2012 *J Coat Technol Res* **9** 347
[191] Phillips R, Hansen P and Eisenbraun E 2012 *J Vac Sci Technol , A* **30** 01A125
[192] Erdmanis M, Karvonen L, Saleem M R, Ruoho M, Pale V, Tervonen A, Honkanen S and Tittonen I 2012 *J Lightwave Technol* **30** 2488
[193] Gong B, Kim D H and Parsons G N 2012 *Langmuir* **28** 11906
[194] Marin E, Guzman L, Lanzutti A, Ensinger W and Fedrizzi L 2012 *Thin Solid Films* **522** 283
[195] Marin E, Lanzutti A, Lekka M, Guzman L, Ensinger W and Fedrizzi L 2012 *Surf Coat Technol* **211** 84
[196] Dalapati G K, Wong T K S, Li Y, Chia C K, Das A, Mahata C, Gao H, Chattopadhyay S, Kumar M K, Seng H L, Maiti C K and Chi D Z 2012 *Nanoscale Res Lett* **7** 99, 8
[197] Luo J, Xia X, Luo Y, Guan C, Liu J, Qi X, Ng C F, Yu T, Zhang H and Fan H J 2013 *Adv Energy Mater* **3** 737
[198] Luka G, Witkowski B S, Wachnicki L, Andrzejczuk M, Lewandowska M and Godlewski M 2013 *CrystEngComm* **15** 9949
[199] Prasittichai C, Avila J R, Farha O K and Hupp J T 2013 *J Am Chem Soc* **135** 16328
[200] Huang Y, Pandraud G and Sarro P M 2013 *J Vac Sci Technol , A* **31** 01A148
[201] Kargar A, Sun K, Jing Y, Choi C, Jeong H, Jung G Y, Jin S and Wang D 2013 *ACS Nano* **7** 9407
[202] Lei Y, Lu J, Zhao H, Liu B, Low K, Wu T, Libera J A, Greeley J P, Chupas P J, Miller J T and Elam J W 2013 *J Phys Chem C* **117** 11141
[203] Kim D H, Woodroof M, Lee K and Parsons G N 2013 *ChemSusChem* **6** 1014
[204] Lee M, Su C, Lin Y, Liao S, Chen J, Perng T, Yeh J and Shih H C 2013 *J Power Sources* **244** 410
[205] Lin Z, Jiang C, Zhu C and Zhang J 2013 *ACS Appl Mater Interfaces* **5** 713
[206] Tarre A, Moldre K, Niilisk A, Mandar H, Aarik J and Rosental A 2013 *J Vac Sci Technol , A* **31** 01A118
[207] Yu I, Wang Y, Cheng H, Yang Z and Lin C 2013 *Int J Photoenergy* 431614
[208] McDonnell S, Longo R C, Seitz O, Ballard J B, Mordi G, Dick D, Owen J H G, Randall J N, Kim J, Chabal Y J, Cho K and Wallace R M 2013 *J Phys Chem C* **117** 20250
[209] Guo H, Chen H, Zhang X, Zhang P, Liu J, Liu H and Cui Y 2013 *Opt Eng* **52** 063402
[210] Chang Y, Liu C, Cheng H and Chen C 2013 *ACS Appl Mater Interfaces* **5** 3549
[211] Yin J, Xu Q, Wang Z, Yao X and Wang Y 2013 *J Mater Chem C* **1** 1029
[212] McClure C D, Oldham C J, Walls H J and Parsons G N 2013 *J Vac Sci Technol , A* **31** 061506
[213] Yang J, Tong L, Yang Y, Chen X, Huang J, Chen R and Wang Y 2013 *J Mater Chem C* **1** 5133
[214] Szilagyi I M, Santala E, Heikkila M, Pore V, Kemell M, Nikitin T, Teucher G, Firkala T, Khriachtchev L, Rasanen M, Ritala M and Leskela M 2013 *Chem Vap Deposition* **19** 149
[215] Munoz-Rojas D, Sun H, Iza D C, Weickert J, Chen L, Wang H, Schmidt-Mende L and MacManus-Driscoll J L 2013 *Prog Photovoltaics* **21** 393
[216] Sun X, Xie M, Travis J J, Wang G, Sun H, Lian J and George S M 2013 *J Phys Chem C* **117** 22497

[217] Biener M M, Biener J, Wang Y M, Shin S J, Tran I C, Willey T M, Perez F N, Poco J F, Gammon S A, Fournier K B, van Buuren A W, Satcher J H and Hamza A V 2013 *ACS Appl Mater Interfaces* **5** 13129
[218] Saleem M R, Honkanen S and Turunen J 2013 *Proc SPIE* **8613** 86130C
[219] Hanson K, Losego M D, Kalanyan B, Parsons G N and Meyer T J 2013 *Nano Lett* **13** 4802
[220] Shi X, Ueno K, Oshikiri T and Misawa H 2013 *J Phys Chem C* **117** 24733
[221] Xia X, Zeng Z, Li X, Zhang Y, Tu J, Fan N C, Zhang H and Fan H J 2013 *Nanoscale* **5** 6040
[222] Alasaarela T, Karvonen L, Jussila H, Saynatjoki A, Mehravar S, Norwood R A, Peyghambarian N, Kieu K, Tittonen I and Lipsanen H 2013 *Opt Lett* **38** 3980
[223] Wang Q, Wang X, Wang Z, Huang J and Wang Y 2013 *J Membr Sci* **442** 57
[224] Erdmanis M, Karvonen L, Saynatjoki A, Tu X, Liow T Y, Lo Q G, Vanska O, Honkanen S and Tittonen I 2013 *Opt Express* **21** 9974
[225] Erdmanis M, Karvonen L, Saynatjoki A, Honkanen S and Tittonen I 2013 *Proc SPIE* **8629** 86291J
[226] Park I, Leem J, Lee H and Min Y 2013 *Bull Korean Chem Soc* **34** 519
[227] Delapati G K, Chia C K, Mahata C, Krishnamoorthy S, Tan C C, Tan H R, Maiti C K and Chi D 2013 *IEEE Trans Electron Devices* **60** 192
[228] Peng Q, Kalanyan B, Hoertz P G, Miller A, Kim D H, Hanson K, Alibabaei L, Liu J, Meyer T J, Parsons G N and Glass J T 2013 *Nano Lett* **13** 1481
[229] Vannucci A K, Alibabaei L, Losego M D, Concepcion J J, Kalanyan B, Parsons G N and Meyer T J 2013 *Proc Natl Acad Sci USA* **110** 20918
[230] Phillips R, O'Toole A, He X, Hansen R, Geer R and Eisenbraun E 2013 *J Mater Res* **28** 461
[231] Alibabaei L, Brennaman M K, Norris M R, Kalanyan B, Song W, Losego M D, Concepcion J J, Binstead R A, Parsons G N and Meyer T J 2013 *Proc Natl Acad Sci U S A* **110** 20008
[232] Saleem M R, Ali R, Honkanen S and Turunen J 2013 *Thin Solid Films* **542** 257
[233] Ban C, Xie M, Sun X, Travis J J, Wang G, Sun H, Dillon A C, Lian J and George S M 2013 *Nanotechnology* **24** 424002
[234] Song S, Song Z, Peng C, Gao L, Gu Y, Zhang Z, Lv Y, Yao D, Wu L and Liu B 2013 *Nanoscale Res Lett* **8** 77
[235] Chen H, Guo H, Zhang P, Zhang X, Liu H, Wang S and Cui Y 2013 *Appl Phys Express* **6** 022101/1
[236] Rosental A, Tarre A, Gerst A, Kasikov A, Lu J, Ottosson M and Uustare T 2013 *IEEE Sens J* **13** 1648
[237] Shi J, Li Z, Kvit A, Krylyuk S, Davydov A V and Wang X 2013 *Nano Lett* **13** 5727
[238] Chang W, Hsueh Y, Huang S, Liu K, Kei C and Perng T 2013 *J Mater Chem A* **1** 1987
[239] Suh D, Choi D and Weber K J 2013 *J Appl Phys* **114** 154107
[240] Niemelä J, Yamauchi H and Karppinen M 2014 *Thin Solid Films* **551** 19
[241] Guan C, Wang X, Zhang Q, Fan Z, Zhang H and Fan H J 2014 *Nano Lett* **14** 4852
[242] Rao Z, Wan J, Li C, Chen B, Liu J, Huang C and Xia Y 2014 *Plasma Sci Technol* **16** 239
[243] Ren W, Zhang H, Kong D, Liu B, Yang Y and Cheng C 2014 *Phys Chem Chem Phys* **16** 22953
[244] Chervinskii S, Matikainen A, Honkanen S, Dergachev A and Lipovskii A A 2014 *Nanoscale Res Lett* **9** 398
[245] Lyytinen J, Berdova M, Franssila S and Koskinen J 2014 *J Vac Sci Technol , A* **32** 01A102
[246] Chen H, Chen P, Huang S and Perng T 2014 *Chem Commun (Cambridge, U K)* **50** 4379
[247] Chen H, Chen P, Kuo J, Hsueh Y and Perng T 2014 *RSC Adv* **4** 40482
[248] Rao Z, Liu B, Li C, Xia Y and Wan J 2014 *Rare Met (Beijing, China)* **33** 583
[249] Mukherjee C, Das T, Mahata C, Maiti C K, Chia C K, Chiam S Y, Chi D Z and Dalapati G K 2014 *ACS Appl Mater Interfaces* **6** 3263
[250] Murakami K, Rommel M, Hudec B, Rosova A, Husekova K, Dobrocka E, Rammula R, Kasikov A, Han J H, Lee W, Song S J, Paskaleva A, Bauer A J, Frey L, Froehlich K, Aarik J and Hwang C S 2014 *ACS Appl Mater Interfaces* **6** 2486
[251] Roussey M, Descrovi E, Hyrinen M, Angelini A, Kuittinen M and Honkanen S 2014 *Opt Express* **22** 27236
[252] Lyytinen J, Berdova M, Hirvonen P, Liu X W, Franssila S, Zhou Q and Koskinen J 2014 *RSC Adv* **4** 37320
[253] Saha D, Ajimsha R S, Rajiv K, Mukherjee C, Gupta M, Misra P and Kukreja L M 2014 *Appl Surf Sci* **315** 116
[254] Eustache E, Tilmant P, Morgenroth L, Roussel P, Patriarche G, Troadec D, Rolland N, Brousse T and Lethien C 2014 *Adv Energy Mater* **4** 1301612/1
[255] Shao D, Sun H, Xin G, Lian J and Sawyer S 2014 *Appl Surf Sci* **314** 872

[256] Qiu J, Zeng G, Pavaskar P, Li Z and Cronin S B 2014 *Phys Chem Chem Phys* **16** 3115
[257] Hansen P, Fjellvag H, Finstad T G and Nilsen O 2014 *Chem Vap Deposition* **20** 274
[258] Chua Y P G, Gunasooriya G T K K, Saeys M and Seebauer E G 2014 *J Catal* **311** 306
[259] Hansen P, Fjellvag H, Finstad T G and Nilsen O 2014 *RSC Adv* **4** 11876
[260] Saleem M R, Honkanen S and Turunen J 2014 *IOP Conf Ser : Mater Sci Eng* **60** 012008/1
[261] Saleem M R, Honkanen S and Turunen J 2014 *Proc SPIE* **8974** 897417
[262] Leem J, Park I, Li Y, Zhou W, Jin Z, Shin S and Min Y 2014 *Bull Korean Chem Soc* **35** 1195
[263] Longo R C, McDonnell S, Dick D, Wallace R M, Chabal Y J, Owen J H G, Ballard J B, Randall J N and Cho K 2014 *J Vac Sci Technol , B* **32** 03D112
[264] Bagge-Hansen M, Wichmann A, Wittstock A, Lee J R I, Ye J, Willey T M, Kuntz J D, van Buuren T, Biener J, Baumer M and Biener M M 2014 *J Phys Chem C* **118** 4078
[265] Aarik L, Arroval T, Rammula R, Mandar H, Sammelselg V, Hudec B, Husekova K, Frohlich K and Aarik J 2014 *Thin Solid Films* **565** 19
[266] Berdova M, Ylitalo T, Kassamakov I, Heino J, Torma P T, Kilpi L, Ronkainen H, Koskinen J, Haeggstrom E and Franssila S 2014 *Acta Mater* **66** 370
[267] Lei Y, Liu B, Lu J, Libera J A, Greeley J P and Elam J W 2014 *J Phys Chem C* **118** 22611
[268] Scuderi V, Impellizzeri G, Privitera V, Romano L, Scuderi M, Nicotra G, Bergum K, Svensson B G and Irrera A 2014 *Nanoscale Res Lett* **9** 458
[269] Alibabaei L, Farnum B H, Kalanyan B, Brennaman M K, Losego M D, Parsons G N and Meyer T J 2014 *Nano Lett* **14** 3255
[270] Turkevych I, Kosar S, Pihosh Y, Mawatari K, Kitamori T, Ye J and Shimamura K 2014 *J Ceram Soc Jpn* **122** 393
[271] Arroval T, Aarik L, Rammula R, Maendar H, Aarik J, Hudec B, Husekova K and Froehlich K 2014 *Phys Status Solidi A* **211** 425
[272] Li Z, Yao C, Wang F, Cai Z and Wang X 2014 *Nanotechnology* **25** 504005
[273] Singh A, Nehm F, Mueller-Meskamp L, Hossbach C, Albert M, Schroeder U, Leo K and Mikolajick T 2014 *Org Electron* **15** 2587
[274] Lee J, Jackson D H K, Li T, Winans R E, Dumesic J A, Kuech T F and Huber G W 2014 *Energy Environ Sci* **7** 1657
[275] Lee G, Katiyar R S, Lai B, Phatak C and Auciello O 2014 *MRS Commun* **4** 67
[276] Sintonen S, Ali S, Ylivaara O M E, Puurunen R L and Lipsanen H 2014 *J Vac Sci Technol , A* **32** 01A111
[277] Atanasov S E, Oldham C J, Slusarski K A, Taggart-Scarff J, Sherman S A, Senecal K J, Filocamo S F, McAllister Q P, Wetzel E D and Parsons G N 2014 *J Mater Chem A* **2** 17371
[278] Song W, Vannucci A K, Farnum B H, Lapides A M, Brennaman M K, Kalanyan B, Alibabaei L, Concepcion J J, Losego M D, Parsons G N and Meyer T J 2014 *J Am Chem Soc* **136** 9773
[279] Zeng G, Qiu J, Li Z, Pavaskar P and Cronin S B 2014 *ACS Catal* **4** 3512
[280] Lee J W, Lee J, Kim C, Cho C and Moon J H 2014 *Sci Rep* **4** 6804
[281] Suh D and Weber K 2014 *Phys Status Solidi RRL* **8** 40
[282] Kraus T J, Nepomnyashchii A B and Parkinson B A 2014 *ACS Appl Mater Interfaces* **6** 9946
[283] Kim D H, Losego M D, Hanson K, Alibabaei L, Lee K, Meyer T J and Parsons G N 2014 *Phys Chem Chem Phys* **16** 8615
[284] Xue Z, Jiang C, Wang L, Liu W and Liu B 2014 *J Phys Chem C* **118** 16352
[285] Wang W, Wen H, Cheng C, Hung C, Chou W, Yau W, Yang P and Lai Y 2014 *Microelectron Reliab* **54** 2754
[286] Jukk K, Kongi N, Tarre A, Rosental A, Treshchalov A B, Kozlova J, Ritslaid P, Matisen L, Sammelselg V and Tammeveski K 2014 *J Electroanal Chem* **735** 68
[287] Chen G, Yeh C, Yeh M, Ho S and Chen H 2015 *Chem Commun* **51** 14750
[288] Suh D 2015 *Phys Status Solidi RRL* **9** 344
[289] Ismagilov R R, Tuyakova F T, Kleshch V I, Obraztsova E A and Obraztsov A N 2015 *Phys Status Solidi C* **12** 1022
[290] Iatsunskyi I, Kempinski M, Nowaczyk G, Jancelewicz M, Pavlenko M, Zaleski K and Jurga S 2015 *Appl Surf Sci* **347** 777
[291] Qiu J, Zeng G, Ha M, Hou B, Mecklenburg M, Shi H, Alexandrova A N and Cronin S B 2015 *Chem Mater* **27** 7977
[292] Su C, Wang C, Hsueh Y, Gurylev V, Kei C and Perng T 2015 *Nanoscale* **7** 19222

[293] Qiu J, Zeng G, Ha M, Ge M, Lin Y, Hettick M, Hou B, Alexandrova A N, Javey A and Cronin S B 2015 *Nano Lett* **15** 6177
[294] Sweet W J and Parsons G N 2015 *Langmuir* **31** 7274
[295] Cameron D C, Krumpolec R, Ivanova T V, Homola T and Cernak M 2015 *Appl Surf Sci* **345** 216
[296] Buchalska M, Surowka M, Hamalainen J, Iivonen T, Leskela M and Macyk W 2015 *Catal Today* **252** 14
[297] Tian M, Wang W, Liu Y, Jungjohann K L, Thomas Harris C, Lee Y and Yang R 2015 *Nano Energy* **11** 500
[298] Lewis R, Liew L, Xu S, Lee Y and Yang R 2015 *Sci Bull* **60** 701
[299] Iatsunskyi I, Jancelewicz M, Nowaczyk G, Kempinski M, Peplinska B, Jarek M, Zaleski K, Jurga S and Smyntyna V 2015 *Thin Solid Films* **589** 303
[300] Cho H, Chen M V, MacRae A C and Meng Y S 2015 *ACS Appl Mater Interfaces* **7** 16231
[301] Lyytinen J, Liu X, Ylivaara O M E, Sintonen S, Iyer A, Ali S, Julin J, Lipsanen H, Sajavaara T, Puurunen R L and Koskinen J 2015 *Wear* **342-343** 270
[302] Ubnoske S M, Peng Q, Meshot E R, Parker C B and Glass J T 2015 *J Phys Chem C* **119** 26119
[303] Hoshian S, Jokinen V, Hjort K, Ras R H A and Franssila S 2015 *ACS Appl Mater Interfaces* **7** 15593
[304] Iatsunskyi I, Coy E, Viter R, Nowaczyk G, Jancelewicz M, Baleviciute I, Zaleski K and Jurga S 2015 *J Phys Chem C* **119** 20591
[305] Ali R, Saleem M R, Paakkonen P and Honkanen S 2015 *Nanomaterials* **5** 792
[306] Mann H S, Lang B N, Schwab Y, Niemelä J, Karppinen M and Scarel G 2015 *J Vac Sci Technol , A* **33** 01A124
[307] Niemelä J and Karppinen M 2015 *Dalton Trans* **44** 591
[308] Kraus T J, Nepomnyashchii A B and Parkinson B A 2015 *J Vac Sci Technol , A* **33** 01A135
[309] Marin E, Lanzutti A, Paussa L, Guzman L and Fedrizzi L 2015 *Mater Corros* **66** 907
[310] Al-Haddad A, Wang Z, Xu R, Qi H, Vellacheri R, Kaiser U and Lei Y 2015 *J Phys Chem C* **119** 16331
[311] Niemelä J, Hirose Y, Hasegawa T and Karppinen M 2015 *Appl Phys Lett* **106** 042101
[312] Ahmadzada T, McKenzie D R, James N L, Yin Y and Li Q 2015 *Thin Solid Films* **591** 131
[313] Liu K, Su C and Perng T 2015 *RSC Adv* **5** 88367
[314] Knauf R R, Kalanyan B, Parsons G N and Dempsey J L 2015 *J Phys Chem C* **119** 28353
[315] Niemelä J, Hirose Y, Shigematsu K, Sano M, Hasegawa T and Karppinen M 2015 *Appl Phys Lett* **107** 192102
[316] Liu H F, Wang Y D, Lin M, Ong L T, Tee S Y and Chi D Z 2015 *RSC Adv* **5** 48647
[317] Iatsunskyi I, Pavlenko M, Viter R, Jancelewicz M, Nowaczyk G, Baleviciute I, Zaleski K, Jurga S, Ramanavicius A and Smyntyna V 2015 *J Phys Chem C* **119** 7164
[318] Gieraltowska S, Wachnicki L, Witkowski B S, Mroczynski R, Dluzewski P and Godlewski M 2015 *Thin Solid Films* **577** 97
[319] Cordova I A, Peng Q, Ferrall I L, Rieth A J, Hoertz P G and Glass J T 2015 *Nanoscale* **7** 12226
[320] Kim H J, Jackson D H K, Lee J, Guan Y, Kuech T F and Huber G W 2015 *ACS Catal* **5** 3463
[321] Yao Z, Wang C, Li Y and Kim N 2015 *Nanoscale Res Lett* **10** 1
[322] Ye J, Baumgaertel A C, Wang Y M, Biener J and Biener M M 2015 *ACS Nano* **9** 2194
[323] Luka G, Wachnicki L, Jakiela R and Lusakowska E 2015 *J Phys D* **48** 495305
[324] Gurylev V, Su C and Perng T 2015 *J Catal* **330** 177
[325] Tian L, Soum-Glaude A, Volpi F, Salvo L, Berthome G, Coindeau S, Mantoux A, Boichot R, Lay S, Brize V, Blanquet E, Giusti G and Bellet D 2015 *J Vac Sci Technol A* **33** 01A141
[326] Zeng G, Qiu J, Hou B, Shi H, Lin Y, Hettick M, Javey A and Cronin S B 2015 *Chem Eur J* **21** 13502
[327] Zhan Z, Xu R, Mi Y, Zhao H and Lei Y 2015 *ACS Nano* **9** 4583
[328] Zhang H, Zhang D, Qin X and Cheng C 2015 *J Phys Chem C* **119** 27875
[329] Zhang H, Ren W and Cheng C 2015 *Nanotechnology* **26** 1
[330] Zhang H, Shuang S, Wang G, Guo Y, Tong X, Yang P, Chen A, Dong C and Qin Y 2015 *RSC Adv* **5** 4343
[331] Zhang W, Dong J, Li C, Chen S, Zhan C, Panneerselvam R, Yang Z, Li J and Zhou Y 2015 *J Raman Spectrosc* **46** 1200
[332] Kim J, Kang J S, Shin J, Kim J, Han S, Park J, Min Y, Ko M J and Sung Y 2015 *Nanoscale* **7** 8368
[333] Zhu Z, Liu B, Zhang H, Ren W, Cheng C, Wu S, Gu M and Chen H 2015 *Opt Express* **23** 7085
[334] Kumagai H, Matsumoto M, Kawamura Y, Toyoda K and Obara M 1994 *Jpn J Appl Phys* **33** 7086
[335] Kumagai H, Matsumoto M, Toyoda K, Obara M and Suzuki M 1995 *Thin Solid Films* **263** 47

[336] Kumagai H, Toyoda K, Kobayashi K, Obara M and Iimura Y 1997 *Appl Phys Lett* **70** 2338
[337] King D M, Zhou Y, Hakim L F, Liang X, Li P and Weimer A W 2009 *Ind Eng Chem Res* **48** 352
[338] Liang X, Lynn A D, King D M, Bryant S J and Weimer A W 2009 *ACS Appl Mater Interfaces* **1** 1988
[339] Zhou Y, King D M, Li J, Barrett K S, Goldfarb R B and Weimer A W 2010 *Ind Eng Chem Res* **49** 6964
[340] Liang X and Patel R L 2014 *Ceram Int* **40** 3097
[341] Aarik J, Arroval T, Aarik L, Rammula R, Kasikov A, Mandar H, Hudec B, Husekova K and Frohlich K 2013 *J Cryst Growth* **382** 61
[342] Aarik L, Arroval T, Rammula R, Mandar H, Sammelselg V and Aarik J 2013 *Thin Solid Films* **542** 100
[343] Moldre K, Aarik L, Mandar H, Niilisk A, Rammula R, Tarre A and Aarik J 2015 *J Cryst Growth* **428** 86
[344] Kubala N G, Rowlette P C and Wolden C A 2009 *J Phys Chem C* **113** 16307
[345] Kubala N G and Wolden C A 2010 *Thin Solid Films* **518** 6733
[346] Hudec B, Husekova K, Rosova A, Soltys J, Rammula R, Kasikov A, Uustare T, Micusik M, Omastova M, Aarik J and Frohlich K 2013 *J Phys D: Appl Phys* **46** 385304
[347] Sammelselg V, Tarre A, Lu J, Aarik J, Niilisk A, Uustare T, Netšipailo I, Rammula R, Pärna R and Rosental A 2010 *Surf Coat Technol* **204** 2015
[348] Aarik J, Aidla A, Uustare T, Kukli K, Sammelselg V, Ritala M and Leskelä M 2002 *Appl Surf Sci* **193** 277
[349] Rooth M, Quinlan R A, Widenkvist E, Lu J, Grennberg H, Holloway B C, Hårsta A and Jansson U 2009 *J Cryst Growth* **311** 373
[350] Soroka I L, Rooth M, Lu J, Boman M, Svedlindh P, Carlsson J and Hårsta A 2009 *J Appl Phys* **106** 084313
[351] Wang H and Wang F 2013 *J Power Sources* **233** 1
[352] Kukli K, Ritala M, Schuisky M, Leskelä M, Sajavaara T, Keinonen J, Uustare T and Hårsta A 2000 *Chem Vap Deposition* **6** 303
[353] Kukli K, Aidla A, Aarik J, Schuisky M, Hårsta A, Ritala M and Leskelä M 2000 *Langmuir* **16** 8122
[354] Schuisky M, Hårsta A, Aidla A, Kukli K, Kiisler A and Aarik J 2000 *J Electrochem Soc* **147** 3319
[355] Schuisky M, Aarik J, Kukli K, Aidla A and Hårsta A 2001 *Langmuir* **17** 5508
[356] Schuisky M, Kukli K, Aarik J, Lu J and Hårsta A 2002 *J Cryst Growth* **235** 293
[357] Pore V, Kivelä T, Ritala M and Leskelä M 2008 *Dalton Trans* 6467
[358] Döring H, Hashimoto K and Fujishima A 1992 *Ber Bunsen-Ges Phys Chem* **96** 620
[359] Ritala M, Leskelä M, Niinistö L and Haussalo P 1993 *Chem Mater* **5** 1174
[360] Aarik J, Aidla A, Uustare T, Ritala M and Leskelä M 2000 *Appl Surf Sci* **161** 385
[361] Rahtu A and Ritala M 2002 *Chem Vap Deposition* **8** 21
[362] Lim J W, Yun S J and Lee J H 2004 *Electrochem Solid-State Lett* **7** F73
[363] Lim J W and Yun S J 2004 *Electrochem Solid-State Lett* **7** H33
[364] Seo E K, Lee J W, Sung-Suh H and Sung M M 2004 *Chem Mater* **16** 1878
[365] Jeong D K, Park N H, Jung S H, Jung W G, Shin H, Lee J G and Kim J Y 2004 *Mater Sci Forum* **449-452** 1165
[366] Shin H, Jeong D, Lee J, Sung M M and Kim J 2004 *Adv Mater* **16** 1197
[367] Jeong D, Lee J, Shin H, Lee J, Kim J and Sung M 2004 *J Korean Phys Soc* **45** 1249
[368] Kim W D, Hwang G W, Kwon O S, Kim S K, Cho M, Jeong D S, Lee S W, Seo M H, Hwang C S, Min Y and Cho Y J 2005 *J Electrochem Soc* **152** C552
[369] Park K S, Seo E K, Do Y R, Kim K and Sung M M 2006 *J Am Chem Soc* **128** 858
[370] Sinha A, Hess D W and Henderson C L 2006 *Electrochem Solid-State Lett* **9** G330
[371] Kim S K, Hwang G W, Kim W and Hwang C S 2006 *Electrochem Solid-State Lett* **9** F5
[372] Knez M, Kadri A, Wege C, Gösele U, Jeske H and Nielsch K 2006 *Nano Lett* **6** 1172
[373] Qiu S and Starr T L 2007 *J Electrochem Soc* **154** H472
[374] Watanabe T, Hoffmann-Eifert S, Yang L, Rüdiger A, Kügeler C, Hwang C S and Waser R 2007 *J Electrochem Soc* **154** G134
[375] Chen X, Knez M, Berger A, Nielsch K, Gösele U and Steinhart M 2007 *Angew Chem , Int Ed* **46** 6829
[376] Ko C H and Lee W 2007 *J Solid State Electrochem* **11** 1391
[377] Lee B H, Ryu M K, Choi S, Lee K, Im S and Sung M M 2007 *J Am Chem Soc* **129** 16034
[378] Shan C X, Hou X, Choy K and Choquet P 2008 *Surf Coat Technol* **202** 2147
[379] Qin Y, Liu L, Yang R, Gösele U and Knez M 2008 *Nano Lett* **8** 3221
[380] Langner A, Knez M, Müller F and Gösele U 2008 *Appl Phys A: Mater Sci Process* **93** 399

[381] Bae C, Kim S, Ahn B, Kim J, Sung M M and Shin H 2008 *J Mater Chem* **18** 1362
[382] Shan C X, Hou X and Choy K 2008 *Surf Coat Technol* **202** 2399
[383] King D M, Liang X, Zhou Y, Carney C S, Hakim L F, Li P and Weimer A W 2008 *Powder Technol* **183** 356
[384] Xie Q, Musschoot J, Deduytsche D, Van Meirhaeghe R L, Detavernier C, Van den Berghe S, Jiang Y, Ru G, Li B and Qu X 2008 *J Electrochem Soc* **155** H688
[385] Lee B H, Lee K H, Im S and Sung M M 2008 *Org Electron* **9** 1146
[386] Kim G, Lee S, Michler G H, Roggendorf H, Gösele U and Knez M 2008 *Chem Mater* **20** 3085
[387] Hua Y, King W P and Henderson C L 2008 *Microelectron Eng* **85** 934
[388] Hamann T W, Martinson A B F, Elam J W, Pellin M J and Hupp J T 2008 *J Phys Chem C* **112** 10303
[389] Hamann T W, Farha O K and Hupp J T 2008 *J Phys Chem C* **112** 19756
[390] Lin Y, Zhou S, Liu X, Sheehan S and Wang D 2009 *J Am Chem Soc* **131** 2772
[391] Kwon H, Park H, Kim B and Ha J S 2009 *J Electrochem Soc* **156** G13
[392] Kim H, Pippel E, Gösele U and Knez M 2009 *Langmuir* **25** 13284
[393] Yang Y, Scholz R, Fan H J, Hesse D, Gösele U and Zacharias M 2009 *ACS Nano* **3** 555
[394] Kim A, Park H, Lee K, Jeong K, Kim C, Lee E and Lee J 2009 *Electron Mater Lett* **5** 35
[395] Lee S, Pippel E, Gösele U, Dresbach C, Qin Y, Chandran C V, Bräuniger T, Hause G and Knez M 2009 *Science* **324** 488
[396] Standridge S D, Schatz G C and Hupp J T 2009 *Langmuir* **25** 2596
[397] Joo J and Rossnagel S M 2009 *J Korean Phys Soc* **54** 1048
[398] Szeghalmi A, Helgert M, Brunner R, Heyroth F, Gösele U and Knez M 2009 *Appl Opt* **48** 1727
[399] Qin Y, Kim Y, Zhang L, Lee S, Yang R B, Pan A, Mathwig K, Alexe M, Gösele U and Knez M 2010 *Small* **6** 910
[400] Luo Y, Kim K, Seo H O, Kim M J, Tai W S, Lee K H, Lim D C and Kim Y D 2010 *Bull Korean Chem Soc* **31** 1661
[401] Lee J, Ju H, Lee J K, Kim H S and Lee J 2010 *Electrochem Commun* **12** 210
[402] Park H H, Kang P S, Kim G T and Ha J S 2010 *Appl Phys Lett* **96** 102908
[403] Lu J and Stair P 2010 *Angew Chem , Int Ed* **49** 2547
[404] Gu D, Baumgart H, Abdel-Fattah T and Namkoong G 2010 *ACS Nano* **4** 753
[405] Kang Y, Su Kim C, Sung You D, Hoon Jung S, Lim K, Kim D, Kim J, Hyung Kim S, Shin Y, Kwon S and Kang J 2011 *Appl Phys Lett* **99** 073308
[406] Choi J, Kwon S, Jeong Y, Kim I and Kim K 2011 *J Electrochem Soc* **158** B749
[407] Sellers M C K and Seebauer E G 2011 *Thin Solid Films* **519** 2103
[408] Shin J, Kim I, Biju K P, Jo M, Park J, Lee J, Jung S, Lee W, Kim S, Park S and Hwang H 2011 *J Appl Phys* **109** 033712
[409] Choi S, Park J Y, Lee C, Lee J G and Kim S S 2011 *J Am Ceram Soc* **94** 1974
[410] Sellers M C K and Seebauer E G 2011 *Appl Phys A: Mater Sci Process* **104** 583
[411] Yoon J, Jung S and Kim J 2011 *Mater Chem Phys* **125** 342
[412] Kim D W, Kim K, Seo H O, Dey N K, Kim M J, Kim Y D, Lim D C and Lee K H 2011 *Catal Lett* **141** 854
[413] Gu D, Baumgart H, Tapily K, Shrestha P, Namkoong G, Ao X and Müller F 2011 *Nano Res* **4** 164
[414] Seo H O, Park S, Shim W H, Kim K, Lee K H, Jo M Y, Kim J H, Lee E, Kim D, Kim Y D and Lim D C 2011 *J Phys Chem C* **115** 21517
[415] Kim K, Dey N K, Seo H O, Kim Y D, Lim D C and Lee M 2011 *Appl Catal , A: General* **408** 148
[416] Sree S P, Dendooven J, Smeets D, Deduytsche D, Aerts A, Vanstreels K, Baklanov M R, Seo J W, Temst K, Vantomme A, Detavernier C and Martens J A 2011 *J Mater Chem* **21** 7692
[417] Qian L, Shen B, Qin G W and Das B 2011 *J Chem Phys* **134** 014707/1
[418] Li X, Fu Y, Liu X, Li A and Hui,L.,Wu,D. 2011 *Appl Phys A: Mater Sci Process* **105** 763
[419] Kim K, Nam J W, Seo H O, Kim Y D and Lim D C 2011 *J Phys Chem C* **115** 22954
[420] Kim S K, Hoffmann-Eifert S and Waser R 2011 *Electrochem Solid-State Lett* **14** H146
[421] Kim S K, Hoffmann-Eifert S, Reiners M and Waser R 2011 *J Electrochem Soc* **158** D6
[422] Xiangbo Meng and Dongsheng Geng and Jian Liu and Ruying Li and,Xueliang Sun 2011 *Nanotechnology* **22** 165602
[423] Li T C, Fabregat-Santiago F, Farha O K, Spokoyny A M, Raga S R, Bisquert J, Mirkin C A, Marks T J and Hupp J T 2011 *J Phys Chem C* **115** 11257
[424] Kugeler C, Zhang J, Hoffmann-Eifert S, Kim S K and Waser R 2011 *J Vac Sci Technol B* **29** 01AD01/1

[425] Dey N K, Kim M J, Kim K, Seo H O, Kim D, Kim Y D, Lim D C and Lee K H 2011 *J Mol Catal A: Chem* **337** 33
[426] Korhonen J T, Kettunen M, Ras R H A and Ikkala O 2011 *ACS Appl Mater Interfaces* **3** 1813
[427] Thimsen E 2011 *Chem Mater* **23** 4612
[428] Lee H J, Seo H O, Kim D W, Kim K, Luo Y, Lim D C, Ju H, Kim J W, Lee J and Kim Y D 2011 *Chem Commun* **47** 5605
[429] Yanguas-Gil A and Elam J W 2012 *J Vac Sci Technol , A* **30** 01A159
[430] Williams P A, Ireland C P, King P J, Chater P A, Boldrin P, Palgrave R G, Claridge J B, Darwent J R, Chalker P R and Rosseinsky M J 2012 *J Mater Chem* **22** 20203
[431] Kubrin R, Lee H S, Zierold R, Yu A, Janssen R, Nielsch K, Eich M and Schneider G A 2012 *J Am Ceram Soc* **95** 2226
[432] Kariniemi M, Niinistö J, Vehkamäki M, Kemell M, Ritala M, Leskelä M and Putkonen M 2012 *J Vac Sci Technol , A* **30** 01A115
[433] Jin S, Martinson A B F and Wiederrecht G P 2012 *J Phys Chem C* **116** 3097
[434] Kim D H, Koo H, Jur J S, Woodroof M, Kalanyan B, Lee K, Devine C K and Parsons G N 2012 *Nanoscale* **4** 4731
[435] dela Torre R, Larkin J, Singer A and Meller A 2012 *Nanotechnology* **23** 385308/1
[436] Lee J, Hong K S, Shin K and Jho J Y 2012 *J Ind Eng Chem (Amsterdam, Neth)* **18** 19
[437] Yantara N, Mathews N, Jinesh K B, Mulmudi H K and Mhaisalkar S G 2012 *Electrochim Acta* **85** 486
[438] Lee S Y, Jeon C, Kim S H, Kim Y, Jung W, An K and Park C 2012 *Jpn J Appl Phys* **51** 031102
[439] Huang J, Lee M and Kim J 2012 *J Vac Sci Technol , A* **30** 01A128/1
[440] Cheng H, Wang F, Chu J P, Santhanam R, Rick J and Lo S 2012 *J Phys Chem C* **116** 7629
[441] McDaniel M D, Posadas A, Ngo T Q, Dhamdhere A, Smith D J, Demkov A A and Ekerdt J G 2012 *J Vac Sci Technol B* **30** 04E111
[442] Shalav A, Venkatachalam D K and Elliman R G 2012 *Appl Phys A: Mater Sci Process* **107** 749
[443] Seo S, Jung E, Lim C, Chae H and Cho S M 2012 *Thin Solid Films* **520** 6690
[444] Cho J W, Park S J, Kim J, Kim W, Park H K, Do Y R and Min B K 2012 *ACS Appl Mater Interfaces* **4** 849
[445] Park S, Seo H O, Kim K, Lee J E, Kwon J, Kim Y D and Lim D C 2012 *Phys Status Solidi RRL* **6** 196
[446] Seo H O, Sim C W, Kim K, Kim Y D, Park J H, Lee B C, Lee K H and Lim D C 2012 *Radiat Phys Chem* **81** 290
[447] Seo S, Jung E, Lim C, Chae H and Cho S M 2012 *Appl Phys Express* **5** 035701
[448] McDaniel M D, Posadas A, Wang T, Demkov A A and Ekerdt J G 2012 *Thin Solid Films* **520** 6525
[449] Oh J, Na H, Mok I, Kim J, Lee K and Sohn H 2012 *Appl Phys A: Mater Sci Process* **108** 679
[450] Seo H O, Sim C W, Kim K, Kim Y D and Lim D C 2012 *Chem Eng J* **183** 381
[451] Chen H, Blaber M G, Standridge S D, DeMarco E J, Hupp J T, Ratner M A and Schatz G C 2012 *J Phys Chem C* **116** 10215
[452] Choun M, Chung S, Jeon H, Uhm S and Lee J 2012 *Electrochem Commun* **24** 108
[453] Noh J H, Ding B, Han H S, Kim J S, Park J H, Park S B, Jung H S, Lee J and Hong K S 2012 *Appl Phys Lett* **100** 084104/1
[454] Panda S K, Yoon Y, Jung H S, Yoon W and Shin H 2012 *J Power Sources* **204** 162
[455] Park S, Seo H O, Kim K, Shim W H, Heo J, Cho S, Kim Y D, Lee K H and Lim D C 2012 *J Phys Chem C* **116** 15348
[456] Xu Q, Yang J, Dai J, Yang Y, Chen X and Wang Y 2013 *J Membr Sci* **448** 215
[457] Ku S J, Jo G C, Bak C H, Kim S M, Shin Y R, Kim K H, Kwon S H and Kim J 2013 *Nanotechnology* **24** 085301/1
[458] Dirnstorfer I, Maehne H, Mikolajick T, Knaut M, Albert M and Dubnack K 2013 *J Vac Sci Technol , A* **31** 01A116
[459] Suh Y J, Lu N, Park S Y, Lee T H, Lee S H, Cha D K, Lee M G, Huang J, Kim S, Sohn B, Kim G, Ko M J, Kim J and Kim M J 2013 *Micron* **46** 35
[460] Lin X, Yu K, Lu G, Chen J and Yuan C 2013 *J Phys D: Appl Phys* **46** 024004/1
[461] Zhang X, Belharouak I, Li L, Lei Y, Elam J W, Nie A, Chen X, Yassar R S and Axelbaum R L 2013 *Adv Energy Mater* **3** 1299
[462] Meng X, Banis M N, Geng D, Li X, Zhang Y, Li R, Abou-Rachid H and Sun X 2013 *Appl Surf Sci* **266** 132

[463] Ngo T Q, Posadas A, Seo H, Hoang S, McDaniel M D, Utess D, Triyoso D H, Buddie Mullins C, Demkov A A and Ekerdt J G 2013 *J Appl Phys* **114** 084901/1
[464] Wang D, Zhang L, Lee W, Knez M and Liu L 2013 *Small* **9** 1025
[465] Notley S M and Fogden A 2013 *Appl Surf Sci* **285** 220
[466] Chandiran A K, Yella A, Stefik M, Heiniger L, Comte P, Nazeeruddin M K and Gratzel M 2013 *ACS Appl Mater Interfaces* **5** 3487
[467] Li J, Chen X, Xu W, Nam C and Shi Y 2013 *Thin Solid Films* **536** 275
[468] Bae C, Zierold R, Montero Moreno J M, Kim H, Shin H, Bachmann J and Nielsch K 2013 *J Mater Chem C* **1** 621
[469] Xu Q, Yang Y, Yang J, Wang X, Wang Z and Wang Y 2013 *J Membr Sci* **443** 62
[470] Katz M J, Vermeer M J D, Farha O K, Pellin M J and Hupp J T 2013 *Langmuir* **29** 806
[471] Avril L, Decams J M and Imhoff L 2013 *Phys Procedia* **46** 33
[472] Dai H, Zhou Y, Chen L, Guo B, Li A, Liu J, Yu T and Zou Z 2013 *Nanoscale* **5** 5102
[473] Kim K, Lim D C, Seo H O, Lee J Y, Seo B Y, Lee D J, Song Y, Cho S, Lim J and Kim Y D 2013 *Appl Surf Sci* **279** 380
[474] Park Y J, Na K, Park G, Kim R S and Anderson T J 2013 *J Nanosci Nanotechnol* **13** 4207
[475] Son H, Prasittichai C, Mondloch J E, Luo L, Wu J, Kim D W, Farha O K and Hupp J T 2013 *J Am Chem Soc* **135** 11529
[476] Kim M, Bae C, Kim H, Yoo H, Montero Moreno J M, Jung H S, Bachmann J, Nielsch K and Shin H 2013 *J Mater Chem A* **1** 14080
[477] Gu Y, Lu H, Geng Y, Ye Z, Zhang Y, Sun Q, Ding S and Zhang D W 2013 *Nanoscale Res Lett* **8** 107
[478] Melendez-Ceballos A, Fernandez-Valverde S M, Barrera-Diaz C, Albin V, Lair V, Ringuede A and Cassir M 2013 *Int J Hydrogen Energy* **38** 13443
[479] Seo H O, Kim D H, Kim K, Park E J, Sim C W and Kim Y D 2013 *Adsorption* **19** 1181
[480] Cheng C, Zhang H, Ren W, Dong W and Sun Y 2013 *Nano Energy* **2** 779
[481] Park H K, Yoon S W, Choi D Y and Do Y R 2013 *J Mater Chem C* **1** 1732
[482] Siles P, Pauli M, Bufon C, Ferreira S, Bettini J, Schmidt O and Malachias A 2013 *Nanotechnology* **24** 035702
[483] Sellers M C K and Seebauer E G 2013 *AIChE J* **59** 1049
[484] Seo H O, Sim J K, Kim K, Kim Y D, Lim D C and Kim S H 2013 *Appl Catal , A* **451** 43
[485] Hu C, McDaniel M D, Ekerdt J G and Yu E T 2013 *IEEE Electron Device Lett* **34** 1385
[486] Kärkkäinen I, Shkabko A, Heikkilä M, Niinistö J, Ritala M, Leskelä M, Hoffmann-Eifert S and Waser R 2014 *Phys Status Solidi A* **211** 301
[487] Hudec B, Paskaleva A, Jancovic P, Derer J, Fedor J, Rosova A, Dobrocka E and Frohlich K 2014 *Thin Solid Films* **563** 10
[488] Chen H, Lin Q, Xu Q, Yang Y, Shao Z and Wang Y 2014 *J Membr Sci* **458** 217
[489] Katoch A, Kim J and Kim S S 2014 *ACS Appl Mater Interfaces* **6** 21494
[490] Hu C, McDaniel M D, Posadas A, Demkov A A, Ekerdt J G and Yu E T 2014 *Nano Lett* **14** 4360
[491] Panda S K, Lee S, Yoon W and Shin H 2014 *J Power Sources* **249** 59
[492] Lu H, Xie Z, Geng Y, Zhang Y, Sun Q, Wang P, Ding S and Zhang D W 2014 *Appl Phys A: Mater Sci Process* **117** 1479
[493] Huang J, Lee M, Lucero A, Cheng L and Kim J 2014 *J Phys Chem C* **118** 23306
[494] Sellers M C K and Seebauer E G 2014 *Mater Lett* **114** 44
[495] Correa Baena J P and Agrios A G 2014 *J Phys Chem C* **118** 17028
[496] Li X, Liu J, Meng X, Tang Y, Banis M N, Yang J, Hu Y, Li R, Cai M and Sun X 2014 *J Power Sources* **247** 57
[497] Jeon W, Lee W, Yoo Y W, An C H, Han J H, Kim S K and Hwang C S 2014 *J Mater Chem C* **2** 9993
[498] Yin X, Battaglia C, Lin Y, Chen K, Hettick M, Zheng M, Chen C, Kiriya D and Javey A 2014 *ACS Photonics* **1** 1245
[499] Tallarida M, Das C and Schmeisser D 2014 *Beilstein J Nanotechnol* **5** 77
[500] Yang X, Liu R, Du C, Dai P, Zheng Z and Wang D 2014 *ACS Appl Mater Interfaces* **6** 12005
[501] Yoo H, Kim M, Bae C, Lee S, Kim H, Ahn T K and Shin H 2014 *J Phys Chem C* **118** 9726
[502] Melendez-Ceballos A, Albin V, Ringuede A, Fernandez-Valverde S M and Cassir M 2014 *Int J Hydrogen Energy* **39** 12233
[503] Benner F, Jordan P M, Richter C, Simon D K, Dirnstorfer I, Knaut M, Bartha J W and Mikolajick T 2014 *J Vac Sci Technol , B* **32** 03D110

[504] Popovici M, Redolfi A, Aoulaiche M, van den Berg J A, Douhard B, Swerts J, Bailey P, Kaczer B, Groven B, Meersschaut J, Conard T, Moussa A, Adelmann C, Delabie A, Fazan P, Van Elshocht S and Jurczak M 2015 *Microelectron Eng* **147** 108
[505] Reckers P, Dimamay M, Klett J, Trost S, Zilberberg K, Riedl T, Parkinson B A, Broetz J, Jaegermann W and Mayer T 2015 *J Phys Chem C* **119** 9890
[506] Son H, Kim C H, Kim D W, Jeong N C, Prasittichai C, Luo L, Wu J, Farha O K, Wasielewski M R and Hupp J T 2015 *ACS Appl Mater Interfaces* **7** 5150
[507] Ratzsch S, Kley E, Tuennermann A and Szeghalmi A 2015 *Nanotechnology* **26** 24003
[508] Mali S S, Shim C S, Park H K, Heo J, Patil P S and Hong C K 2015 *Chem Mater* **27** 1541
[509] Lin Y, Hsu C, Tseng M, Shyue J and Tsai F 2015 *ACS Appl Mater Interfaces* **7** 22610
[510] Spende A, Sobel N, Lukas M, Zierold R, Riedl J C, Gura L, Schubert I, Moreno Josep M M, Nielsch K, Stuhn B, Hess C, Trautmann C and Toimil-Molares M E 2015 *Nanotechnology* **26** 335301
[511] McDowell M T, Lichterman M F, Carim A I, Liu R, Hu S, Brunschwig B S and Lewis N S 2015 *ACS Appl Mater Interfaces* **7** 15189
[512] Li M, Li X, Li W, Meng X, Yu Y and Sun X 2015 *Electrochem Commun* **57** 43
[513] Visentin F, El Habra N, Favaro M, Battiston S, Gerbasi R, Crociani L and Galenda A 2015 *Chem Vap Deposition* **21** 300
[514] Aghaee M, Maydannik P S, Johansson P, Kuusipalo J, Creatore M, Homola T and Cameron D C 2015 *J Vac Sci Technol , A* **33** 041512
[515] Sasinska A, Singh T, Wang S, Mathur S and Kraehnert R 2015 *J Vac Sci Technol , A* **33** 01A152
[516] Das C, Henkel K, Tallarida M, Schmeisser D, Gargouri H, Kärkkäinen I, Schneidewind J, Gruska B and Arens M 2015 *J Vac Sci Technol , A* **33** 01A144
[517] Bak C H, Ku S J, Jo G C, Jung K, Lee H J, Kwon S H and Kim J 2015 *Polymer* **60** 267
[518] Eitan Barlaz D and Seebauer E G 2015 *CrystEngComm* **17** 2101
[519] Xiao X, Liu X, Cao G, Zhang C, Xia L, Xu W and Xiao S 2015 *Polym Eng Sci* **55** 1296
[520] Xiao X, Liu X, Chen F, Fang D, Zhang C, Xia L and Xu W 2015 *ACS Appl Mater Interfaces* **7** 21326
[521] Lin Y, Kapadia R, Yang J, Zheng M, Chen K, Hettick M, Yin X, Battaglia C, Sharp I D, Ager J W and Javey A 2015 *J Phys Chem C* **119** 2308
[522] Kim M, Lee J, Lee S, Seo S, Bae C and Shin H 2015 *ChemSusChem* **8** 2363
[523] Kim I S and Martinson A B F 2015 *J Mater Chem A* **3** 20092
[524] Das C, Tallarida M and Schmeisser D 2015 *Nanoscale* **7** 7726
[525] Kim D H, Kim S Y, Han S W, Cho Y K, Jeong M, Park E J and Kim Y D 2015 *Appl Catal , A* **495** 184
[526] Kim D H, Jeong M, Seo H O and Kim Y D 2015 *Phys Chem Chem Phys* **17** 599
[527] Katz M J, DeVries Vermeer M J, Farha O K, Pellin M J and Hupp J T 2015 *J Phys Chem B* **119** 7162
[528] Guerra-Nunez C, Zhang Y, Li M, Chawla V, Erni R, Michler J, Park H G and Utke I 2015 *Nanoscale* **7** 10622
[529] Yao X, Li J, Kong L and Wang Y 2015 *Nanotechnology* **26** 1
[530] Cho C, Lee J, Lee D C and Moon J H 2015 *Electrochim Acta* **166** 350
[531] Wang D, Yan Y, Schaaf P, Sharp T, Schoenherr S, Ronning C and Ji R 2015 *J Vac Sci Technol , A* **33** 01A102
[532] Gun Y, Song G Y, Quy V H V, Heo J, Lee H, Ahn K and Kang S H 2015 *ACS Appl Mater Interfaces* **7** 20292
[533] Zhang H, Canlas C, Jeremy Kropf A, Elam J W, Dumesic J A and Marshall C L 2015 *J Catal* **326** 172
[534] Hsu W, Sutter-Fella C M, Hettick M, Cheng L, Chan S, Chen Y, Zeng Y, Zheng M, Wang H, Chiang C and Javey A 2015 *Sci Rep* **5** 16028
[535] Zhang Y, Guerra-Nunez C, Utke I, Michler J, Rossell M D and Erni R 2015 *J Phys Chem C* **119** 3379
[536] Barreca D, Carraro G, Warwick M E A, Kaunisto K, Gasparotto A, Gombac V, Sada C, Turner S, Van Tendeloo G, Maccato C and Fornasiero P 2015 *Cryst Eng Comm* **17** 6219
[537] Li Q, Dong C, Nie A, Liu J, Zhou W and Wang H 2012 *Langmuir* **28** 15809
[538] Liang X, King D M, Li P and Weimer A W 2009 *J Am Ceram Soc* **92** 649
[539] Nie A, Liu J, Li Q, Cheng Y, Dong C, Zhou W, Wang P, Wang Q, Yang Y, Zhu Y, Zeng Y and Wang H 2012 *J Mater Chem* **22** 10665
[540] Szeghalmi A, Kley E B and Knez M 2010 *J Phys Chem C* **114** 21150
[541] Szeghalmi A, Helgert M, Brunner R, Heyroth F, Gösele U and Knez M 2010 *Adv Funct Mater* **20** 2053
[542] Wang H, Ma D, Ma F and Xu K 2012 *J Vac Sci Technol B* **30** 040601
[543] Wang H, Xu S and Gordon R G 2010 *Electrochem Solid-State Lett* **13** G75

[544] Williams V O, Jeong N C, Prasittichai C, Farha O K, Pellin M J and Hupp J T 2013 *Prepr - Am Chem Soc , Div Energy Fuels* **58** 409
[545] Yu K, Lin X, Lu G, Wen Z, Yuan C and Chen J 2012 *RSC Adv* **2** 7843
[546] Kim S, Han T H, Kim J, Gwon H, Moon H, Kang S, Kim S O and Kang K 2009 *ACS Nano* **3** 1085
[547] Kim S K, Kim W, Kim K, Hwang C S and Jeong J 2004 *Appl Phys Lett* **85** 4112
[548] Kim S K, Kim K, Kwon O S, Lee S W, Jeon C B, Park W Y, Hwang C S and Jeong J 2005 *Electrochemical and Solid-State Letters* **8** F59
[549] Kim S K, Lee S Y, Seo M, Choi G and Hwang C S 2007 *J Appl Phys* **102** 024109
[550] Tanner C M, Perng Y, Frewin C, Saddow S E and Chang J P 2007 *Appl Phys Lett* **91** 203510
[551] Kim S K, Choi G, Lee S Y, Seo M, Lee S W, Han J H, Ahn H, Han S and Hwang C S 2008 *Adv Mater* **20** 1429
[552] Kim S K, Choi G J, Kim J H and Hwang C S 2008 *Chem Mater* **20** 3723
[553] Rai V R and Agarwal S 2008 *J Phys Chem C* **112** 9552
[554] Kim S K, Choi G and Hwang C S 2008 *Electrochem Solid-State Lett* **11** G27
[555] Choi G, Kim S K, Lee S Y, Park W Y, Seo M, Choi B J and Hwang C S 2009 *Journal of The Electrochemical Society* **156** G71
[556] Han J H, Han S, Lee W, Lee S W, Kim S K, Gatineau J, Dussarrat C and Hwang C S 2011 *Appl Phys Lett* **99** 022901
[557] Seo M, Ho Rha S, Keun Kim S, Hwan Han J, Lee W, Han S and Seong Hwang C 2011 *J Appl Phys* **110** 024105
[558] Kim S K, Han S, Han J H, Lee W and Hwang C S 2011 *Phys Status Solidi RRL* **5** 262
[559] Cianci E, Lattanzio S, Seguini G, Vassanelli S and Fanciulli M 2012 *Thin Solid Films* **520** 4745
[560] Cleveland E R, Henn-Lecordier L and Rubloff G W 2012 *J Vac Sci Technol , A* **30** 01A150/1
[561] Lehnert W, Ruhl G and Gschwandtner A 2012 *J Vac Sci Technol , A* **30** 01A152
[562] Kukli K, Lu J, Link J, Kemell M, Puukilainen E, Heikkila M, Hoxha R, Tamm A, Hultman L, Stern R, Ritala M and Leskela M 2014 *Thin Solid Films* **565** 165
[563] Kukli K, Kemell M, Dimri M C, Puukilainen E, Tamm A, Stern R, Ritala M and Leskela M 2014 *Thin Solid Films* **565** 261
[564] Jeon W, Yoo S, Kim H K, Lee W, An C H, Chung M J, Cho C J, Kim S K and Hwang C S 2014 *ACS Appl Mater Interfaces* **6** 21632
[565] Jeon W, Rha S H, Lee W, An C H, Chung M J, Kim S H, Cho C J, Kim S K and Hwang C S 2015 *Phys Status Solidi RRL* **9** 410
[566] Sridharan K, Jang E, Park Y M and Park T J 2015 *Chem - Eur J* **21** 19136
[567] Kil D, Lee J and Roh J 2002 *Chem Vap Deposition* **8** 195
[568] Lim J W, Yun S J and Kim H 2007 *J Electrochem Soc* **154** G239
[569] Kim J, Kim J, Ahn J, Park P and Kang S 2007 *J Electrochem Soc* **154** H1008
[570] Niskanen A, Arstila K, Leskelä M and Ritala M 2007 *Chem Vap Deposition* **13** 152
[571] Jeon W, Chung H, Joo D and Kang S 2008 *Electrochem Solid-State Lett* **11** H19
[572] Jung Wook Lim and Sun Jin Yun and Hyun,Tak Kim 2008 *Jpn J Appl Phys* **47** 6934
[573] Choi B J, Oh S H, Choi S, Eom T, Shin Y C, Kim K M, Yi K, Hwang C S, Kim Y J, Park H C, Baek T S and Hong S K 2009 *J Electrochem Soc* **156** H59
[574] Rai V R and Agarwal S 2009 *J Phys Chem C* **113** 12962
[575] Joo D, Park J and Kang S 2009 *Electrochem Solid-State Lett* **12** H77
[576] Choi G, Kim S K, Won S, Kim H J and Hwang C S 2009 *J Electrochem Soc* **156** G138
[577] Lim J W, Yun S J and Kim J H 2009 *ETRI J* **31** 675
[578] Park J, Jeong J K, Mo Y and Kim S 2009 *Appl Phys Lett* **94** 042105
[579] Nam S, Rooks M J, Kim K and Rossnagel S M 2009 *Nano Lett* **9** 2044
[580] Dingemans G, Seguin R, Engelhart P, Sanden M C M v d and Kessels W M M 2010 *Phys Status Solidi (RRL)* **4** 10
[581] Nam S, Lee M, Lee S, Lee D, Rossnagel S M and Kim K 2010 *Nano Lett* **10** 3324
[582] Jeong H Y, Lee J Y, Ryu M and Choi S 2010 *Phys Status Solidi RRL* **4** 28
[583] Kim K M, Song S J, Kim G H, Seok J Y, Lee M H, Yoon J H, Park J and Hwang C S 2011 *Adv Funct Mater* **21** 1587
[584] Tallarida M, Friedrich D, Städter M, Michling M and Schmeisser D 2011 *J Nanosci Nanotechnol* **11** 8049
[585] Young Jeong H, Kyu Kim S, Yong Lee J and Choi S 2011 *J Electrochem Soc* **158** H979

[586] Kim K M, Choi B J, Lee M H, Kim G H, Song S J, Seok J Y, Yoon J H, Han S and Hwang C S 2011 *Nanotechnology* **22** 254010
[587] Hwan Kim G, Ho Lee J, Yeong Seok J, Ji Song S, Ho Yoon J, Jean Yoon K, Hwan Lee M, Min Kim K, Dong Lee H, Wook Ryu S, Joo Park T and Seong Hwang C 2011 *Appl Phys Lett* **98** 262901
[588] Lee J, Lee S J, Han W B, Jeon H, Park J, Kim H, Yoon C S and Jeon H 2012 *ECS J Solid State Sci Technol* **1** Q63
[589] Taschuk M T, Harris K D, Smetaniuk D P and Brett M J 2012 *Sens Actuators, B* **162** 1
[590] Kyung M K, Seungwu H, Hwang C S and Hwang C S 2012 *Nanotechnology* **23** 035201
[591] Kurian S, Sudhagar P, Lee J, Song D, Cho W, Lee S, Kang Y S and Jeon H 2013 *J Mater Chem A* **1** 4370
[592] Jung M, Yun Y J, Chu M and Kang M G 2013 *Chem - Eur J* **19** 8543
[593] Lee J, Lee S J, Han W B, Jeon H, Park J, Jang W, Yoon C S and Jeon H 2013 *Phys Status Solidi A* **210** 276
[594] Jeun J, Park K, Kim D, Kim W, Kim H, Lee B, Kim H, Yu W, Kang K and Hong S 2013 *Nanoscale* **5** 8480
[595] Song S J, Seok J Y, Yoon J H, Kim K M, Kim G H, Lee M H and Hwang C S 2013 *Sci Rep* **3** 3443
[596] Park S, Lee J, Jang J S, Rhu H, Yu H, You B Y, Kim C S, Kim K J, Cho Y J, Baik S and Lee W 2013 *Nanotechnology* **24** 295202
[597] Kim D, Kim W, Kim S and Hong S 2014 *ACS Appl Mater Interfaces* **6** 11817
[598] Rauwel E, Clavel G, Willinger M, Rauwel P and Pinna N 2008 *Angew Chem , Int Ed* **120** 3648
[599] Rauwel E, Willinger M, Ducroquet F, Rauwel P, Matko I, Kiselev D and Pinna N 2008 *J Phys Chem C* **112** 12754
[600] Rauwel E, Ducroquet F, Rauwel P, Willinger M, Matko I and Pinna N 2009 *J Vac Sci Technol B* **27** 230
[601] Willinger M, Neri G, Bonavita A, Micali G, Rauwel E, Herntrich T and Pinna N 2009 *Phys Chem Chem Phys* **11** 3615
[602] Bernal Ramos K, Clavel G, Marichy C, Cabrera W, Pinna N and Chabal Y J 2013 *Chem Mater* **25** 1706
[603] Kahouli A, Marichy C, Sylvestre A and Pinna N 2015 *J Appl Phys* **117** 154101
[604] Han T H, Oh J K, Park J S, Kwon S, Kim S and Kim S O 2009 *J Mater Chem* **19** 3512
[605] Han T H, Moon H, Hwang J O, Seok S I, Im S H and Kim S O 2010 *Nanotechnology* **21** 185601
[606] Won S, Suh S, Lee S W, Choi G, Hwang C S and Kim H J 2010 *Electrochem Solid-State Lett* **13** G13
[607] Ritala M, Leskelä M and Rauhala E 1994 *Chem Mater* **6** 556
[608] Ritala M, Juppo M, Kukli K, Rahtu A and Leskelä M 1999 *J Phys IV France* **9** Pr8-1021
[609] Aarik J, Aidla A, Sammelselg V, Uustare T, Ritala M and Leskelä M 2000 *Thin Solid Films* **370** 163
[610] Rahtu A, Kukli K and Ritala M 2001 *Chem Mater* **13** 817
[611] Aarik J, Karlis J, Mändar H, Uustare T and Sammelselg V 2001 *Appl Surf Sci* **181** 339
[612] Kim I, Tuller H L, Kim H and Park J 2004 *Appl Phys Lett* **85** 4705
[613] Wang J J, Deng X, Varghese R, Nikolov A, Sciortino P, Liu F and Chen L 2005 *Opt Lett* **30** 1864
[614] Alekhin A P, Gudkova S A, Markeev A M, Mitiaev A S, Sigarev A A and Toknova V F 2010 *Appl Surf Sci* **257** 186
[615] Alekhin A P, Lapushkin G I, Markeev A M, Sigarev A A and Toknova V F 2010 *J Surf Invest* **80** 1091
[616] Grigal I P, Markeev A M, Gudkova S A, Chernikova A G, Mityaev A S and Alekhin A P 2012 *Appl Surf Sci* **258** 3415
[617] Alekhin A P, Markeev A M, Ovchinnikov D V, Solov'ev A A and Toknova V F 2013 *Russ J Appl Chem* **86** 326
[618] Pore V, Rahtu A, Leskelä M, Ritala M, Sajavaara T and Keinonen J 2004 *Chem Vap Deposition* **10** 143
[619] Kemell M, Pore V, Ritala M, Leskelä M and Lindén M 2005 *J Am Chem Soc* **127** 14178
[620] Alén P, Vehkamäki M, Ritala M and Leskelä M 2006 *J Electrochem Soc* **153** G304
[621] Kemell M, Pore V, Ritala M and Leskelä M 2006 *Chem Vap Deposition* **12** 419
[622] Kemell M, Pore V, Tupala J, Ritala M and Leskelä M 2007 *Chem Mater* **19** 1816
[623] Färm E, Kemell M, Ritala M and Leskelä M 2008 *J Phys Chem C* **112** 15791
[624] Färm E, Kemell M, Ritala M and Leskelä M 2008 *Thin Solid Films* **517** 972
[625] Heikkilä M, Puukilainen E, Ritala M and Leskelä M 2009 *J Photochem Photobiol A* **204** 200
[626] Pore V, Ritala M, Leskelä M, Saukkonen T and Järn M 2009 *Cryst Growth Des* **9** 2974
[627] Popovici M, Van Elshocht S, Menou N, Swerts J, Pierreux D, Delabie A, Brijs B, Conard T, Opsomer K, Maes J W, Wouters D J and Kittl J A 2010 *J Electrochem Soc* **157** G1

[628] Popovici M, Kim M, Tomida K, Swerts J, Tielens H, Moussa A, Richard O, Bender H, Franquet A, Conard T, Altimime L, Elshocht S V and Kittl J A 2011 *Microelectron Eng* **88** 1517
[629] Popovici M, Swerts J, Tomida K, Radisic D, Kim M, Kaczer B, Richard O, Bender H, Delabie A, Moussa A, Vrancken C, Opsomer K, Franquet A, Pawlak M A, Schaekers M, Altimime L, Van Elshocht S and Kittl J A 2011 *Phys Status Solidi RRL* **5** 19
[630] Pore V, Dimri M, Khanduri H, Stern R, Lu J, Hultman L, Kukli K, Ritala M and Leskelä M 2011 *Thin Solid Films* **519** 3318
[631] Popovici M, Delabie A, Adelmann C, Meersschaut J, Franquet A, Tallarida M, van den Berg J, Richard O, Swerts J, Tomida K, Kim M, Tielens H, Bender H, Conard T, Jurczak M, Van Elshocht S and Schmeisser D 2013 *ECS J Solid State Sci Technol* **2** N23
[632] Zhou G, Ren J and Zhang S 2013 *Adv Mater Res* **750-752** 1052
[633] Zhou G, Ren J and Zhang S 2013 *Adv Mater Res* **785-786** 832
[634] Lim G T and Kim D 2006 *Thin Solid Films* **498** 254
[635] Maeng W J and Kim H 2006 *Electrochem Solid-State Lett* **9** G191
[636] Xie Q, Jiang Y, Detavernier C, Deduytsche D, Van Meirhaeghe R L, Ru G, Li B and Qu X 2007 *J Appl Phys* **102** 083521
[637] Alessandri I, Zucca M, Ferroni M, Bontempi E and Depero L E 2009 *Small* **5** 336
[638] Alessandri I and Depero L E 2010 *ACS Appl Mater Interfaces* **2** 594
[639] Swaminathan S, Shandalov M, Oshima Y and McIntyre P C 2010 *Appl Phys Lett* **96** 082904
[640] Bontempi E, Zanola P, Gelfi M, Zucca M, Depero L E, Girault B, Goudeau P, Geandier G, Bourhis E L and Renault P 2010 *Nucl Instrum Methods Phys Res B* **268** 365
[641] Gerasopoulos K, Chen X, Culver J, Wang C and Ghodssi R 2010 *Chem Commun* **46** 7349
[642] Cleveland E R, Banerjee P, Perez I, Lee S B and Rubloff G W 2010 *ACS Nano* **4** 4637
[643] Gougousi T and Lacis J W 2010 *Thin Solid Films* **518** 2006
[644] Gerasopoulos K, McCarthy M, Banerjee P, Fan X, Culver J N and Ghodssi R 2010 *Nanotechnology* **21** 055304
[645] Borgese L, Bontempi E, Gelfi M, Depero L E, Goudeau P, Geandier G and Thiaudière D 2011 *Acta Mater* **59** 2891
[646] Nam T, Kim J, Kim M, Kim H and Kim W 2011 *J Korean Phys Soc* **59** 452
[647] Tétreault N, Heiniger L, Stefik M, Labouchère P L, Arsenault É, Nazeeruddin N K, Ozin G A and Grätzel M 2011 *ECS Trans* **41** 303
[648] Ahn J, Geppert I, Gunji M, Holland M, Thayne I, Eizenberg M and McIntyre P C 2011 *Appl Phys Lett* **99** 232902
[649] Yuan Z, Nainani A, Sun Y, Lin J J, Pianetta P and Saraswat K C 2011 *Appl Phys Lett* **98** 172106
[650] Haspert L C, Banerjee P, Henn-Lecordier L and Rubloff G W 2011 *J Vac Sci Technol B* **29** 041807/1
[651] Kang H, Lee C, Kim D, Kim J, Choi W and Kim H 2011 *Appl Catal , B: Environmental* **104** 6
[652] Dendooven J, Pulinthanathu Sree S, De Keyser K, Deduytsche D, Martens J A, Ludwig K F and Detavernier C 2011 *J Phys Chem C* **115** 6605
[653] Chen Y W, Prange J D, Dühnen S, Park Y, Gunji M, Chidsey C E D and McIntyre P C 2011 *Nat Mater* **10** 539
[654] Hu J, Saraswat K C and Philip Wong H 2011 *Appl Phys Lett* **99** 092107
[655] Lin J J, Roy A M, Nainani A, Sun Y and Saraswat K C 2011 *Appl Phys Lett* **98** 092113
[656] Pulinthanathu Sree S, Dendooven J, Jammaer J, Masschaele K, Deduytsche D, D'Haen J, Kirschhock C E A, Martens J A and Detavernier C 2012 *Chem Mater* **24** 2775
[657] Wittig R, Waller E, von Freymann G and Steiner R 2012 *J Laser Appl* **24** 042011
[658] Dendooven J, Devloo-Casier K, Levrau E, Van Hove R, Pulinthanathu Sree S, Baklanov M R, Martens J A and Detavernier C 2012 *Langmuir* **28** 3852
[659] Thomas M A, Cui J B and Watanabe F 2012 *ECS Trans* **45** 41
[660] Kim C E and Yun I 2012 *Appl Surf Sci* **258** 3089
[661] Lin M C, Nien L, Chen C, Lee C and Chen M 2012 *Appl Phys Lett* **101** 023112/1
[662] Borgese L, Gelfi M, Bontempi E, Goudeau P, Geandier G, Thiaudiere D and Depero L E 2012 *Surf Coat Technol* **206** 2459
[663] Kim H, Ko K and Kang H 2012 *ECS Trans* **50** 127
[664] Jin S H, Jun G H, Hong S H and Jeon S 2012 *Carbon* **50** 4483
[665] Langston M C, Dasgupta N P, Jung H J, Logar M, Huang Y, Sinclair R and Prinz F B 2012 *J Phys Chem C* **116** 24177

[666] Kim C E and Yun I 2012 *ECS Trans* **45** 89
[667] Moshe H, Vanbel M, Valev V K, Verbiest T, Dressler D and Mastai Y 2013 *Chem - Eur J* **19** 10295
[668] Petrochenko P E, Scarel G, Hyde G K, Parsons G N, Skoog S A, Zhang Q, Goering P L and Narayan R J 2013 *Jom* **65** 550
[669] Okyay A K, Oruc F B, Cimen F and Aygun L E 2013 *Proc SPIE* **8626** 862616
[670] Chandiran A K, Comte P, Humphry-Baker R, Kessler F, Yi C, Nazeeruddin M K and Graetzel M 2013 *Adv Funct Mater* **23** 2775
[671] Ui T, Kudo M and Suzuki T 2013 *Phys Status Solidi C* **10** 1417
[672] Alessandri I 2013 *J Am Chem Soc* **135** 5541
[673] Dasgupta N P, Liu C, Andrews S, Prinz F B and Yang P 2013 *J Am Chem Soc* **135** 12932
[674] Abendroth B, Moebus T, Rentrop S, Strohmeyer R, Vinnichenko M, Weling T, Stoecker H and Meyer D C 2013 *Thin Solid Films* **545** 176
[675] Kawasaki M, Chen M, Yang J, Chiou W and Shiojiri M 2013 *Appl Phys Lett* **102** 091603
[676] Satpati A K, Arroyo-Curras N, Ji L, Yu E T and Bard A J 2013 *Chem Mater* **25** 4165
[677] Ye L and Gougousi T 2013 *ACS Appl Mater Interfaces* **5** 8081
[678] Chakrabarti B, Galatage R V and Vogel E M 2013 *IEEE Electron Device Lett* **34** 867
[679] Sree S P, Dendooven J, Masschaele K, Hamed H M, Deng S, Bals S, Detavernier C and Martens J A 2013 *Nanoscale* **5** 5001
[680] Scheuermann A G, Lawrence J P, Gunji M, Chidsey C E D and McIntyre P C 2013 *ECS Trans* **58** 75
[681] Colombi P, Bergese P, Bontempi E, Borgese L, Federici S, Keller S S, Boisen A and Depero L E 2013 *Meas Sci Technol* **24** 125603/1
[682] Scheuermann A G, Prange J D, Gunji M, Chidsey C E D and McIntyre P C 2013 *Energy Environ Sci* **6** 2487
[683] Zhang G Z, Wu H, Chen C, Wang T, Wang P Y, Mai L Q, Yue J and Liu C 2014 *Appl Phys Lett* **104** 163503
[684] Lichterman M F, Carim A I, McDowell M T, Hu S, Gray H B, Brunschwig B S and Lewis N S 2014 *Energy Environ Sci* **7** 3334
[685] Kayaci F, Vempati S, Ozgit-Akgun C, Donmez I, Biyikli N and Uyar T 2014 *Nanoscale* **6** 5735
[686] Liang Y and Liao W 2014 *RSC Adv* **4** 19482
[687] Goren E, Ungureanu M, Zazpe R, Rozenberg M, Hueso L E, Stoliar P, Tsur Y and Casanova F 2014 *Appl Phys Lett* **105** 143506
[688] Kavan L, Tetreault N, Moehl T and Gratzel M 2014 *J Phys Chem C* **118** 16408
[689] Deng S, Verbruggen S W, Lenaerts S, Martens J A, Van den Berghe S, Devloo-Casier K, Devulder W, Dendooven J, Deduytsche D and Detavernier C 2014 *J Vac Sci Technol , A* **32** 01A123
[690] Kim S, Heo K, Yoo S C, Choi S G and Chang S W 2014 *J Korean Phys Soc* **65** 1118
[691] Salihoglu O 2014 *J Vac Sci Technol , B* **32** 051201
[692] McDowell M T, Lichterman M F, Spurgeon J M, Hu S, Sharp I D, Brunschwig B S and Lewis N S 2014 *J Phys Chem C* **118** 19618
[693] Brittman S, Yoo Y, Dasgupta N P, Kim S, Kim B and Yang P 2014 *Nano Lett* **14** 4665
[694] Nabatame T, Ohi A, Chikyo T, Kimura M, Yamada H and Ohishi T 2014 *J Vac Sci Technol , B* **32** 03D121
[695] Abdellatef S A, Ohi A, Nabatame T and Taniguchi A 2014 *Biomater Sci* **2** 330
[696] Sperling B A, Hoang J, Kimes W A, Maslar J E, Steffens K L and Nguyen N V 2014 *J Vac Sci Technol , A* **32** 031513
[697] Wu Y, Yang X, Chen H, Zhang K, Qin C, Liu J, Peng W, Islam A, Bi E, Ye F, Yin M, Zhang P and Han L 2014 *Appl Phys Express* **7** 052301
[698] Wang J, Zhang P, Song X and Gao L 2014 *RSC Adv* **4** 21318
[699] Yum J, Moehl T, Yoon J, Chandiran A K, Kessler F, Gratia P and Gratzel M 2014 *J Phys Chem C* **118** 16799
[700] Pan S, Zhao Y, Huang G, Wang J, Baunack S, Gemming T, Li M, Zheng L, Schmidt O G and Mei Y 2015 *Nanotechnology* **26** 364001
[701] Lu H, Tian W, Guo J and Li L 2015 *Sci Rep* **5** 12765
[702] Li X, Bassi P S, Boix P P, Fang Y and Wong L H 2015 *ACS Appl Mater Interfaces* **7** 16960
[703] Luo H, Fang Z, Song N, Garvey T, Lopez R and Meyer T J 2015 *ACS Appl Mater Interfaces* **7** 25121
[704] Li C, Hisatomi T, Watanabe O, Nakabayashi M, Shibata N, Domen K and Delaunay J 2015 *Energy Environ Sci* **8** 1493

[705] Lu H, Ma Y, Gu B, Tian W and Li L 2015 *J Mater Chem A* **3** 16445
[706] Shaner M R, Hu S, Sun K and Lewis N S 2015 *Energy Environ Sci* **8** 203
[707] Salmistraro M, Sassolini S, Weber-Bargioni A, Cabrini S and Alessandri I 2015 *Microelectron Eng* **143** 69
[708] Michaux K E, Gambardella A A, Alibabaei L, Ashford D L, Sherman B D, Binstead R A, Meyer T J and Murray R W 2015 *J Phys Chem C* **119** 17023
[709] Schmidt D O, Hoffmann-Eifert S, Zhang H, La Torre C, Besmehn A, Noyong M, Waser R and Simon U 2015 *Small* **11** 6444
[710] Henegar A J and Gougousi T 2015 *ECS J Solid State Sci Technol* **4** P298
[711] Han Y, Pringle J M and Cheng Y 2015 *Photochem Photobiol* **91** 315
[712] Haider A, Cansizoglu H, Cansizoglu M F, Karabacak T, Okyay A K and Biyikli N 2015 *J Vac Sci Technol , A* **33** 01A110
[713] Trejo O, Roelofs K E, Xu S, Logar M, Sarangi R, Nordlund D, Dadlani A L, Kravec R, Dasgupta N P, Bent S F and Prinz F B 2015 *Nano Lett* **15** 7829
[714] Garvey T R, Farnum B H and Lopez R 2015 *Nanoscale* **7** 2400
[715] Verlage E, Hu S, Liu R, Jones R J R, Sun K, Xiang C, Lewis N S and Atwater H A 2015 *Energy Environ Sci* **8** 3166
[716] Seo J, Kim H J, Pekarek R T and Rose M J 2015 *J Am Chem Soc* **137** 3173
[717] Digdaya I A, Han L, Buijs T W F, Zeman M, Dam B, Smets A H M and Smith W A 2015 *Energy Environ Sci* **8** 1585
[718] Iancu A T, Logar M, Park J and Prinz F B 2015 *ACS Appl Mater Interfaces* **7** 5134
[719] Didden A, Hillebrand P, Dam B and van de Krol R 2015 *Int J Photoenergy* 1
[720] Chen W, Ren W, Zhang Y, Liu M and Ye Z 2015 *Ceram Int* **41** S278
[721] Xie Z, Liu X, Wang W, Wang X, Liu C, Xie Q, Li Z and Zhang Z 2015 *Nano Energy* **11** 400
[722] Charlton M R, Dylla A G and Stevenson K J 2015 *J Phys Chem C* **119** 28285
[723] Yoon J, Kim S, Kim D, Kim I, Hong S, No K and Hong S 2015 *Small* **11** 3750
[724] Alibabaei L, Sherman B D, Norris M R, Brennaman M K and Meyer T J 2015 *Proc Natl Acad Sci U S A* **112** 5899
[725] Li L, Xu C, Zhao Y, Chen S and Ziegler K J 2015 *ACS Appl Mater Interfaces* **7** 12824
[726] Li S, Zhang P, Song X and Gao L 2015 *ACS Appl Mater Interfaces* **7** 18560
[727] Zhang G, Wu Y, Ding H, Zhu Y, Li J, Lin Y, Jiang S, Zhang Q, Pan N, Luo Y and Wang X 2015 *RSC Adv* **5** 71883
[728] Zhang G, Wu H, Chen C, Wang T, Yue J and Liu C 2015 *Nanoscale Res Lett* **10** 76
[729] Pheamhom R, Sunwoo C and Kim D 2006 *J Vac Sci Technol A* **24** 1535
[730] Seger B, Tilley D S, Pedersen T, Vesborg P C K, Hansen O, Graetzel M and Chorkendorff I 2013 *RSC Adv* **3** 25902
[731] Seger B, Tilley S D, Pedersen T, Vesborg P C K, Hansen O, Graetzel M and Chorkendorff I 2013 *J Mater Chem A* **1** 15089
[732] Kim B, Li Y, Jung H, Kim J Y, Lee D, Kim B, Son H J, Ko M J and Kim D 2014 *Nano* **9** 1440011
[733] Tilley S D, Schreier M, Azevedo J, Stefik M and Graetzel M 2014 *Adv Funct Mater* **24** 303
[734] Cho H, Shin N, Kim K, Kim B and Kim D 2015 *Synth Met* **207** 31
[735] Rose M and Bartha J W 2009 *Appl Surf Sci* **255** 6620
[736] Kääriäinen T O, Cameron D C and Tanttari M 2009 *Plasma ProcessesPolym* **6** 631
[737] Kaariainen T O, Kelly P J, Cameron D C, Beake B, Li H, Barker P M and Struller C F 2012 *J Vac Sci Technol , A* **30** 01A132
[738] Moitzheim S, Nimisha C S, Deng S, Cott D J, Detavernier C and Vereecken P M 2014 *Nanotechnology* **25** 504008
[739] Kurttepeli M, Deng S, Verbruggen S W, Guzzinati G, Cott D J, Lenaerts S, Verbeeck J, Van Tendeloo G, Detavernier C and Bals S 2014 *J Phys Chem C* **118** 21031
[740] Verbruggen S W, Deng S, Kurttepeli M, Cott D J, Vereecken P M, Bals S, Martens J A, Detavernier C and Lenaerts S 2014 *Appl Catal , B* **160-161** 204
[741] Schindler P, Logar M, Provine J and Prinz F B 2015 *Langmuir* **31** 5057
[742] Jin C, Liu B, Sun J and Lei Z 2015 *Nanoscale Res Lett* **10** 95
[743] Deng S, Kurttepeli M, Cott D J, Bals S and Detavernier C 2015 *J Mater Chem A* **3** 2642
[744] Kanomata K, Pansila P, Ahmmad B, Kubota S, Hirahara K and Hirose F 2014 *Appl Surf Sci* **308** 328
[745] Park J, Lee W, Lee G, Kim I, Shin B and Yoom S 2004 *Integrated Ferroelectr* **68** 129

[746] Lee C, Kim J, Son J Y, Choi W and Kim H 2009 *Appl Catal B* **91** 628
[747] Lee C, Kim J, Son J Y, Maeng W J, Jo D, Choi W and Kim H 2009 *J Electrochem Soc* **156** D188
[748] Byung-Woo Kang and Woong-Sun Kim and Chang-Mook Hwang and Dae-Yong Moon and Jay-Jung Kim and Jae-Gun Park,and Jong 2010 *Jpn J Appl Phys , Part 1* **49** 08JG05
[749] Lee C, Kim J, Gu G H, Jo D, Park C G, Choi W and Kim H 2010 *Thin Solid Films* **518** 4757
[750] Xie Q, Musschoot J, Schaekers M, Caymax M, Delabie A, Lin D, Qu X, Jiang Y, den Berghe S V and Detavernier C 2011 *Electrochem Solid-State Lett* **14** G27
[751] Kääriäinen T O, Lehti S, Kääriäinen M and Cameron D C 2011 *Surf Coat Technol* **205** S475
[752] Rumaiz A K, Woicik J C, Weiland C, Xie Q, Siddons D P, Jaffari G H and Detavernier C 2012 *Appl Phys Lett* **101** 222110
[753] Wei D, Hossain T, Garces N Y, Nepal N, Meyer H M,III, Kirkham M J, Eddy C R, Jr. and Edgar J H 2013 *ECS J Solid State Sci Technol* **2** N110
[754] Bulusu A, Behm H, Sadeghi-Tohidi F, Bahre H, Baumert E, Samet D, Hopmann C, Winter J, Pierron O and Graham S 2013 *Dig Tech Pap - Soc Inf Disp Int Symp* **44** 361
[755] Han D, Choi D and Park J 2014 *Thin Solid Films* **552** 155
[756] Jin M, Jo J, Kim J, An K, Jeong M S, Kim J and Yoo J 2014 *ACS Appl Mater Interfaces* **6** 11649
[757] Pointet J, Gonon P, Latu-Romain L, Bsiesy A and Vallee C 2014 *J Vac Sci Technol , A* **32** 01A120
[758] Kim L H, Kim K, Park S, Jeong Y J, Kim H, Chung D S, Kim S H and Park C E 2014 *ACS Appl Mater Interfaces* **6** 6731
[759] Garces N Y, Meyer D J, Wheeler V D, Liliental-Weber Z, Gaskill D K and Eddy C R 2014 *J Vac Sci Technol , B* **32** 03D101
[760] Jin M, Jo J and Yoo J 2015 *Org Electron* **19** 83
[761] Bulusu A, Graham S, Bahre H, Behm H, Boeke M, Dahlmann R, Hopmann C and Winter J 2015 *Adv Eng Mater* **17** 1057
[762] Tao Q, Kueltzo A, Singh M, Jursich G and Takoudis C G 2011 *J Electrochem Soc* **158** G27
[763] Tao Q, Jursich G M and Takoudis C G 2011 *IEEE Transactions on Semiconductor Manufacturing* **24** 139
[764] Tao Q, Overhage K, Jursich G and Takoudis C 2012 *Thin Solid Films* **520** 6752
[765] Patel S, Butt A, Tao Q, Rossero A. J I, Royhman D, Sukotjo C and Takoudis C G 2014 *Colloids Surf , B* **115** 280
[766] Zhang Q, Zhu B, Zhang L and Ding S 2014 *Microelectron Eng* **122** 1
[767] Katamreddy R, Wang Z, Omarjee V, Rao P V, Dussarrat C and Blasco N 2009 *ECS Trans* **25** 217
[768] Lee J P, Park M H, Chung T M, Kim Y and Sung M M 2004 *Bull Korean Chem Soc* **25** 475
[769] Watanabe T, Hoffmann-Eifert S, Hwang C S and Waser R 2006 *J Electrochem Soc* **153** F199
[770] Watanabe T, Hoffmann-Eifert S, Peter F, Mi S, Jia C, Hwang C S and Waser R 2007 *J Electrochem Soc* **154** G262
[771] Lee S W, Kwon O S, Han J H and Hwang C S 2008 *Appl Phys Lett* **92** 222903
[772] Kim S K, Hoffmann-Eifert S, Mi S and Waser R 2009 *J Electrochem Soc* **156** D296
[773] Lee S W, Han J H, Kim S K, Han S, Lee W and Hwang C S 2011 *Chem Mater* **23** 976
[774] Lee S W, Han J H, Han S, Lee W, Jang J H, Seo M, Kim S K, Dussarrat C, Gatineau J, Min Y and Hwang C S 2011 *Chem Mater* **23** 2227
[775] Potts S E, Keuning W, Langereis E, Dingemans G, van de Sanden M C M and Kessels W M M 2010 *J Electrochem Soc* **157** P66
[776] Blanquart T, Niinistö J, Gavagnin M, Longo V, Pallem V R, Dussarrat C, Ritala M and Leskelä M 2012 *Chem Mater* **24** 3420
[777] Kaipio M, Blanquart T, Tomczak Y, Niinistö J, Gavagnin M, Longo V, Wanzenböck H D, Pallem V R, Dussarrat C, Puukilainen E, Ritala M and Leskelä M 2014 *Langmuir* **30** 7395
[778] Rose M, Niinistö J, Michalowski P, Gerlich L, Wilde L, Endler I and Bartha J W 2009 *J Phys Chem C* **113** 21825
[779] Rose M, Bartha J W and Endler I 2010 *Appl Surf Sci* **256** 3778
[780] Zhou G, Ren J and Zhang S 2012 *Thin Solid Films* **524** 179
[781] Zydor A, Kessler V G and Elliott S D 2012 *Phys Chem Chem Phys* **14** 7954
[782] Longo V, Leick N, Roozeboom F and Kessels W M M 2011 *ECS Trans* **41** 63
[783] Tran T H Y, Haije W G, Longo V, Kessels W M M and Schoonman J 2011 *J Membr Sci* **378** 438
[784] Zhao C, Hedhili M N, Li J, Wang Q, Yang Y, Chen L and Li L 2013 *Thin Solid Films* **542** 38
[785] Kang C, Jeon H, Jang W, Song H, Kim H, Kim H and Jeon H 2015 *Phys Status Solidi A* **212** 674

[786] Profijt H B, van de Sanden M C M and Kessels W M M 2011 *Electrochem Solid-State Lett* **15** G1
[787] Di Giacomo F, Zardetto V, D'Epifanio A, Pescetelli S, Matteocci F, Razza S, Di Carlo A, Licoccia S, Kessels W M M, Creatore M and Brown T M 2015 *Adv Energy Mater* **5** 1401808
[788] Reiners M, Xu K, Aslam N, Devi A, Waser R and Hoffmann-Eifert S 2013 *Chem Mater* **25** 2934
[789] Dang V, Parala H, Kim J H, Xu K, Srinivasan N B, Edengeiser E, Havenith M, Wieck A D, de los Arcos T, Fischer R A and Devi A 2014 *Phys Status Solidi A* **211** 416
[790] Kaipio M, Blanquart T, Banerjee M, Xu K, Niinistö J, Longo V, Mizohata K, Devi A, Ritala M and Leskelä M 2014 *Chem Vap Dep* **20** 209
[791] Niinistö J, Hatanpää T, Kariniemi M, Mäntymäki M, Costelle L, Mizohata K, Kukli K, Ritala M and Leskelä M 2012 *Chem Mater* **24** 2002
[792] Lee M K, Yen C F and Yang S 2011 *EEE Trans Electron Devices* **58** 3885
[793] Lee M and Yen C 2012 *Phys Status Solidi A* **209** 2147
[794] Lee M and Yen C 2014 *Appl Phys A: Mater Sci Process* **116** 2051
[795] Lee M and Yen C 2015 *Thin Solid Films* **595** 12
[796] Yen C and Lee M 2014 *Solid-State Electron* **100** 1
[797] Yen C, Lee M and Lee J 2014 *Solid-State Electron* **92** 1
[798] Anderson V R, Cavanagh A S, Abdulagatov A I, Gibbs Z M and George S M 2014 *J Vac Sci Technol , A* **32** 01A114/1
[799] Malygin A A, Drozd V E, Malkov A A and Smirnov V M 2015 *Chem Vap Dep* **21** 216
[800] Keränen J, Iiskola E, Guimon C, Auroux A and Niinistö L 2000 *Stud Surf Sci Catal* **143** 777
[801] Kim Y and Kim D 2012 *Korean J Chem Eng* **29** 969
[802] Profijt H B, van de Sanden M C M and Kessels W M M 2012 *Electrochem Solid-State Lett* **15** G1
[803] Zydor A and Elliot S D 2011 *J Nanosci Nanotechnol* **11** 8089
[804] Zhang Y, Creatore M, Ma Q, El Boukili A, Gao L, Verheijen M A, Verhoeven M W G M and Hensen E J M 2015 *Appl Surf Sci* **330** 476
[805] Wu Y, Potts S E, Hermkens P M, Knoops H C M, Roozeboom F and Kessels W M M 2013 *Chem Mater* **25** 4619
[806] Knapas K, Rahtu A and Ritala M 2010 *Langmuir* **26** 848
[807] Hirose Y, Yamada N, Nakao S, Hitosugi T, Shimada T and Hasegawa T 2009 *Phys Rev B* **79** 165108
[808] Ginley DS, Hosono H, Paine DC editors.
Handbook of Transparent Conductors. : Springer; 2010
[809] Scanlon D O, Dunnill C W, Buckeridge J, Shevlin S A, Logsdail A J, Woodley S M, Catlow C R, Powell M J, Palgrave R G, Parkin I P, Watson G W, Keal T W, Sherwood P, Walsh A and Sokol A A 2013 *Nat Mater* **12** 798
[810] Luttrell T, Halpegamage S, Tao J, Kramer A, Sutter E and Batzill M 2014 *Scientific Reports* **4** 4043
[811] Chen C, Li P, Wang G, Yu Y, Duan F, Chen C, Song W, Qin Y and Knez M 2013 *Angew Chem , Int Ed* **52** 9196
[812] Singh R, Bapat R, Qin L, Feng H and Polshettiwar V 2016 *ACS Catal* **6** 2770
[813] Kim B, Li Y, Jung H, Kim J Y, Lee D, Kim B, Son H J, Kim D and Ko M J 2014 *NANO* **09** 1440011
[814] Liang Y, Wang C, Kei C, Hsueh Y, Cho W and Perng T 2011 *J Phys Chem C* **115** 9498
[815] Lange S, Arroval T, Saar R, Kink I, Aarik J and Krumme A 2015 *Polym Plast Technol Eng* **54** 301
[816] Korhonen J T, Hiekkataipale P, Malm J, Karppinen M, Ikkala O and H.A. R R 2011 *ACS nano* **5** 1967
[817] Schröder S, Dogan Ö, Schneidewind J, Bertotti G, Keil S, Gargouri H, Arens M, Brose E, Bruns J, Wolansky D, Tillack B, Vassanelli S, Szyszka B and Thewes R 2015 *2015 6th International Workshop on Advances in Sensors and Interfaces (IWASI)* 21
[818] Hoshian S, Jokinen V and Franssila S 2016 *2016 IEEE 29th International Conference on Micro Electro Mechanical Systems (MEMS)* 547
[819] Wang C, Wang H, Yao Q, Yan H, Li J and Lu J 2016 *J Phys Chem C* **120** 478
[820] Acauan L, Dias A C, Pereira M B, Horowitz F and Bergmann C P 2016 *ACS Appl Mater Interfaces* **8** 16444
[821] Marichy C, Donato N, Latino M, Willinger M G, Tessonnier J, Neri G and Pinna N 2015 *Nanotechnology* **26** 024004
[822] Xie M, Sun X, Zhou C, Cavanagh A S, Sun H, Hu T, Wang G, Lian J and George S M 2015 *J Electrochem Soc* **162** A974
[823] Li M, Li X, Li W, Meng X, Yu Y and Sun X 2015 *Electrochem Commun* **57** 43
[824] Xing W, Buettner-Garrett J, Krysiak M, Kelly J and King D M 2014 *ECS Trans* **61** 13

[825] Lotfabad E M, Kalisvaart P, Cui K, Kohandehghan A, Kupsta M, Olsen B and Mitlin D 2013 *Phys Chem Chem Phys* **15** 13646
[826] Mohanty D, Dahlberg K, King D M, David L A, Sefat A S, Wood D L, Daniel C, Dhar S, Mahajan V, Lee M and Albano F 2016 *Scientific Reports* **6** 245
[827] Qin C, Cao J, Chen J, Dai G, Wu T, Chen Y, Tang Y, Li A and Chen Y 2016 *Dalton Trans* **45** 9669
[828] Deng S, Verbruggen S W, He Z, Cott D J, Vereecken P M, Martens J A, Bals S, Lenaerts S and Detavernier C 2014 *RSC Adv* **4** 11648
[829] Shin H, Jeong D K, Lee J, Sung M M and Kim J 2004 *Adv Mater* **16** 1197
[830] Kang T, Smith A P, Taylor B E and Durstock M F 2009 *Nano Lett* **9** 601
[831] Carvajal C G, Rout S, Mundle R and Pradhan A K 2017 *Langmuir* **33** 11
[832] Zhang H, Ren W and Cheng C 2015 *Nanotechnology* **26** 0957
[833] Guan C, Wang X, Zhang Q, Fan Z, Zhang H and Fan H J 2014 *Nano Lett* **14** 4852
[834] Kim M, Lee J, Lee S, Seo S, Bae C and Shin H 2015 *ChemSusChem* **8** 2363
[835] Zhong Y, Ma Y, Guo Q, Liu J, Wang Y, Yang M and Xia H 2017 *Scientific Reports* **7** 2045
[836] Tan L K, Kumar M K, An W W and Gao H 2010 *ACS Applied Materials & Interfaces* **2** 498
[837] Liu L, Karuturi S K, Su L T and Yoong A T I 2011 *Energy & Environmental Science* **4** 209
[838] Graugnard E, King J S, Gaillot D P and Summers C J 2006 *Adv Funct Mater* **16** 1187
[839] Yoshimura T, Tatsuura S and Sotoyama W 1991 *Appl Phys Lett* **59** 482
[840] Kubono A, Yuasa N, Shao H, Umemoto S and Okui N 1996 *Thin Solid Films* **289** 107
[841] Lee B H, Ryu M K, Choi S, Lee K, Im S and Sung M M 2007 *J Am Chem Soc* **129** 16034
[842] Nilsen O, Klepper K, Nielsen H and Fjellvaåg H 2008 *ECS Trans* **16** 3
[843] Dameron A A, Seghete D, Burton B B, Davidson S D, Cavanagh A S, Bertrand J A and George S M 2008 *Chem Mater* **20** 3315
[844] Yoon K, Han K and Sung M 2012 *Nanoscale Res Lett* **7** 71
[845] Niemelä J, Giri A, Hopkins P E and Karppinen M 2015 *J Mater Chem A* **3** 11527
[846] Niemelä J, Karttunen A J and Karppinen M 2015 *J Mater Chem C* **3** 10349
[847] Abdulagatov A I, Hall R A, Sutherland J L, Lee B H, Cavanagh A S and George S M 2012 *Chem Mater* **24** 2854
[848] Ishchuk S, Taffa D H, Hazut O, Kaynan N and Yerushalmi R 2012 *ACS Nano* **6** 7263
[849] Abdulagatov A I, Terauds K E, Travis J J, Cavanagh A S, Raj R and George S M 2013 *J Phys Chem C* **117** 17442
[850] Nilsen O, Haug K R, Finstad T and Fjellvåg H 2013 *Chem Vap Dep* **19** 174
[851] Sood A, Sundberg P, Malm J and Karppinen M 2011 *Appl Surf Sci* **257** 6435
[852] Sundberg P, Sood A, Liu X, Johansson L and Karppinen M 2012 *Dalton Trans* **41** 10731